1

INVESTIGATION OF THE HIGH ANGLE OF ATTACK DYNAMICS OF THE F-15B USING BIFURCATION ANALYSIS

THESIS

Robert J. McDonnell
Captain, USAF

AFIT/GAE/ENY/90D-16

DEPARTMENT OF THE AIR FORCE
AIR UNIVERSITY
AIR FORCE INSTITUTE OF TECHNOLOGY

Wright-Patterson Air Force Base, Ohio

AFIT/GAE/ENY/90D-16

1

INVESTIGATION OF THE HIGH
ANGLE OF ATTACK DYNAMICS OF THE
F-15B USING BIFURCATION ANALYSIS

THESIS

Robert J. McDonnell
Captain, USAF

AFIT/GAE/ENY/90D-16

AFIT/GAE/ENY/90D-16

INVESTIGATION OF THE HIGH ANGLE OF ATTACK DYNAMICS OF THE F-15B USING BIFURCATION ANALYSIS

THESIS

Presented to the Faculty of the School of Engineering

of the Air Force Institute of Technology

Air University

In Partial Fulfillment of the

Requirements for the Degree of

Master of Science of Aeronautical Engineering

Robert J. McDonnell, B.S.

Captain, USAF

December 1990

Acknowledgements

This work done in this thesis owes much to the people who previously opened up this avenue of investigation. First of all I'd like to thank my advisor, Captain Jim Planeaux for his interest in bifurcation theory and the help he provided in completing this work. Dan Baumann is also recognized for his work in developing the F-15 model used in the thesis and the valuable information he provided. I would also like to thank my thesis committee, Dr. Robert Calico, Dr. Curtis Spenny, and Dr. Brad Liebst, for their valuable comments during the review of this document. I also want to remember Captain Wayne Wilsdon, who helped me struggle through Wings and Bodies, Computational Fluids, and Panelling Methods, and who's tragic death made us all aware of how precious life really is. And to my family and friends, thanks for all your advice and support throughout this ordeal.

Captain Robert J. McDonnell

Table of Contents

List of Figures

List of Tables

List of Symbols

α : angle of attack, degrees

$\bar{\alpha}$: angular acceleration vector

β : sideslip angle, degrees

δ_a : aileron deflection angle, degrees

δ_e : elevator deflection angle, degrees

$\delta_{\Delta e}$: differential elevator deflection angle, degrees

δ_{pv} : pitch thrust vector angle, degrees

δ_r : rudder defection angle, degrees

δ_{yv} : yaw thrust vector angle, degrees

$\Delta C_{l\beta}$: rolling moment increment due to 2-place canopy

$\Delta C_{n\beta}$: yawing moment increment due to 2-place canopy

$\Delta C_{n\beta *}$: asymmetric yawing moment increment

$\Delta C_{y\beta *}$: asymmetric side force increment

λ : control parameter

ϕ : bank angle, degrees

ψ : heading angle, degrees

ρ : period, seconds

θ : pitch angle, degrees

$\bar{a}$: translational acceleration vector

b : wing span, feet

C_D : drag coefficient

C_L : lift coefficient

C_l : rolling moment coefficient

$C_{l\beta}$: partial derivative of rolling moment due to sideslip

$C_{l\delta a}$: partial derivative of rolling moment due to aileron deflection

$C_{l\delta e}$: partial derivative of rolling moment due to elevator deflection

$C_{l\delta\Delta e}$: Partial derivative of rolling moment due to differential elevator

$C_{l\delta r}$: partial derivative of rolling moment due to rudder deflection

C_{lp} : roll damping

C_{lr} : roll damping due to yaw rate

C_m : pitching moment coefficient

C_{mo} : basic pitching moment coefficient

C_{mq} : pitch damping

C_n : yawing moment coefficient

$C_{n\beta}$: yawing moment due to sideslip

$C_{n\beta^*}$: yawing moment due to sideslip, high angle of attack increment

$C_{n\delta a}$: partial derivative of yawing moment due to aileron deflection

$C_{n\delta e}$: partial derivative of yawing moment due to elevator deflection

$C_{n\delta\Delta e}$: partial derivative of yawing moment due to differential elevator deflection

$C_{n\delta r}$: partial derivative of yawing moment due to rudder deflection

C_{np} : yawing moment due to roll rate

C_{nr} : yaw damping

C_x : x axis force coefficient

C_y : y axis force coefficient

$C_{y\beta}$: side force due to sideslip

$C_{y\beta *}$: asymmetric side force due to sideslip

$C_{y\delta a}$: partial derivative of side force due to aileron deflection

$C_{y\delta e}$: partial derivative of side force due to elevator deflection

$C_{y\delta \Delta e}$: partial derivative of side force due to differential elevator deflection

$C_{y\delta r}$: partial derivative of side force due tp rudder deflection

C_{yp} : side force due to roll rate

C_{yr} : side force due to yaw rate

C_z : z axis force coefficient

$\bar{c}$: mean aerodynamic chord, feet

C.G. : center of gravity

d_{Tx} : offset of thrust from C.G. in x direction, ft

d_{Ty} : offset of thrust from C.G. in y direction, ft

d_{Tz} : offset of thrust from C.G. in z direction, ft

f : vector function describing aircraft dynamics

$\bar{F}$: force acting on airplane

g : gravitational constant, 32,174 ft/sec^2

I : aircraft inertia tensor

I_x : moment of inertia about x axis, slug ft^2

I_{xz} : moment of inertia about y axis, slug ft^2

I_y : moment of inertia about z axis, slug ft^2

I_z : product of inertia in x and z direction, slug ft^2

L : rolling moment, ft lbf

M : pitching moment, ft lbf

m : aircraft mass, slugs

N : yawing moment, ft lbf

$\overline{N}$: moment acting on airplane

p : roll rate, radians/second

q : pitch rate, radians/second

$\overline{q}$: dynamic pressure, lbf/ft^2

r : yaw rate, radians/second

S : wing planform area, ft^2

T : thrust force, lbf

T_l : left engine thrust, lbf

T_{lx} : left engine thrust in x direction, lbf

T_{ly} : left engine thrust in y direction, lbf

T_{lz} : left engine thrust in z direction, lbf

T_r : right engine thrust, lbf

T_{rx} : right engine thrust in x direction, lbf

T_{ry} : right engine thrust in y direction, lbf

T_{rz} : right engine thrust in z direction, lbf

T_x : thrust in x direction, lbf

T_y : thrust in y direction, lbf

T_z : thrust in z direction, lbf

t : time, seconds

u : vector of aircraft states

V_{tr} : aircraft true airspeed, ft/sec

Abstract

Previous studies predicted the F-15B high angle of attack and flat spin behavior using bifurcation analysis. These studies varied control surface deflections to find equilibrium and periodic solutions. The purpose of this ~~thesis~~ research was to use bifurcation analysis to predict the F-15B high angle of attack and flat spin behavior as a result of variable thrust, asymmetric thrust, and thrust vectoring.

Using a previously developed model of the F-15, bifurcation analysis and continuation methods were used to map out the equilibrium and periodic solutions of the model as a function of the thrust parameters. A baseline bifurcation diagram, as a function of alpha and elevator deflection angle, δ_e, of the equilibrium solutions for the F-15 was developed. Thrust was varied and changes were identified. Thrust asymmetries were introduced and their effect on entering and recovering from spins was identified. Thrust vectoring was introduced to see how pitch and yaw vectoring can aid in the entry and recovery from spins. Where deemed necessary, time history simulations were presented to further explain F-15 behavior.

Keywords: Spinning motion; Aerodynamic stability; Jet fighters; Equations of motion; Bifurcation mathematics; Angle of attack; Aerodynamic control surfaces; Theses, (EDC)

INVESTIGATION OF THE HIGH ANGLE OF ATTACK DYNAMICS OF THE F-15B USING BIFURCATION ANALYSIS

I. Introduction

In the military flight environment, pilots must regularly place themselves in the high angle of attack flight regime to out maneuver their opponent. Unfortunately, maintaining controlled flight in this regime is difficult. Loss of control can occur through nonlinear behavior such as stalls, departures, wing rock, nose slice, spin entry, and full spins. In combat these will often lead to fatal results. In peacetime training these are not as dangerous as long as there is enough altitude to recover to controlled flight. However, spins require quite a bit more altitude to recover than the other aircraft motions. As a consequence, many aircrews and their multimillion dollar aircraft are lost in spin accidents. Between the years 1966 and 1970, two hundred fighter aircraft worth 360 million dollars were lost in spin accidents resulting in 100 fatalities (1:1). Even the F-15, the most advanced fighter in the U.S. Air Force today, is not immune to spin losses. Baumann (6:2-4) describes the details of a recent Air Force accident investigation board in which an F-15 was lost due to an flat spin. A routine training flight turned into the total loss of an aircraft because of an inadvertent spin.

Spins

The motion of an airplane in a spin is characterized by an angle of attack between the stall and 90 degrees, and a rapid, wings level descent toward the earth while rotating about a vertical or near vertical axis (24:1). Spins are most commonly entered by stalling the wings and introducing a yaw. The yaw increases the lift on the wing outside of the yaw and further stalls the inside wing. The increased drag on the stalled wing further drives the yaw. Additionally, a rolling moment in the direction of the yaw is introduced by the asymmetric lift distribution. Depending on the severity of the induced motions and the aircraft's physical characteristics, a spin may or may not develop. A developed spin is therefore a complex balance of aerodynamic and inertia forces and moments. Once a spin develops, a recovery to normal flight must be accomplished by stopping the yaw rotation or breaking the stall. Application of a yawing moment about the body z axis opposite the spin is the preferred method of recovery.

Previous Studies

A rough idea of a certain airplane's spin characteristics can be estimated during design by looking at key aerodynamic and inertial factors. However, there is no clear cut design methodology for high angle of attack aerodynamics because of the nonlinear behavior of the fluid dynamics of separated flows, a high dependence on configuration, and a lack of ground test facilities (10:1). Vertical wind tunnels can be used to gain an idea of a design's spin characteristics, however, correlation with full scale aircraft can be questionable because of Reynolds number effects (24:7). Analytical studies can provide an additional tool in predicting the spin characteristics of an airplane.

Analytical predictions of spin behavior have been performed for many years. In 1954, Scher (29) and Burk (8) both demonstrated that spins could be simulated on computers by using wind tunnel aerodynamic coefficients and solving the nonlinear equations of motion. Scher produced time histories of spin entry, developed spins, and spin recovery. Burk produced time histories of spin recoveries using anti-spin yaw moments and found that the applied moment aided the recovery from the spin. Additional time history studies were done in 1959 by Scher, Anglin, and Lawerence using a 60 degree delta wing airplane (30), in 1960 by Neihouse, Klinar, and Scher of the X-15 (24), and in 1972 by Adams of several airplanes (1). In 1966, Grafton produced time histories of spins to determine the effect thrust has on spins (13) and found that generally, applying thrust aided the recovery from spins. These studies were able to simulate spins, but were unable to accurately describe the causes of nonlinear behaviors such as jumps or the onset of oscillatory motion.

In 1979, Carrol and Mehra (9) used a different approach to analytical methods when they applied bifurcation theory and continuation methods to solve the nonlinear equations of motion. Equilibrium solutions of the nonlinear system were traced out by varying control surface deflections. The stability was determined by looking at the eigenvalues of the linearized system. The new method was not a simulation, like the previous studies, but a map of the airplane's equilibrium solutions and therefore offered a more global view of the nonlinear behavior of the aircraft. More important though, the nature of the transitions from stable to unstable equilibrium solutions revealed the causes and onset of nonlinear behavior. Guicheteau (15,16), Hui and Tobak (18), Zagaynov and Goman (36), Hawkins (17), and Jahnke (19,20,21) also used bifurcation analysis to observe the nonlinear behavior of different aircraft configurations, including the development of spins. Barth (5) and Planeaux and Barth (25) investigated the nonlinear behavior of the F-15 using bifurcation analysis and proved its ability to predict the aircraft's motion, including the onset of wing rock. However, their model was not realistic above 40 degrees angle of attack and therefore could not predict spins. Beck (7) and Planeaux, Beck, and Baumann (26) continued this research using control augmentation.

Previous work in F-15 spin research using bifurcation theory was done by Baumann (6). He created an F-15 model that more realistically describes the aero coefficients at high angles of attack by curve fitting F-15 aerodynamic data to angles of attack up to 90 degrees. Using the new F-15 model, Baumann found stable flat spins between 70 and 80 degrees angle of attack. These flat spins correlate well with flight test data. (22,34)

Overview

This paper continues the F-15 spin research accomplished by Baumann using a modified Baumann model which includes control of variable thrust, asymmetric thrust, and thrust vectoring. Bifurcation analysis will be used to determine how effective the thrust parameters are in causing and recovering from flat spins. Although current operational F-15's do not have the capability to vector thrust, nozzles with vectoring features are presently installed on the F-15 STOL demonstrator aircraft presently undergoing flight testing at Edwards AFB, Ca. (28:51). Additionally, the Rockwell/MBB X-31 aircraft will have thrust vectoring paddles installed (27:117). In the X-31 studies, thrust vectoring will be used to evaluate its combat utility at low airspeeds and high angles of attack. Analytical and simulation studies, such as those done by Schneider (31) and Anderson (2), have shown the ability of thrust vectoring to increase an aircraft's agility. However, only the study by Burk (8) has gone on to show the potential use of applied moments in spin recoveries.

Chapter II will discuss in more details, the dynamics of spins and recovery from them. Chapter III will briefly discuss bifurcation theory and the continuation method used to trace out the branches of the bifurcation diagram. Chapter IV will describe the F-15 model and the modifications made to the Baumann F-15 model. Chapter V presents the results that were found during the research. In Chapter VI, the conclusions will be presented and ideas of future research using this technique will be given.

II. Spin Theory

The previous chapter defined spin motion and gave a simple example of how spins are typically entered. This Chapter will look at flat spins and show briefly how the aerodynamics and physical characteristics of an airplane affect its ability to recover from the spin. Most of the information in this chapter is referenced from Neihouse, Klinar, and Scher (24).

The most dangerous of all spins is the flat spin. It is characterized by an angle of attack approaching 90 degrees and high yaw rotation rates. As the plane approaches 90 degrees, the aerodynamic control surfaces become ineffective due to blockage by the wings and fuselage and recovery may be difficult. The inertia characteristics of modern fighter aircraft compound the difficulty in recovering from a flat spin. Since most of the weight is concentrated in the fuselage, the high yaw rotation rate is accompanied by a large amount of angular momentum. The aerodynamic surfaces must provide moments to counter this angular momentum and break the spin. The decreased effectiveness of the control surfaces couples with the large amount of angular momentum to make recovery from flat spins much more difficult. Spin test aircraft are often fitted with drogue parachutes to aid in the recovery from flat spins. However, operational aircraft do not have the luxury of spin parachutes and are often lost due to flat spins. Vectoring an aircraft's thrust against the spin is a potential source of additional moments to decrease the angular momentum. Unfortunately, modern fighters are not equipped with vectoring nozzles either. Asymmetric thrust settings in a multiengine aircraft are another possible source for antispin moments.

Since the main component of motion in a developed spin is the rotation about the z axis (yawing motion), the recovery from the spin therefore necessitates decreasing the rate of yaw rotation, r. Eqn (1) represents the $\dot{r}$ equation of an aircraft in principal axes.

$$\dot{r} = \frac{M_{z,aero}}{I_z} + \frac{I_x - I_y}{I_z}\, p\, q = \frac{\bar{q}\, S\, \bar{c}}{I_z}\, C_n + \frac{I_x - I_y}{I_z}\, p\, q \tag{1}$$

The yawing rate can be reduced by making $\dot{r}$ negative. Most conventional aircraft have inertia characteristics that make the coupled term of $I_x - I_y$ small. Therefore, the aerodynamic yaw moment created by the rudder is the primary moment in recovering from spins for this type of configuration. The inertia characteristics of modern fighter aircraft make the coupled term of $I_x - I_y$ a large negative number. A decrease in the yaw rate can be accomplished by coupling the roll and pitch rates to provide an antispin yaw moment. Assuming that the plane is in a right spin, a negative $\dot{r}$ can be achieved by producing a positive pitch and roll rate. To most pilots this is not intuitive since it requires prospin control inputs (i.e. aileron into the spin and pitch up). Accompanying this with an antispin rudder deflection seems to be the most practical method at recovering from a flat spin. The F-15 flight manual recommends nearly full aileron/differential stabilator deflections in the spin direction to recover from flat spins (34:6-7). The use of yaw thrust vectoring and asymmetric thrust settings can also provide direct antispin yaw moments. Pitch vectoring can provide a coupling term or can provide a nose down moment to try to break the stall.

III. Bifurcation Theory

> Nonlinear phenomena are responsible for a variety of effects. Jumping between modes, sudden onset or vanishing of periodic oscillations, loss or gain of stability, buckling of frames and shells, ignition, combustion, and chaos are but a few examples. Nonlinear phenomena arise in all fields of physics, chemistry, biology, and engineering. The classical mathematical discipline that treats nonlinear phenomena is bifurcation theory. (33,xi)

This chapter will discuss the basic principles of bifurcation theory and their use in understanding nonlinear behavior. Some of the concepts covered will be equilibrium solutions, stability, turning points, bifurcation points and Hopf bifurcations. Most of the information in this chapter is referenced from Seydel (33). The software program used in this research, AUTO, will also be described.

Equilibrium Points

Equilibrium points represent steady states of a dynamical system; the system is at rest or in uniform motion. Equilibrium points are also referred to as *stationary points*. The motion of a non-time dependent system can be modelled mathematically as

$$\dot{u} = f(u) \tag{2}$$

where u is the state vector. The equilibrium states of this system would satisfy the equation

$$f(u) = 0. \quad (3)$$

An aircraft in this state would exhibit no translational or angular accelerations and would have constant roll and pitch angles.

The dependence of the system on some control parameter can be found by varying the parameter and finding any new equilibrium points. The equation can be represented as

$$\dot{u} = f(u,\lambda) \quad (4)$$

where λ is the control parameter. This parameter is called the *bifurcation parameter*. In an aircraft model, these parameters would be such things as the elevator deflection or thrust level. A qualitative idea of system's dependence on the varying parameter is found by plotting the new value of a representative state variable versus the value of the parameter. This diagram is called a *bifurcation diagram*. For the aircraft model with the elevator deflection as the bifurcation parameter, a bifurcation diagram provides an idea of the aircraft's equilibrium motion as the elevator is deflected from one value to another. If the elevator is varied from stop to stop, the global behavior of the aircraft can be found. Unfortunately, these diagrams tell little of the aircraft response over time or of the stability of the equilibrium points.

Stability

The stability of an equilibrium point is determined by identifying whether the system will return to the equilibrium point if it is disturbed. A point is considered *stable* if the response to a small perturbation is small as time goes to infinity. If the response goes to zero as time goes to infinity it is considered *asymptotically stable*. It is *unstable* if the response grows as time goes to infinity. A *neutrally* stable point would neither go to zero nor grow. The size of the perturbation is important since an equilibrium point may be stable for a small perturbation but unstable for a larger one.

Stability can be found by linearizing the system around the equilibrium point. This is a good approximation of the nonlinear system close to the equilibrium point. The stability can then be determined by looking at the eigenvalues of the Jacobian matrix of the linear system. The system is stable if the real parts of the eigenvalues are negative or zero. A positive real part indicates that the point is unstable.

Turning Points

A *turning point* in a nonlinear system has a single eigenvalue equal to zero. Figure 3-1 is a bifurcation diagram with a turning point found in the differential equation

$$\dot{y} = \lambda - y^2. \tag{5}$$

At the turning point or *limit point*, the only equilibrium solution is $\lambda = 0$, $y = 0$. With $\lambda > 0$ there are two solutions. The solution $+\sqrt{\lambda}$ is stable, while $-\sqrt{\lambda}$ is unstable. Turning points do not necessarily separate stable equilibria from unstable equilibria. Unstable solutions can also exist on both sides of the turning point as one eigenvalue crosses zero. Fig. 3-1 also identifies stable equilibria as being solid lines while unstable equilibria are identified by dashed lines.

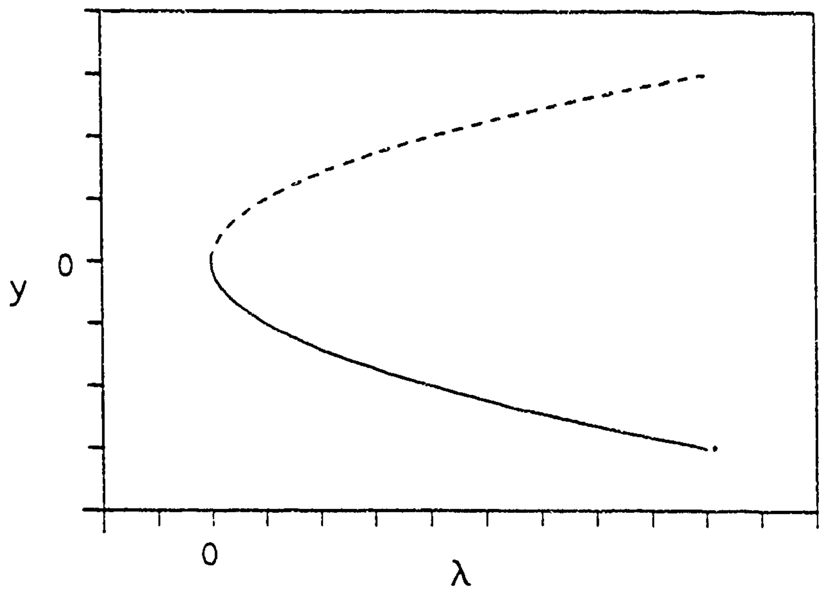

Figure 3-1 Turning Point on a Bifurcation Diagram

A unique phenomenon called *hysteresis* occurs when a branch loses stability at a turning point and then becomes stable at another turning point. Fig. 3-2 is a bifurcation diagram of a typical hysteresis point. Hysteresis leads to jump phenomena between the stable branches as the parameter is varied beyond either limit point. Aircraft can display jump phenomena between stable states, such as the jump from low angle of attack equilibria to a high angle of attack spin. Two good articles dealing with jump phenomena in aircraft maneuvers are written by Schy and Hannah (32) and Young, Schy, and Johnson (35).

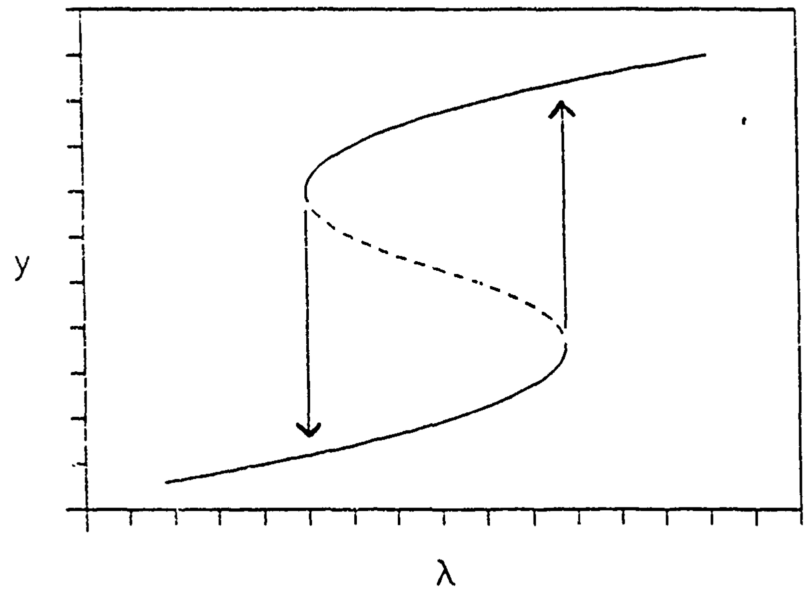

Figure 3-2 Limit Points Showing Hysteresis

Bifurcation Points

Bifurcation points also have one zero eigenvalue. However, unlike a turning point, there are solutions for values of λ on both sides of a bifurcation point. Fig. 3-3 is an example of the *pitchfork bifurcation* that develops in the differential equation

$$y = \lambda y - y^3. \quad (6)$$

For all values of λ the trivial solution, $y = 0$, is an equilibrium solution. Additionally, for $\lambda > 0$ there are two nontrival equilibria, $y = \pm\sqrt{\lambda}$. However, the branch $y = 0$ losses stability at the bifurcation point and a bifurcation of two stable branches occurs. This is referred to as a *supercritical pitchfork*.

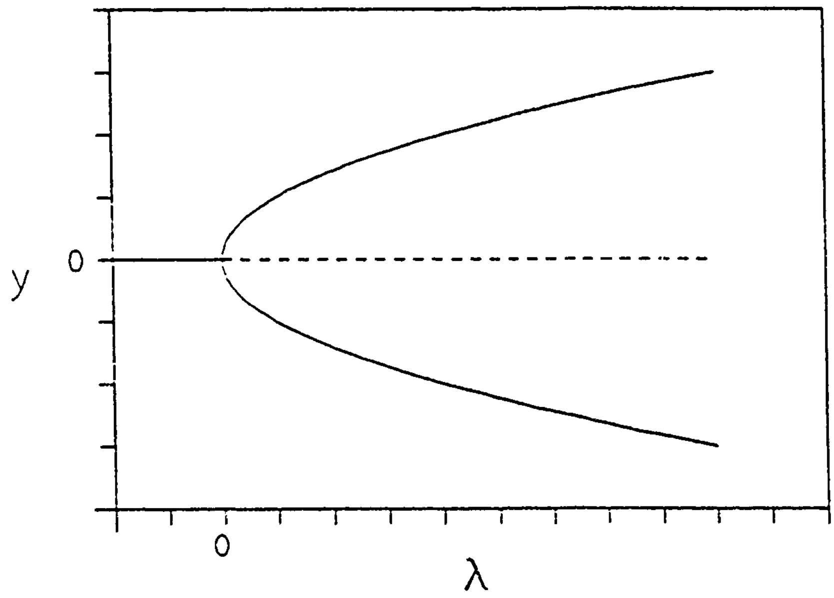

Figure 3-3 Supercritical Pitchfork

If the branch $y = 0$ gains stability at the bifurcation point and a bifurcation of unstable branches occurs, the result is called a *subcritical pitchfork*. Fig. 3-4 is an example of a subcritical bifurcation. The behavior at these bifurcation points is also referred to as a stationary or steady state bifurcation.

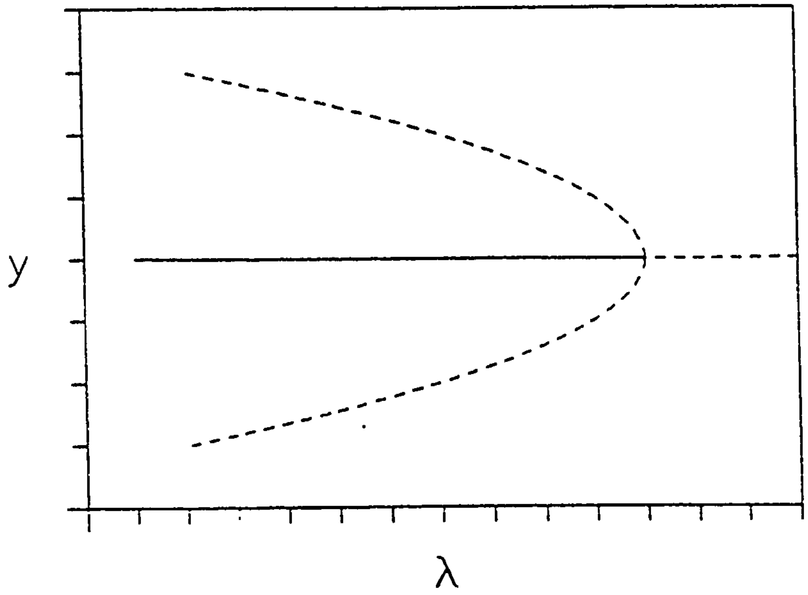

Figure 3-4 Subcritical Pitchfork

Hopf Bifurcation

The types of nonlinear phenomena identified so far are for equilibrium solutions. The type of bifurcation that connects equilibrium solutions with periodic motion is the *Hopf bifurcation*. Periodic solutions arise at points where two eigenvalues of the linearized system become purely imaginary. For an example, a Hopf bifurcation arises from the two equations

$$\begin{aligned} \dot{y}_1 &= -y_2 + y_1(\lambda - y_1^2 - y_2^2) \\ \dot{y}_2 &= y_1 + y_2(\lambda - y_1^2 - y_2^2). \end{aligned} \tag{7}$$

The only equilibrium solution for all λ occurs at $y_1 = y_2 = 0$. However, the eigenvalues are $\lambda \pm i$ which indicates that the equilibrium points are unstable for $\lambda > 0$

and stable for $\lambda < 0$. A Hopf point is located at $\lambda = 0$ since both eigenvalues are purely imaginary. Additionally, a change of stability takes place without a turning point or any branches bifurcating. The exchange of stability occurs through the formation of a family of *limit cycles* at the Hopf point.

Limit cycles are found by putting y_1 and y_2 into polar coordinates

$$y_1 = \rho\cos\theta, \; y_2 = \rho\sin\theta \tag{8}$$

and then substituting them into Eqn (7). By manipulation this yields

$$\dot{\rho} = \rho(\lambda - \rho^2) \tag{9}$$

$$\dot{\theta} = 1. \tag{10}$$

This shows that $\dot{\theta} = 1$ which is not an equilibrium solution. For $\lambda > 0$ the result is a periodic orbit with an amplitude growing by $\sqrt{\lambda}$. Fig. 3-5 shows how this looks in three dimensions. The limit cycle encircles the unstable equilibrium. Fig. 3-6 is an example of a Hopf bifurcation on a bifurcation diagram. A stable branch goes unstable at the Hopf point. The circles represent the maximum amplitude of the limit cycle at λ. Closed circles indicate stable limit cycles and open circles indicate unstable limit cycles.

Periodic solutions lose stability via three mechanisms;

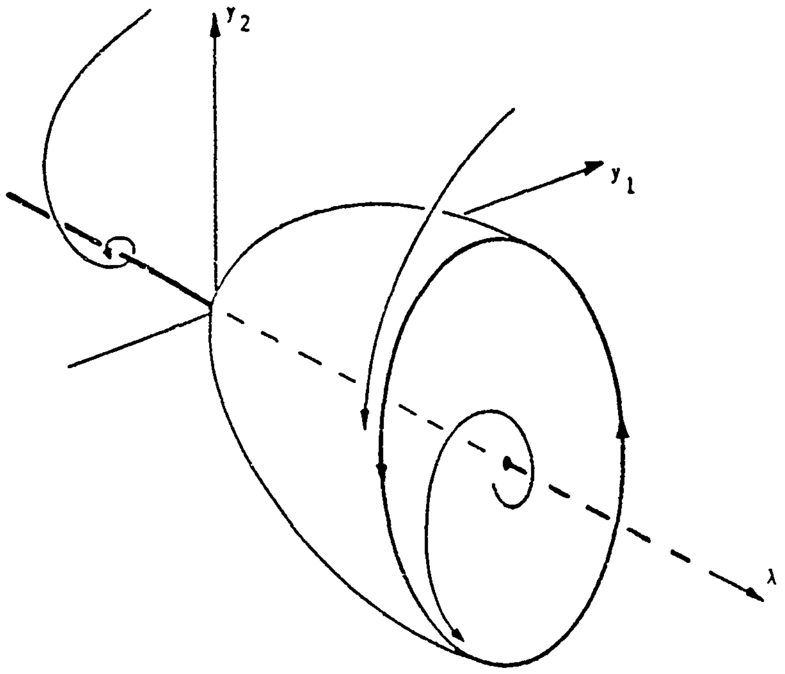

Figure 3-5 Limit Cycles Near a Hopf Bifurcation (26:63)

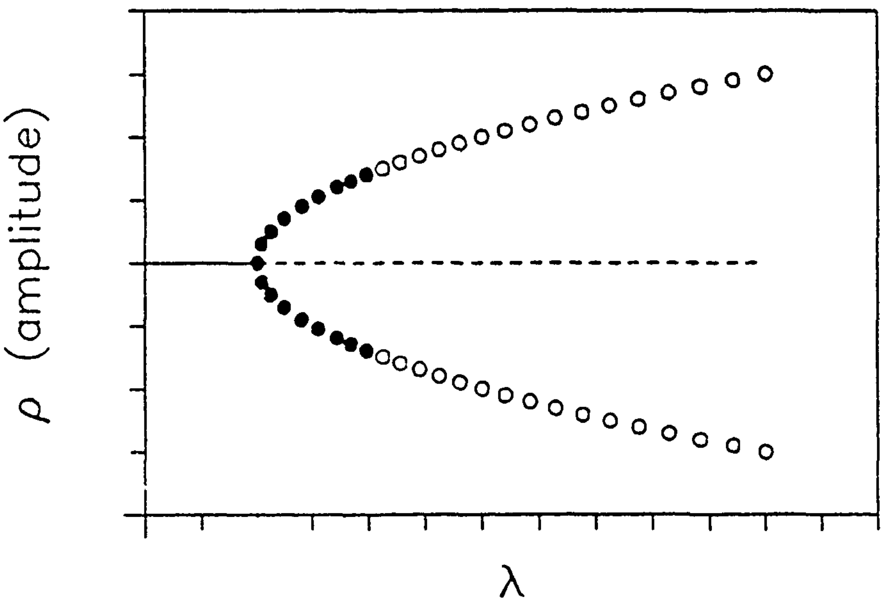

Figure 3-6 Hopf Point on a Bifurcation Diagram

turning points, period doubling, and bifurcation into a torus. Floquet multipliers, which are analogous to eigenvalues, are used to find the stability of a limit cycle.

AUTO Software

The tool used in this research to trace out equilibrium branches, determine stability, identify turning points and bifurcation points, and find limit cycles is the program AUTO written by Doedel (11). From a known starting point, (u_0, λ_0), which satisfies Eqn (3), Doedel uses the psuedo arclength continuation technique to trace out equilibrium solutions for new values of λ. The psuedo arclength technique varies the stepsize along the branch and using the direction vector $(\dot{u}, \dot{\lambda})$ a predictor-corrector algorithm finds the next solution. The predictor/corrector algorithm used is the Newton method. The psuedo arclength technique allows the algorithm to be scaled so it can compute near and past limit points where the direction vector is infinite. Doedel also incorporates an adaptive stepsize. If the solution converges rapidly using the predictor/corrector algorithm, the stepsize is increased to save computation time. Additionally, if the solution does not converge, the stepsize is halved until a minimum stepsize is reached. The program will then signal nonconvergence.

AUTO identifies bifurcation points and turning points by monitoring the Jacobian matrix at each solution and identifying sign changes in the eigenvalues. Using bifurcation analysis, AUTO identifies these changes as limit points, bifurcation points, or Hopf Bifurcations. AUTO continues on the main branch until a user specified number of points is reached or values of λ or u exceed user specified limits. AUTO has the capability to go back to the bifurcation points to compute the branches emanating from the bifurcation point. Additionally, AUTO can go back and compute the limit cycles that begin at the Hopf bifurcations. More information on the capabilities of AUTO can be found in the AUTO user manual (11).

IV. Model Development

Aircraft Description

The F-15B aircraft, which is modelled in this research, is a two seat, high performance, supersonic, all-weather air-superiority fighter. The aircraft's primary mission is aerial combat, however, it can also be configured for ground attack. It is powered by twin Pratt and Whitney F-100 turbofan engines. The model developed for this research includes pitch and yaw thrust vectoring which a baseline F-15B does not have. The vectoring nozzles are assumed to have no effects on the aerodynamic characteristics or weight and balance of the F-15B. Appendix A provides the physical dimensions of the aircraft and weight and balance.

The aircraft's aerodynamic control surfaces are the ailerons, rudder, elevator. Thrust settings can be independently controlled for both right and left engines. For this research, the yaw and pitch angles of the nozzles can also be controlled. Several control characteristics of the F-15B will not be modelled to simplify the research. These include the effects of the Control Augmentation System (CAS), Aileron Rudder Interconnect (ARI), and speedbrake. The differential elevator deflection is also set at a constant gain times the aileron deflection. The F-15 aero coefficients modelled are for low speed flight and constant altitude. Therefore, flight conditions of 20,000 feet and low Mach numbers will be used.

Force and Moment Equations

The force and moment equations used in this research are the body-axis force and moment equations used by Baumann (6:20-21) but modified to include forces and moments due to variable thrust, asymmetric thrust and thrust vectoring. These equations therefore have both aerodynamic and thrust components. The aerodynamic force and moment coefficients were modelled for the F-15 by Baumann. He used a statistical software program to curve fit F-15 aerodynamic data from -20 degrees to 90 degrees angle of attack. These curve fits are fairly representative of the actual F-15 aerodynamic coefficients (23). Some amount of data smoothing can be expected, however, the general trends in the data are maintained. The details of his curve fitting techniques can be found in (6). At low angles of attack, the above coefficients are symmetric with respect to the lateral variables β, p, and r. However, asymmetries are present above 40 degrees angle of attack due to asymmetric shedding of nose vortices (22:3.4).

The thrust components are added to the aerodynamic coefficients to produce combined thrust/aerodynamic force and moment coefficients. The thrust contributions to the modified force coefficients are found by determining the thrust in the body x,y, and z directions as a result of total thrust and any vectoring. The moments are found by determining the contribution by each engine in the body x, y and z direction and multiplying each by the appropriate moment arm to the center of gravity. Asymmetric thrust is modelled using the variables right engine thrust (T_r) and left engine thrust (T_l). Pitch vectoring is modelled using the variable δ_{pv} with a positive value causing the a nose up pitching moment (flow deflected upward). Yaw vectoring is modelled using the variable δ_{yv} with a positive value causing a yaw to the left (flow deflected left). The moment arm offsets are defined as d_{Tx}, d_{Ty}, and d_{Tz}. Fig. 4-1 shows these variables.

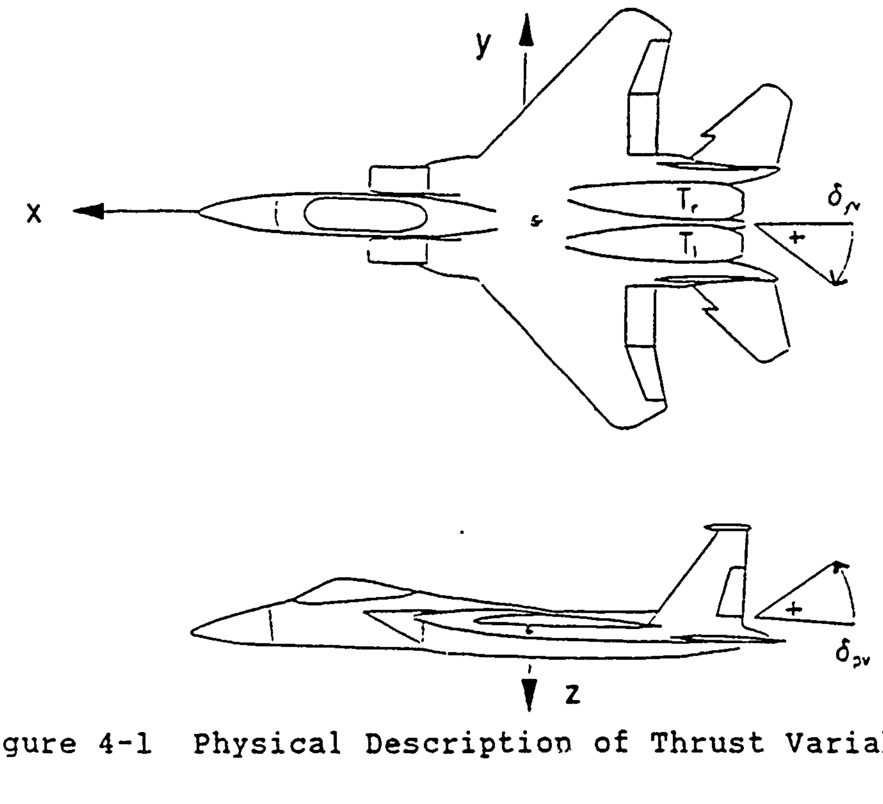

Figure 4-1 Physical Description of Thrust Variables

Etkin (12) was used to verify Baumann's equations and the thrust effects. The resulting equations are:

$$C_x = C_L(\alpha,\delta_e)\sin\alpha - C_D(\alpha,\delta_e)\cos\alpha + T_x/(\bar{q}\ S) \tag{11}$$

$$\begin{aligned} C_y = {} & C_y(\alpha,|\beta|,\delta_e) + C_{y\delta a}(\alpha)\delta_a + C_{y\delta r}(\alpha)\delta_r \\ & + [b/2V_{tr}][C_{yr}(\alpha)r + C_{yp}(\alpha)p] + \Delta C_{y\beta^*}(\alpha,\beta) \\ & + C_{y\delta\Delta e}(\alpha,\delta_e)\delta_{\Delta e} + T_y/(\bar{q},\ S) \end{aligned} \tag{12}$$

$$C_z = -C_L(\alpha,\delta_e)\cos\alpha - C_D(\alpha,\delta_e)\sin\alpha + T_z/(\bar{q}\ S) \tag{13}$$

$$\begin{aligned} C_l = {} & C_{l\beta}(\alpha,|\beta|)\ \beta + C_{l\delta a}(\alpha,\delta_e)\ \delta_a + C_{l\delta r}(\alpha,|\delta_r|)\ \delta_r \\ & + [b/2V_{tr}][C_{lp}(\alpha)\ p + C_{lr}(\alpha)\ r] \\ & + C_{l\delta\Delta e}(\alpha,\delta_e)\ \delta_{\Delta e} + \Delta C_{l\beta}(\alpha,\beta) \\ & + [T_{zr}d_{Ty} - T_{zl}d_{Ty}]/(\bar{q}\ S\ b) \end{aligned} \tag{14}$$

$$\begin{aligned} C_m = {} & C_{mo}(\alpha,\delta_e) + [\bar{c}/(2\ V_{tr})]C_{mq}(\alpha)\ q \\ & + [T_x d_{Tz} - T_z d_{Tx}]/(\bar{q}\ S\ \bar{c}) \end{aligned} \tag{15}$$

$$\begin{aligned} C_n = {} & C_{n\beta}(\alpha,|\beta|,\delta_e)\ \beta + C_{n\delta a}(\alpha)\ \delta_a + C_{n\delta r}(\alpha,|\beta|,|\delta_r|,\delta_e)\ \delta_r \\ & + [b/2V_{tr}][C_{np}(\alpha)\ p + C_{nr}(\alpha)\ r] + C_{n\delta\Delta e}(\alpha,\delta_{\Delta e})\delta_{\Delta e} \\ & + \Delta C_{n\beta}(\alpha,\beta) + \Delta C_{n\beta^*}(\alpha,\beta) \\ & + [T_y d_{Tx} - T_{xr}d_{Ty} - T_{xl}d_{Ty}]/(\bar{q}\ S\ b). \end{aligned} \tag{16}$$

These coefficients are used in the equations of motion.

Equations of Motion

The equations of motion for an airplane are derived from Newton's Law

$$\bar{F} = M\bar{a} \tag{17}$$

$$\bar{N} = I\bar{\alpha} \tag{18}$$

where $\bar{a}$ is the aircraft translational acceleration, $\bar{\alpha}$ is the aircraft rotational acceleration, M is the aircraft mass, I is the aircraft rotational inertia tensor, and $\bar{F}$ and $\bar{N}$ are the forces and moments acting on the aircraft. The result is a twelfth order system. However, by making the following assumptions, rigid aircraft, constant air density, constant gravity, and a flat earth, and by transforming the force and moment equations from the inertial frame to a frame fixed to the aircraft, the equations of motion are reduced from order twelve to order nine. The aircraft state can be described by the nine state variables (α, β, p, q, r, θ, φ, ψ, V). If the xz plane is a plane of symmetry, the following equations are formed. Translational acceleration equations:

$$\dot{\alpha} = q + \left[-\left[\frac{\bar{q}\ S}{mV_{tr}} C_x - \frac{g}{V_{tr}} \sin\theta + r \sin\beta \right] \sin\alpha + \left[\frac{\bar{q}\ S}{mV_{tr}} C_z + \frac{g}{V_{tr}} \cos\theta \cos\phi - p \sin\beta \right] \cos\alpha \right] \sec\beta \tag{19}$$

$$\begin{aligned} \dot{\beta} = &- \left[\left[\frac{\bar{q}\ S}{mV_{tr}} C_x - \frac{g}{V_{tr}} \sin\theta \right] \sin\beta + r \right] \cos\alpha \\ &+ \left[\frac{\bar{q}\ S}{mV_{tr}} C_y + \frac{g}{V_{tr}} \cos\theta \sin\phi \right] \cos\beta \\ &- \left[\left[\frac{\bar{q}\ S}{mV_{tr}} C_z + \frac{g}{V_{tr}} \cos\theta \cos\phi \right] \sin\beta - p \right] \sin\alpha \end{aligned} \tag{20}$$

$$\dot{V}_{tr} = V_{tr} \left[\left[\frac{\bar{q}\ S}{mV_{tr}} C_x - \frac{g}{V_{tr}} \sin\theta \right] \cos\alpha \cos\beta \right.$$

$$+ \left[\frac{\bar{q}\ S}{mV_{tr}} C_y + \frac{g}{V_{tr}} \cos\theta \sin\phi \right] \sin\beta \tag{21}$$

$$\left. + \left[\frac{\bar{q}\ S}{mV_{tr}} C_z + \frac{g}{V_{tr}} \cos\theta \cos\phi \right] \sin\alpha \cos\beta \right].$$

Rotational acceleration equations:

$$\dot{p} = \left[- \left[\frac{I_z - I_y}{I_x} + \frac{I_{xz}^2}{I_x I_z} \right] qr + \left[1 - \frac{I_y - I_x}{I_z} \right] \frac{I_{xz}}{I_x} pq \right.$$

$$\left. + \frac{\bar{q}\ S\ b}{I_x} \left[C_l + \frac{I_{xz}}{I_z} C_n \right] \right] \cdot \left[1 - \frac{I_{xz}^2}{I_x I_z} \right]^{-1} \tag{22}$$

$$\dot{q} = \frac{\bar{q}\ S\ \bar{c}}{I_y} C_m + \frac{I_z - I_x}{I_y} pr + \frac{I_{xz}}{I_y} (r^2 - p^2) \tag{23}$$

$$\dot{r} = \left[\left[\frac{I_{xz}^2}{I_x I_z} - \frac{I_y - I_x}{I_z} \right] pq - \left[1 + \frac{I_z - I_y}{I_x} \right] \frac{I_{xz}}{I_z} qr \right.$$

$$\left. + \frac{\bar{q}\ S\ b}{I_z} \left[\frac{I_{xz}}{I_x} C_l + C_n \right] \right] \cdot \left[1 - \frac{I_{xz}^2}{I_x I_z} \right]^{-1}. \tag{24}$$

The aircraft orientation or Euler angle equations are:

$$\dot{\theta} = q\cos\phi - r\sin\phi \tag{25}$$

$$\dot{\phi} = p + (q\sin\phi + r\cos\phi)\tan\theta \tag{26}$$

$$\dot{\psi} = (q\sin\phi + r\cos\phi)\sec\theta. \tag{27}$$

The yaw angle is decoupled from the rest of the equations via the definition of the Euler angles. The aircraft is first rotated through the yaw axis, then the pitch axis and then the roll axis. The yaw rotation does not change the direction of the gravity vector since the z axis of the aircraft and earth are initially aligned. The result is an eighth order model without the $\dot{\psi}$ orientation equation. The above equations are in the form of Eqn (4) with the state vector $u = [\alpha, \beta, p, q, r, \theta, \phi, V]^T$ and the variable parameters $\lambda = [\delta_a, \delta_r, \delta_e, Tl, Tr, \delta_{pv}, \delta_{yv}]^T$. The purpose of this research is to find the solutions to this set of equations that satisfy Eqn (3).

Model Modifications

In addition to the modifications due to the thrust variables, one curve fit in the Baumann model was revised. Initial elevator sweeps of the Baumann model identified a loss of longitudinal stability at low angles of attack and then a regain of stability shortly later. This loss of stability did not match flight test data. The curve fits for the longitudinal aerodynamic coefficients were compared to the aero database to see if they were in error. The pitch damping derivative was identified as the cause of the problem. The curve fit of C_{mq} in Baumann's model was inaccurate at both low angles of attack and above 70 degrees. A new curve fit was developed to replace the incorrect equation for C_{mq}. Fig. 4-2 compares the original and modified curve fits for C_{mq} and also provides an idea as to how the aero data is modelled.

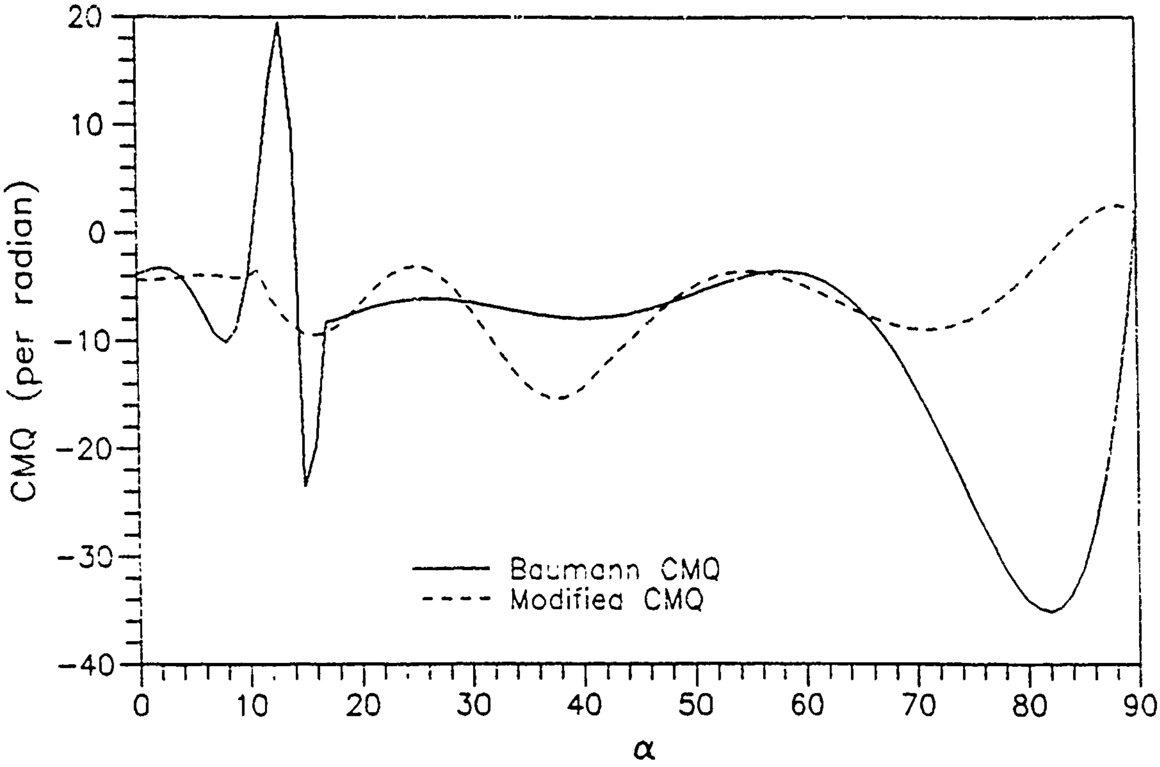

Figure 4-2 Comparison of the Revised and Baumann CMQ

V. Results

The main point of this research was to see the effects of thrust, thrust vectoring, and asymmetric thrust on the spin characteristics and spin recovery of the F-15. Therefore, a baseline of the global spin characteristics of the F-15 had to be established to compare the results against. The Baumann model was initially run, however some irregularities in the data at low alpha necessitated changes in the model. The model used in this research is a modified Baumann model. The new model is first compared to the old model to see the effects of the changes. The new model will then be further evaluated to define the global F-15 spin characteristics. Thrust levels will be varied to see how they affect these spin characteristics. Asymmetric thrust will be introduced to see if it can lead to spins and to see if it can be used to recover from flat spins. Finally, pitch and yaw thrust vectoring will be used to see how they can aid in the recovery from flat spins.

The general technique used in the investigation was to find the global effects of varying the parameter of interest, and then to concentrate on the stable flat spin regime. Additional bifurcation diagrams were developed from a starting point in the stable flat spin region. Time histories are shown in some cases to provide a better understanding of the F-15's behavior.

Comparison with Unmodified Model

The first run in this research was an elevator sweep from a starting point calculated by Baumann (6:32-34). Baumann used a thrust setting of 8300 lbf in his research because it is the thrust setting for trim conditions at 0.6 Mach and 20,000 feet (6:19). The $\alpha-\delta_e$ bifurcation diagram from this elevator sweep indicated a small area of instability bounded by Hopf points at a fairly low angle of attack. As discussed earlier, an incorrect curve fit for C_{mq} was identified as the cause of the instability and also showed that the original curve fit did not represent the high angle of attack data. A new curve fit was found for C_{mq} and was incorporated into the model. Again an elevator sweep was run from the original starting point. The $\alpha-\delta_e$ bifurcation diagram for the modified model did not have the small unstable area. A comparison of the Baumann and modified model in the high α regime was then accomplished using a rudder sweep from a starting point near full elevator deflection. The original elevator sweep did not continue into the spin region and therefore Baumann found that rudder sweeps can be used to reach this area (6:47). Since the new curve for C_{mq} is not as stable in pitch damping at high angles of attack as the old model (see Fig. 4-2), the new model should show a smaller region of stability in the spin region. The $\alpha-\delta_r$ bifurcation diagram of the unmodified model (Fig. 5-1) shows a small region of stable spins with full elevator deflection. The $\alpha-\delta_r$ diagram using the new model (Fig. 5-2) shows the same tracing of equilibrium solutions as Fig. 5-1. However, the stable portion of the branch is no longer present. This matches the expected results that the equilibrium would be less stable. A stable limit-cycle may exist in the modified model in the vicinity of the stable area of the unmodified model. However, the rudder sweep was not able to find these limit cycles because there are no Hopf points present. With full elevator deflection, the new model is similar to the unmodified model except for the loss of the stable spin branch.

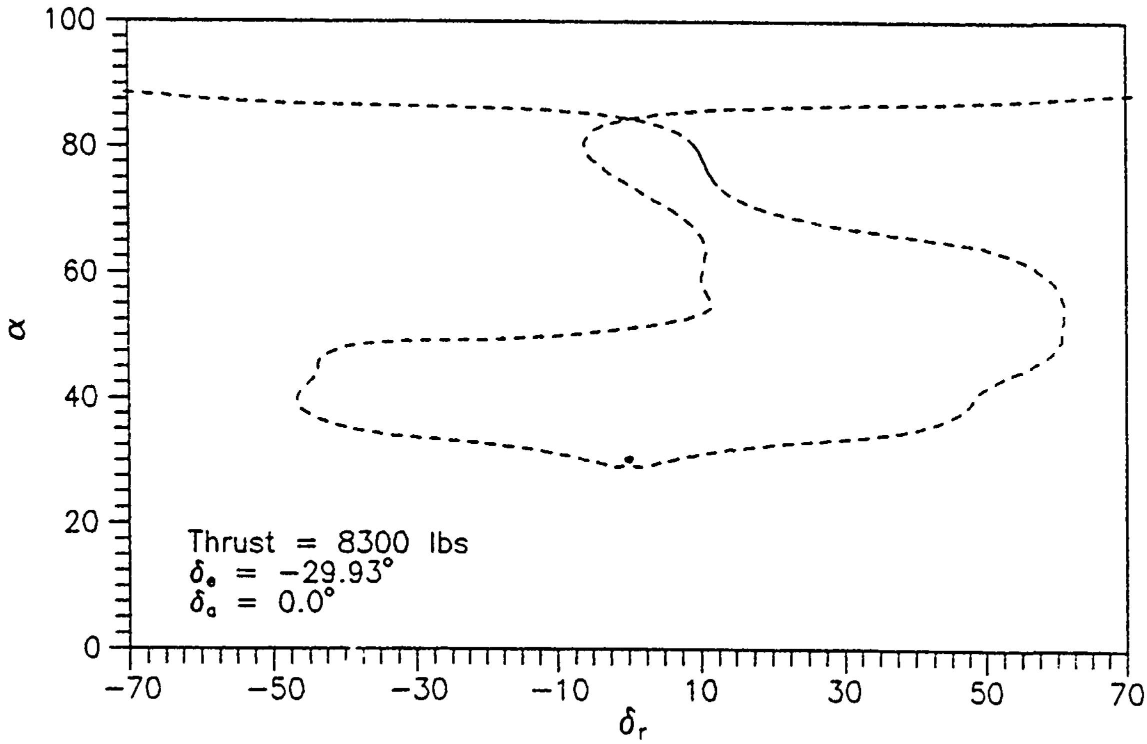

Figure 5-1 Baumann Model Rudder Sweep

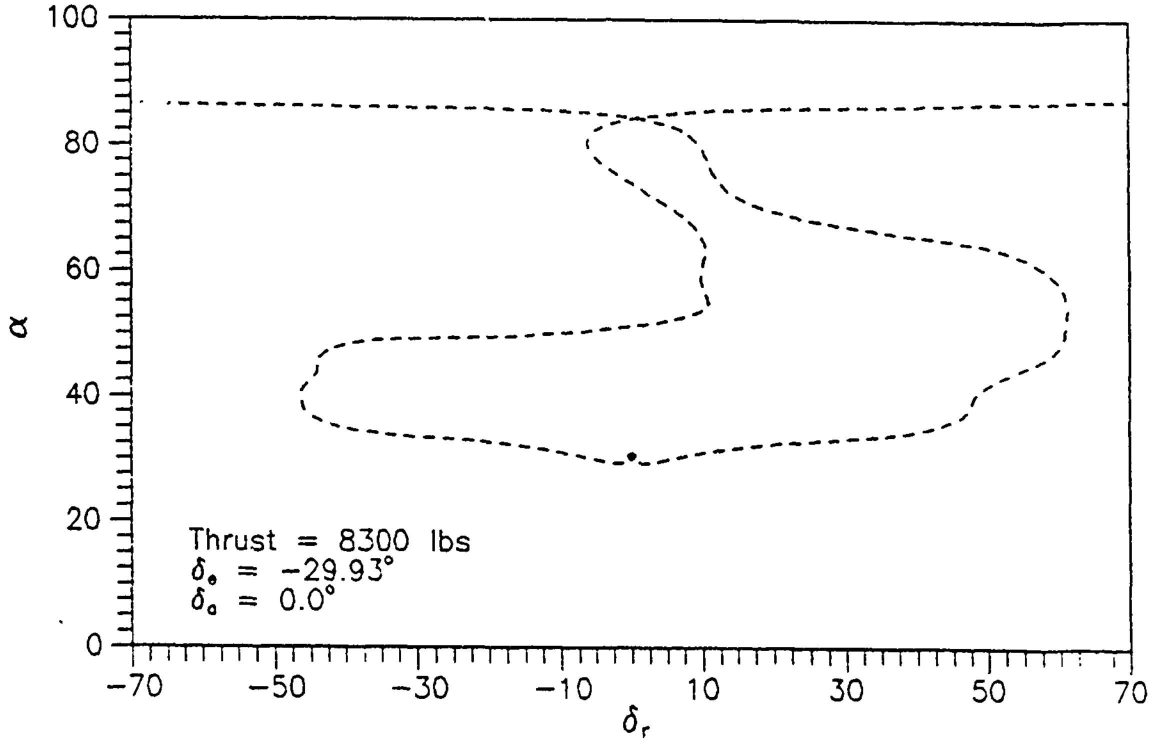

Figure 5-2 Revised Model Rudder Sweep

Baseline Model Spin Characteristics

The previous comparison was done by holding the elevator and ailerons constant and varying the rudder. This introduces asymmetries into the airplane aerodynamics by varying the rudder. A different method of producing bifurcation diagrams is to hold neutral rudder and aileron and vary the elevator. This method provides a global view of the F-15 longitudinal motion in a symmetric configuration as a function of elevator deflection. Any asymmetries identified would therefore be the result of aerodynamic asymmetries and not the result of rudder or aileron inputs. Rudder sweeps are still necessary, however, to provide starting points for high angle of attack branches. Fig. 5-3 is the baseline

$\alpha-\delta_e$ bifurcation diagram of the F-15B for a thrust level of 8300 lbf. This diagram shows only the equilibrium solutions found between the F-15 elevator deflection limits. The entire continuation diagram can be found in Appendix C, Fig. C-1.

Several equilibrium branches are identified in Fig. 5-3. The low angle of attack stable branch loses stability at δ_e = -19.3 degrees and identifies the onset of wing rock. The unstable branches at alpha = 36 degrees and between alpha = 40 degrees and 50 degrees identify spirals. The branch found between alpha = 64 degrees and 84 degrees is the spin branch. It contains both stable and unstable equilibrium and limit-cycle solutions. The stable portion of the branch between δ_e = -21.4 degrees and -15.4 degrees identifies a stable right spin. It is bounded by stable limit-cycles that eventually become unstable. The unstable equilibrium branch connected to the stable branch has a maximum value of the unstable eigenvalue equal to $0.10683 \pm 2.4174i$ at δ_e = 0 degrees. This is important since the positive eigenvalue is a small number. This means that the loss of stability along the branch will most likely not be an immediate event (i.e. long transient). The small stable region at δ_e = -25 degrees identifies a stable left spin. It gains stability via a turning point and loses stability via a Hopf bifurcation and with stable limit-cycles. The larger area of right

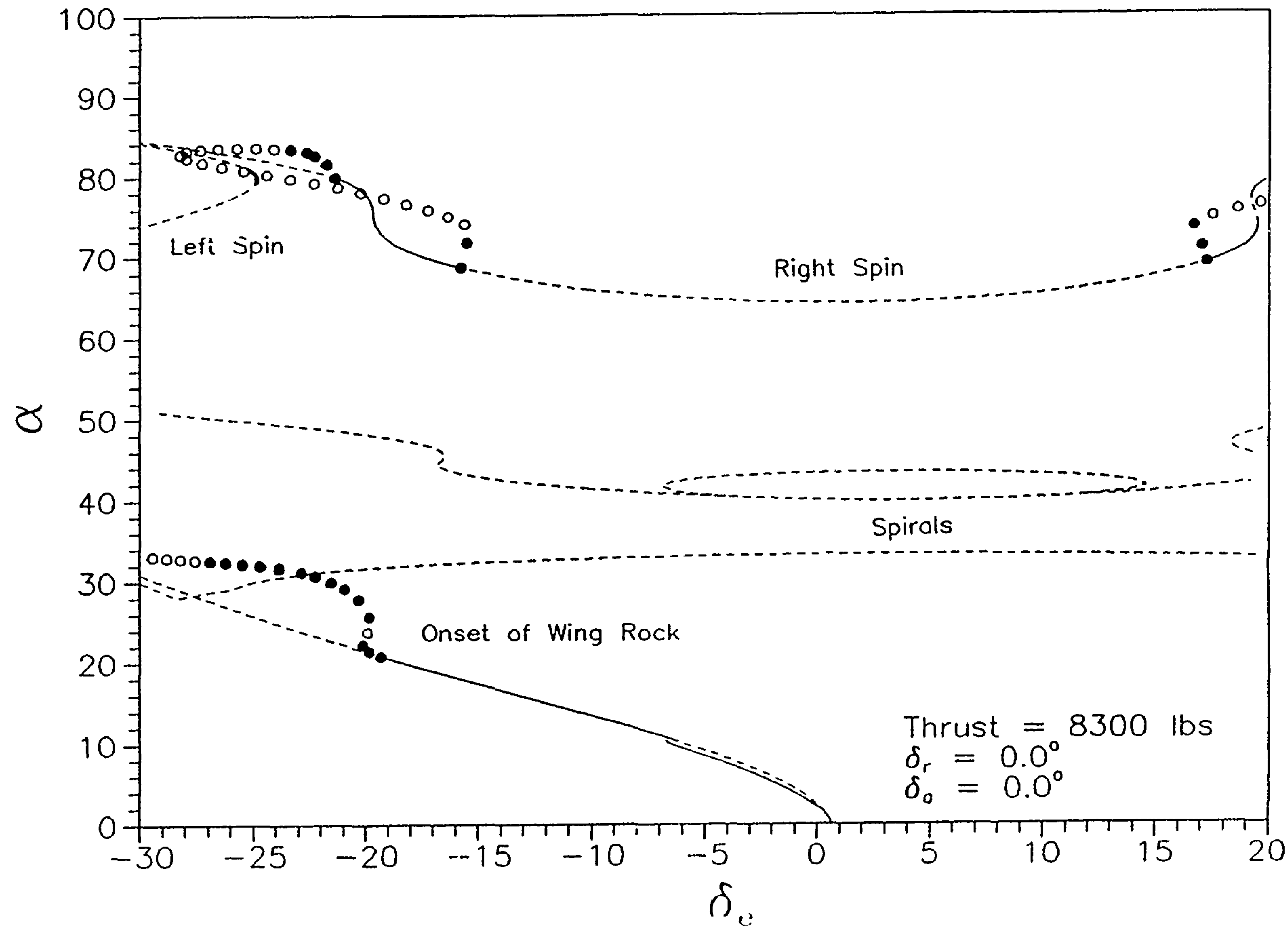

Figure 5-3 Revised Model Elevator Sweep

spin with symmetric controls can be explained by the asymmetric yawing moment above alpha = 40 degrees (22:3.4). The asymmetry favors a right yaw and therefore, a larger right spin region. Of additional interest is that the stable spin branch lies directly above point were wing rock begins. The F-15 could theoretically encounter wing rock and then jump to the stable spin branch.

The F-15 flight manual recommends several methods to recover from spins (34:6-7). The highly oscillatory spin can be recovered by neutralizing the controls. Stable flat spins can be recovered by applying aileron in the direction of the spin. As discussed earlier, by applying aileron in the direction of the spin, a cross coupling inertia effect acts in the direction opposite the yaw. The manual also states that rudder deflection in either direction has little effect on spin recovery. This was also discussed earlier and is a result of the rudder being washed out by the wake off the wings and fuselage. These recovery techniques were applied in a simulation of the stable flat spin at δ_e = -19.14 degrees to see if the model corresponds to actual flight behavior. The selection of δ_e = -19.14 degrees as a starting point is motivated by the fact that it is near the center of the stable branch and corresponds to the onset of wing rock at low α. This starting point will be used in many of the bifurcation diagrams in the following sections.

Fig. 5-4 shows the α - time simulation using elevator for recovery. If the elevator is neutralized, the F-15 will enter an oscillatory spin at a lower angle of attack. If the elevator is deflected to a negative full deflection, the F-15 enters an oscillatory spin at a higher angle of attack. The F-15 will not recover from the flat spin in a reasonable time using elevator alone. Comparing Fig. 5-4 to Fig. 5-3, the oscillatory spins begin at the Hopf points bounding the stable region. These oscillations are centered on the unstable equilibrium branches and can be classified as unstable oscillations because they continue to grow.

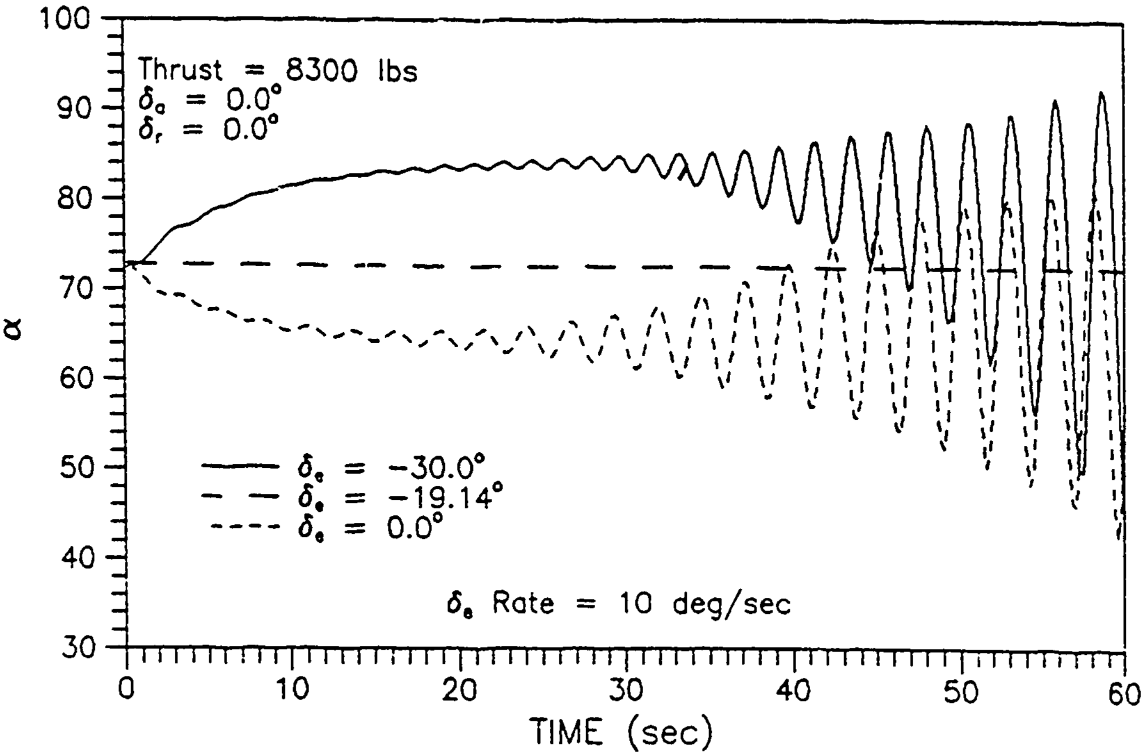

Figure 5-4 Simulation of Spin Recovery Using Elevator

Fig. 5-5 is the simulation using rudder for recovery. A fully deflected antispin rudder recovers the F-15 to wing rock in 13 seconds. A fully deflected prospin rudder drives the F-15 into an unstable oscillatory spin that recovers the F-15 to wing rock in 55 seconds. In a real world situation the F-15 would not have 55 seconds to recover from a flat spin, however this diagram is valuable in revealing the true nature of the oscillatory spin as being unstable. The effectiveness of the rudder to recover from a flat spin in this simulation is contrary to the statement in the F-15 flight manual.

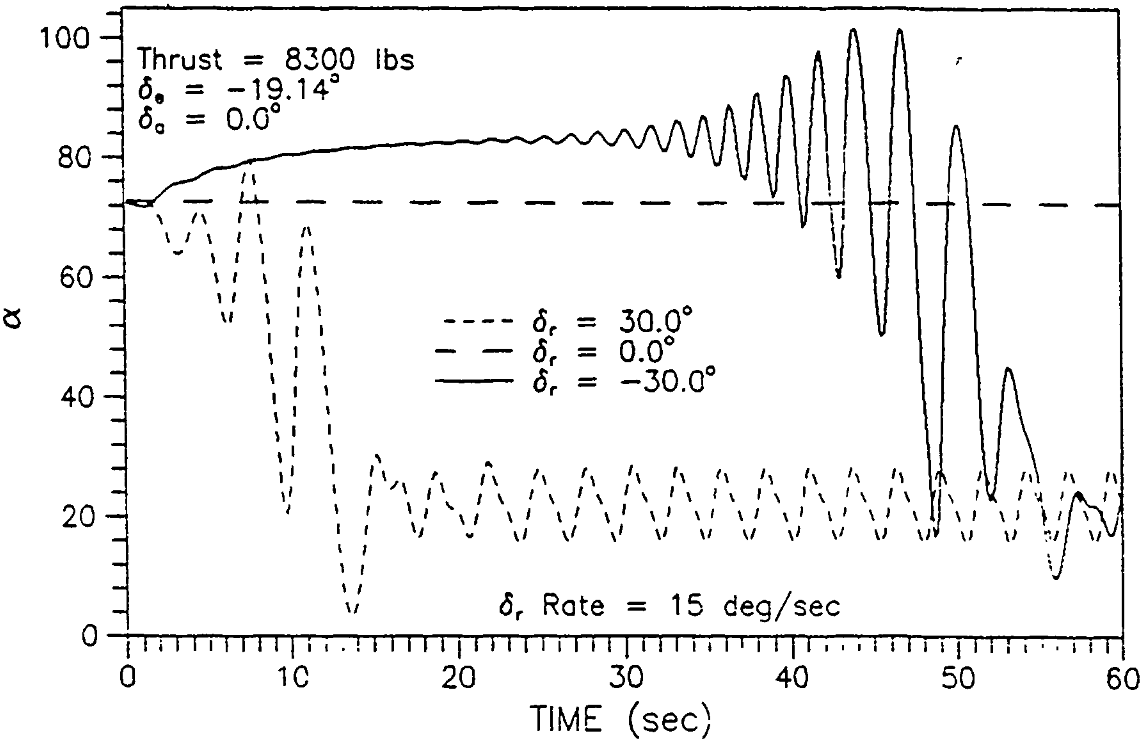

Figure 5-5 Simulation of Spin Recovery Using Rudder

Fig. 5-6 is the recovery attempt using ailerons. Aileron in the direction of the spin actually increase the angle of attack of the spin while aileron opposite the spin reduces the angle of attack. The F-15 should not be able to recover using ailerons alone. The results of this simulation are also contrary to the statements in the F-15 flight manual, at least for δ_e = -19.14 degrees and a thrust level of 8300 lbs.

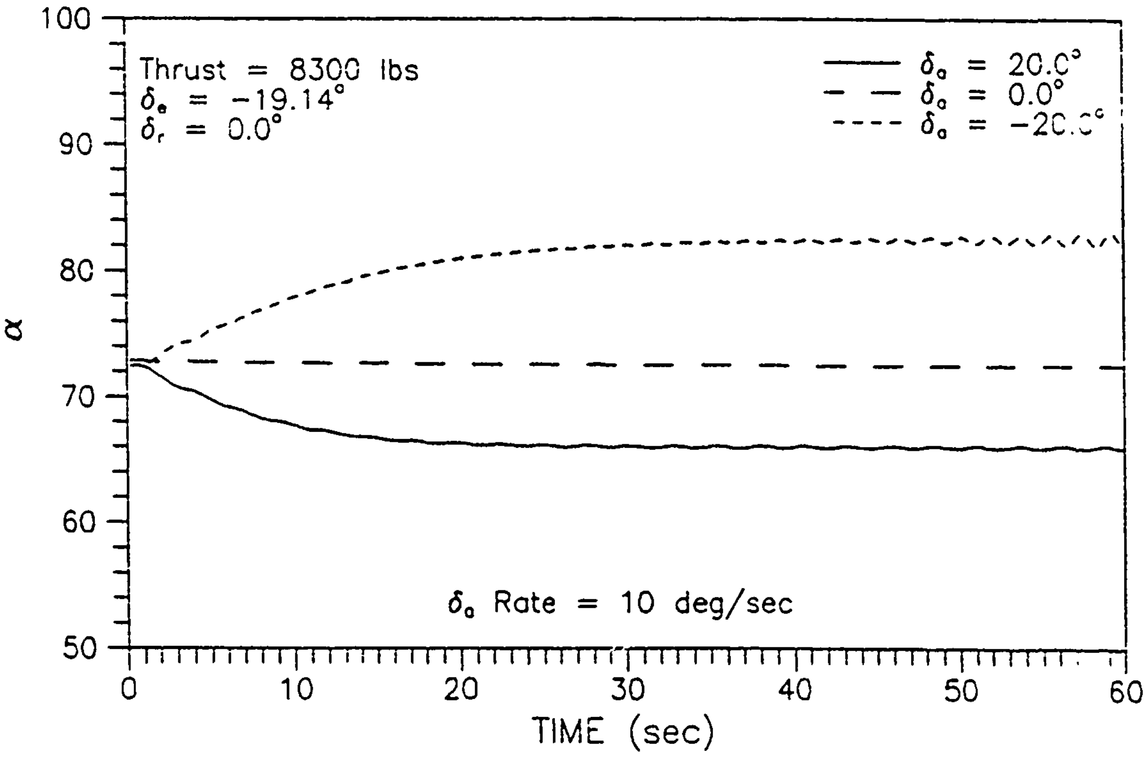

Figure 5-6 Simulation of Spin Recovery Using Ailerons

These discrepancies were investigated by looking at the equations for the aero coefficients due to the aileron and rudder deflections and seeing if they were the cause. The equations of motion were double checked to see if they were correct. Possible cross coupling effects were investigated by looking at the stable spin angular velocities.

The rudder effectiveness is caused by the curve fit for $C_{n\delta r}$. The curve fit is dependent on δ_r, α, β, and δ_e with generally any value of β and negative values of δ_e increasing the rudder effectiveness at high α. Unfortunately, the curve fit makes the rudder deflections twice as effective at large negative values of δ_e than aerodynamic data indicates. Therefore, the model is somewhat inaccurate in the effects of rudder at high angles of attack. The starting points used for the continuation of the high angle of attack branches for the α - δ_e bifurcation diagram are still accurate since at these points the rudder in undeflected.

The ineffectiveness of the ailerons can be explained as a cross coupling effect in the model. Table 1 shows the values of p, q, and r in the stable spin regime for δ_e = -19.14 degrees.

Table I. Stable Spin Angular Velocities

p rad/sec	q rad/sec	r rad/sec
0.6119	-0.0874	1.932

Since $I_x - I_y$ for the F-15 is negative, it couples with a positive p, and negative q to drive the yaw rate - see Eqn (1). Therefore, in the right flat spin region being investigated, prospin aileron deflections are not effective in recovering from the spin and actually drive the yaw rate. Deflections opposite the spin can slow the spin rate, however, there is not enough control authority to completely stop it. This anomaly is therefore a consequence of the spin characteristics and not a problem with the model.

Since the main investigation in this research is thrust effects, the discrepancy due to rudder and aileron is noted but will not be further investigated. The model will be kept in a symmetric δ_r, δ_a configuration during investigation of the thrust effects and therefore these discrepancies will not enter into the rest of the results. The coupling effects will be important during pitch vectoring, and will be discussed more in that section.

Throttling

The effects of varying the thrust level in the model are discussed next. First, throttling was run from the original level of 8300 lbf to see how the model reacted at low angles of attack. The elevator deflection was set at -19.14 degrees with neutral rudder and ailerons. The α - T bifurcation diagram is shown in Fig. 5-7. The diagram is interesting in that α does not change with thrust until the thrust to weight ratio approaches one. At 37,000 lbs thrust, the diagram hits a wall and shoots to α = 90 degrees. For thrust to weight ratios greater than 1, the model is in a constant acceleration and there could be no solutions that would satisfy Eqn (3). From this diagram, however, two starting points were picked to continue up to high angles of attack using rudder sweeps.

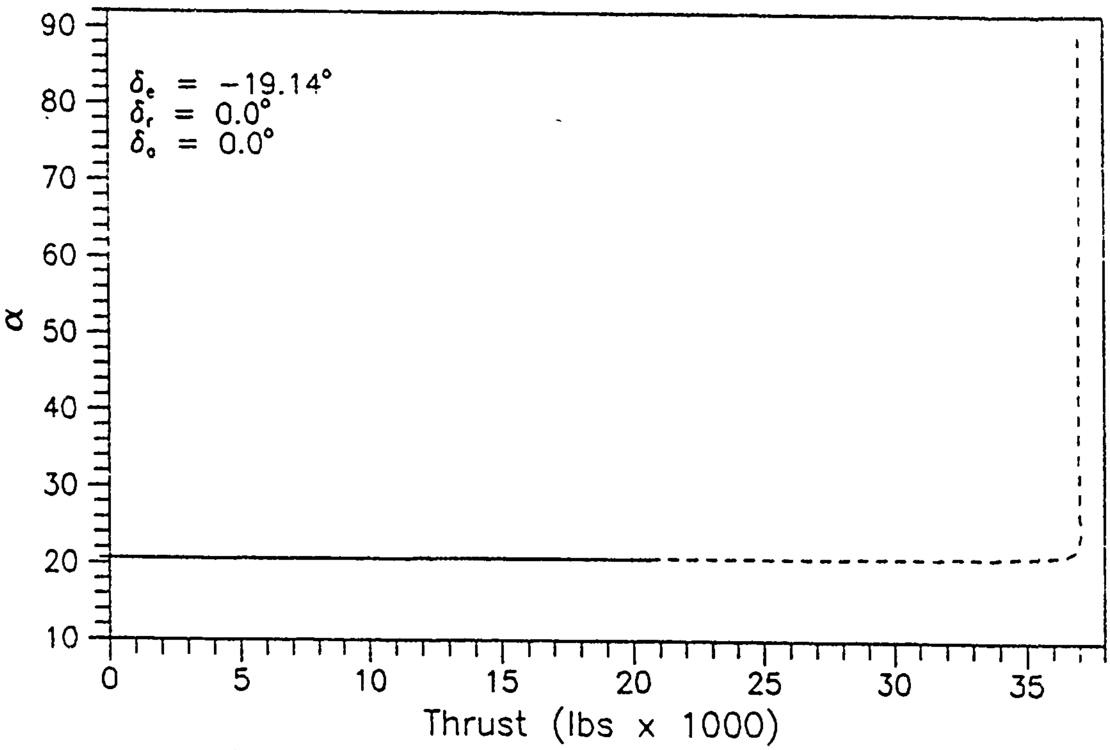

Figure 5-7 Low Alpha Engine Throttling

The two values selected for continuation were 0 lbf and 29200 lbf. The zero thrust value was picked to show a base-line of the spin region with no thrust. The thrust value of 29200 lbf was selected since it is close to the full military power rating (non-afterburning) of the PW F-100 engines. Rudder sweeps were again used to provide high angle of attack starting points for the elevator sweeps. The longitudinal motion, symmetric spin characteristics were then found by doing elevator sweeps with the thrust held at 0 lbf (Fig. 5-8) and at 29200 lbf (Fig. 5-9). The full continuation diagrams of these elevator sweeps can be found in Appendix C.

Comparing the three elevator sweeps for different thrust levels (Figs. 5-3, 5-8, and 5-9) the stable right spin branch decreases in size with thrust. This result can be partly attributed to a nose up moment due to thrust. The engines are located below the aircraft's center of gravity and therefore a pitch-up moment accompanies increases in thrust. This increases the value of q and the cross coupling effect of q and r would bring about an antispin moment. A better understanding of this phenomenon is achieved by creating a bifurcation diagram of α - T from a starting point in the stable spin region. Fig. 5-10 shows that thrust decreases the angle of attack and eventually produces limit cycle behavior with high thrust levels, however it will not bring the plane out of the spin. A simulation was run to show this effect and is shown in Fig. 5-11. The limit cycle behavior becomes apparent in this time history, and as expected, the airplane remains in a

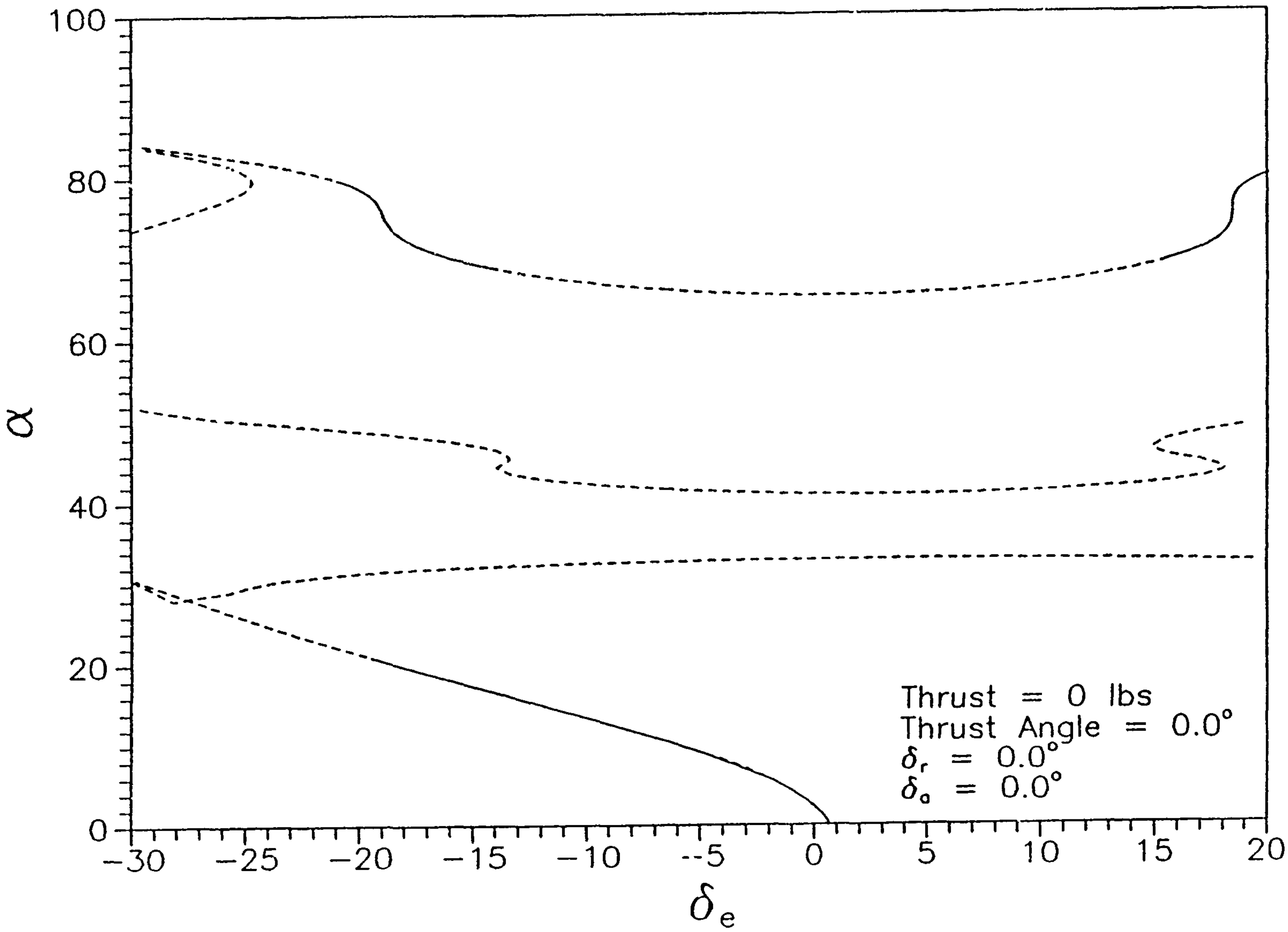

Figure 5-8 Elevator Sweep with Thrust = 0 Pounds

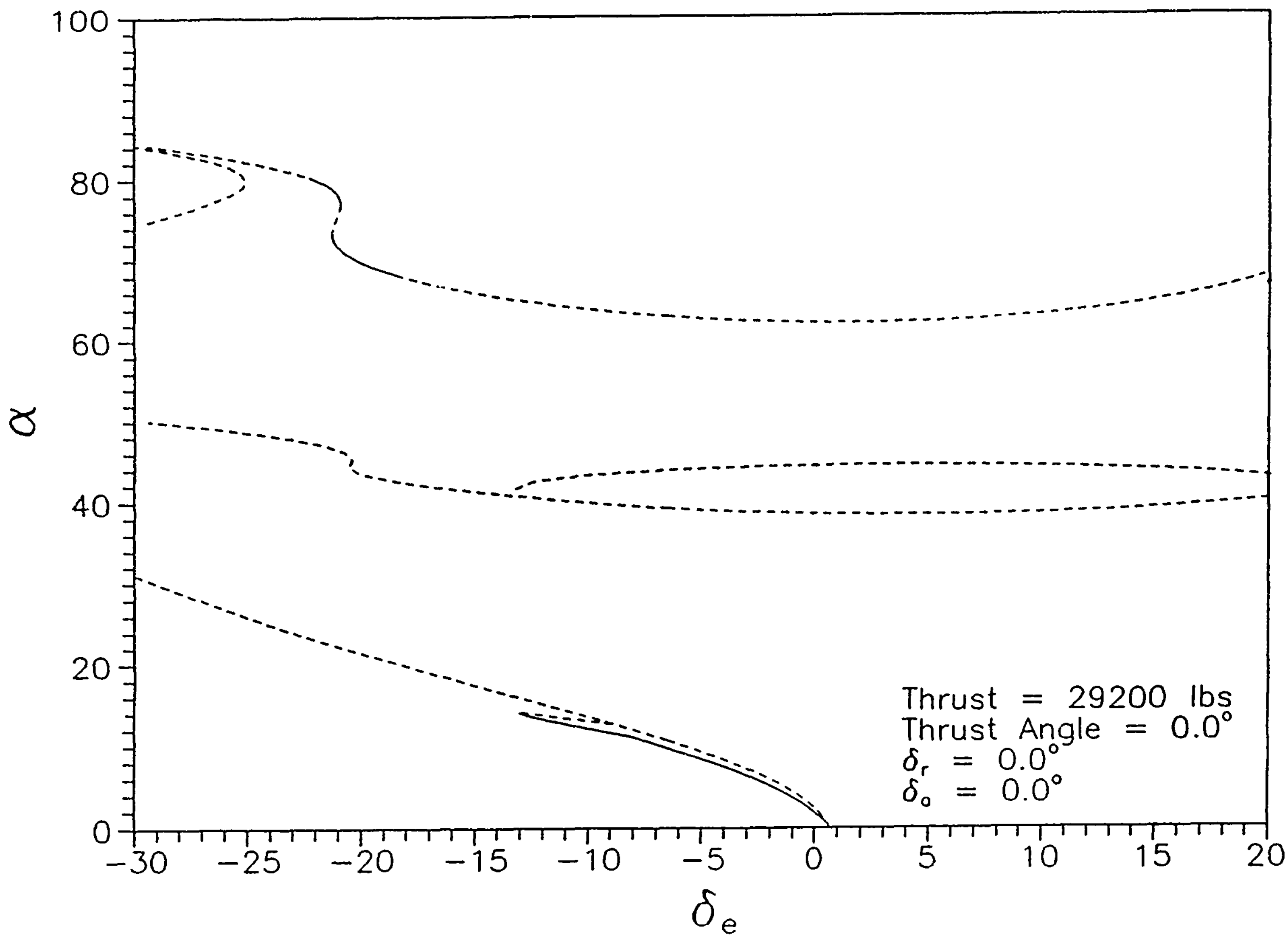

Figure 5-9 Elevator Sweep with Thrust = 29200 pounds

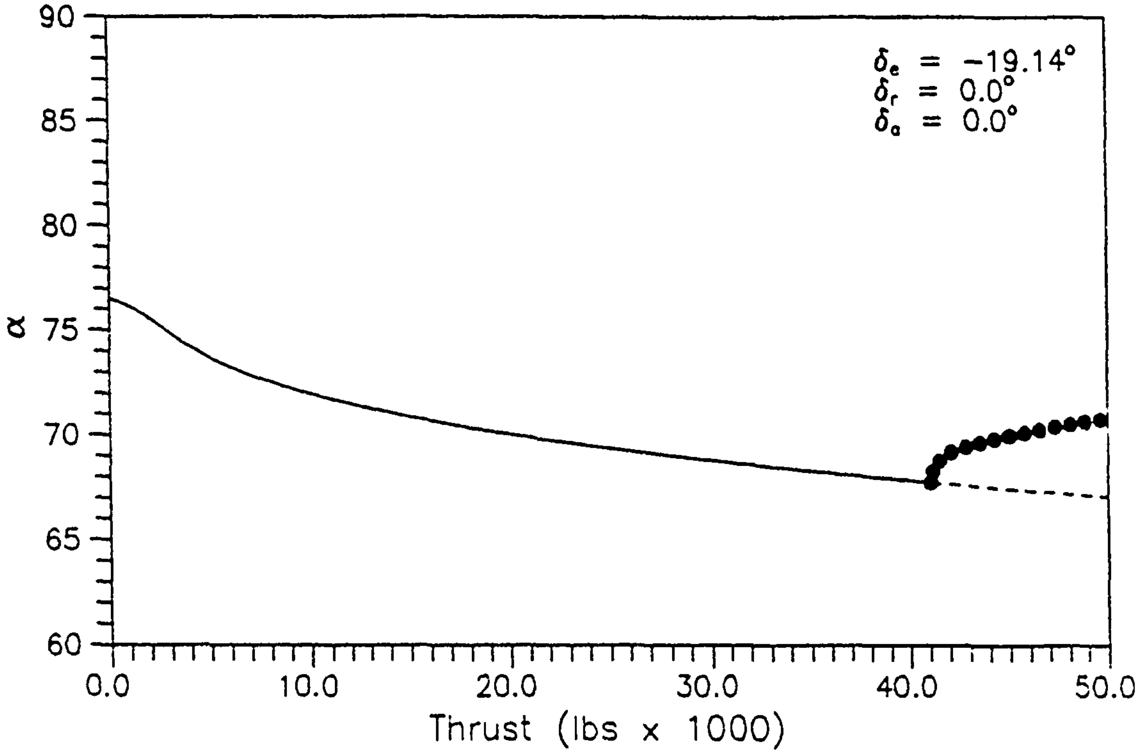

Figure 5-10 Throttling During Flat Spin

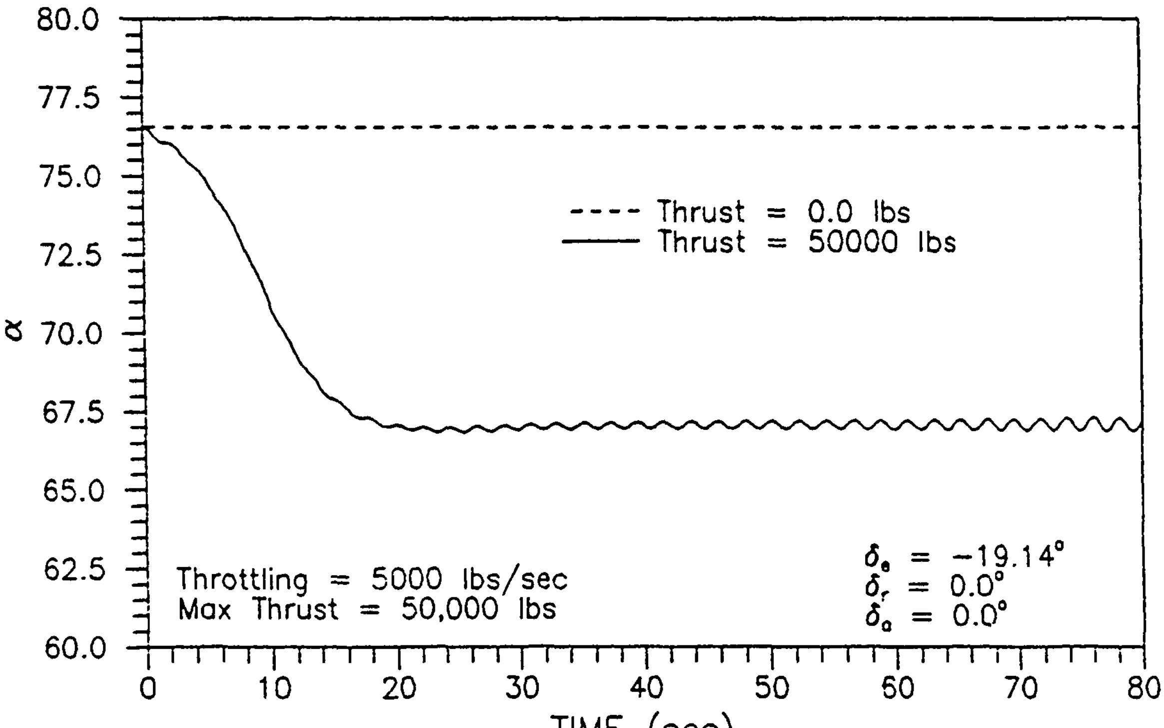

Figure 5-11 Simulation of Throttling in a Flat Spin

mildly oscillatory spin.

For an F-15, higher thrust levels produce spin regions with smaller stable branches. Additionally, higher thrust levels produce spins at lower angles of attack for a given elevator deflection. These effects can aid in the recovery from spins, however, used alone increasing thrust cannot bring the F-15 out of a spin. Grafton (13) came to this same conclusion in her research. She determined that thrust effects are generally small, but have a generally favorable effect on the number of turns required to recover from a relatively nonoscillatory spin.

Asymmetric Thrust

The F-15 has the capability of providing direct yaw moments by using asymmetric thrust. In a spin, the engines can theoretically be throttled to provide an antispin moment. In real world situations, asymmetric thrust usually occurs through the inadvertent flameout of one engine. Both of these cases will be looked at to see how asymmetric thrust can lead to spins, and to see how it can be used to recover from them.

Starting from a low angle of attack equilibrium state and a thrust of 8300 lbs, each engine was throttled and α - T bifurcation diagrams were examined. Figs. 5-12 and 5-13 show that the equilibrium branch continued to the high angle of attack regime through the application of both negative and positive thrust. The negative thrust is unrealistic but does provide a pathway to high α solutions in realistic asymmetric thrust regions. The low angle of attack branch remains stable throughout the range of asymmetries and therefore, jumps to the spin region via limit points should not be expected due to asymmetric thrust alone. A large perturbation may push the F-15 away from the stable branch and cause an attraction to the stable high α solutions. Fig. 5-12 contains a large region of stable equilibria between α = 68 degrees and 80 degrees and identifies a right flat spin. This corresponds to the large region of stable right spin found in the symmetric bifurcation diagrams. In this region, $T_l > T_r$ and a positive yaw moment results. The positive yaw moment drives the plane into the right spin. A left spin branch is also present for an asymmetry of $T_r > T_l$ but contains no stable branch. This branch corresponds to the left spin found in the symmetric bifurcation diagrams. Fig. 5-13 mirrors Fig. 5-12 but also identifies a small stable left spin branch at T_l = -1000 lbf. Although this thrust setting is unrealistic in the real world, it shows that an asymmetry of around 5000 lbf should be able to produce a stable left flat spin. The two figures also identify a small intermediate stable spin region between α = 50 degrees and 58 degrees that is bounded by Hopf points.

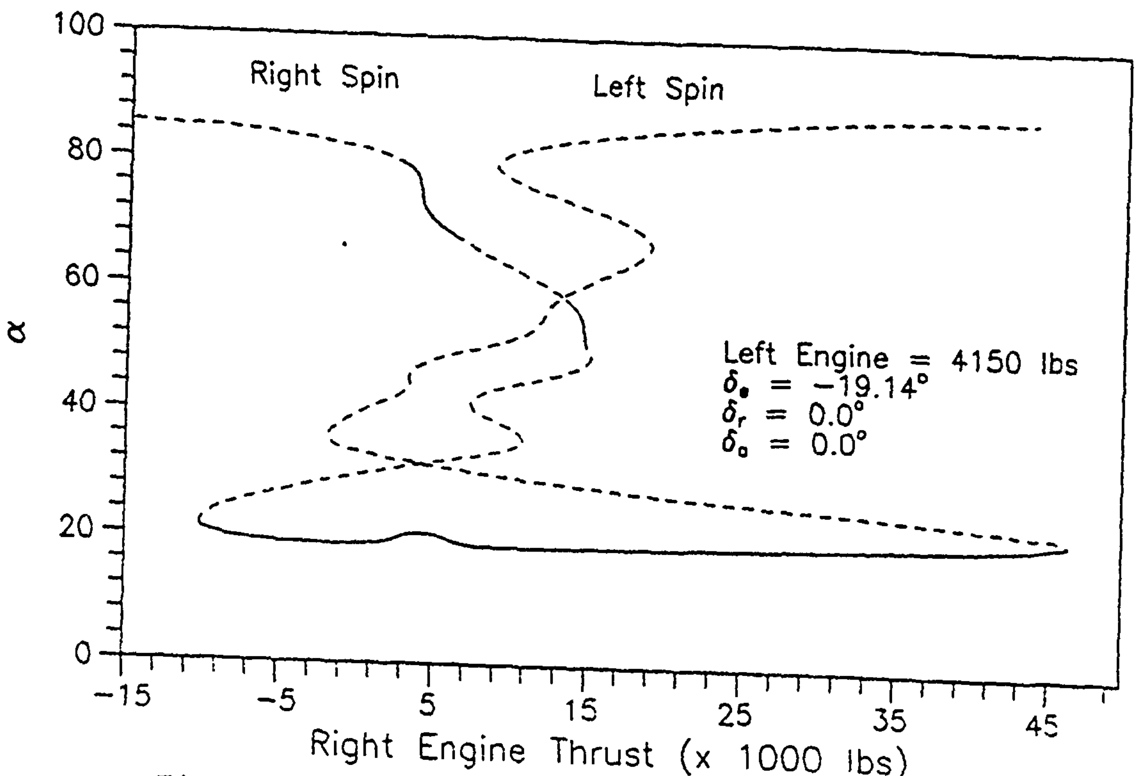

Figure 5-12 Right Engine Asymmetric Thrust

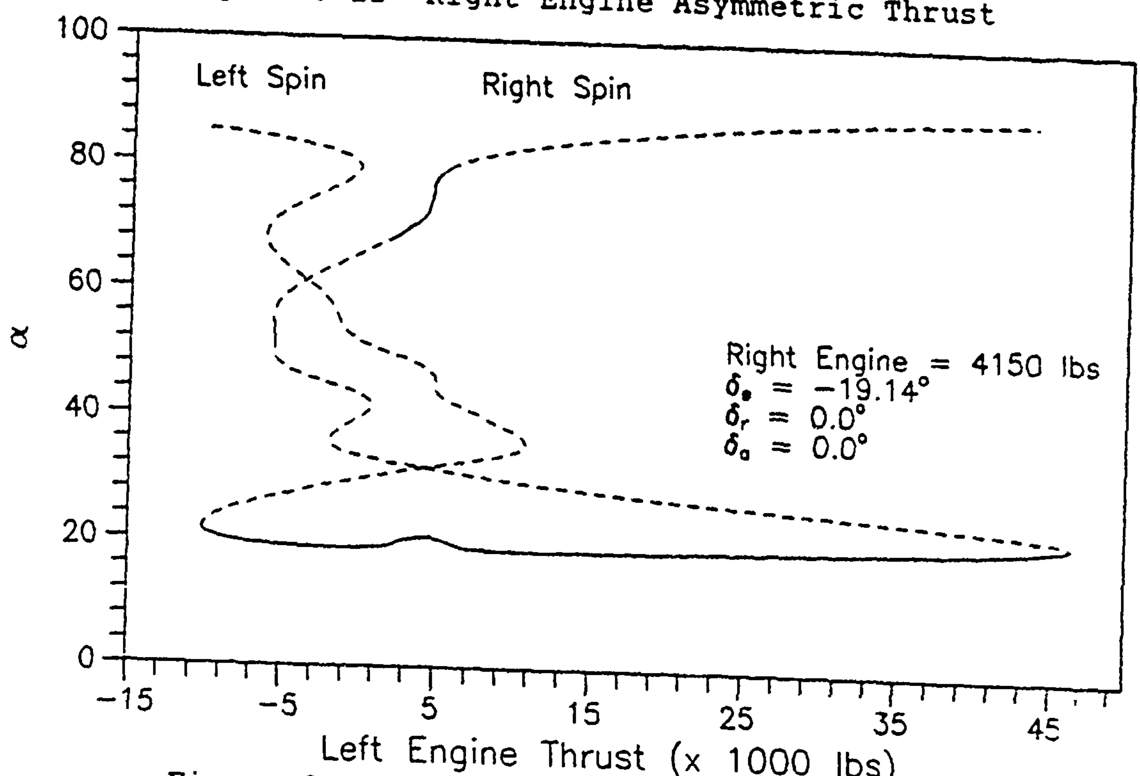

Figure 5-13 Left Engine Asymmetric Thrust

Analysis of the effects of asymmetric thrust due to a flameout were done using elevator sweeps for both right and left engine flameouts from an initial thrust of 8300 lbf. Figs. 5-14 and 5-15 are the $\alpha-\delta_e$ bifurcation diagrams of a right engine flameout and a left engine flameout. The full continuation diagrams can be found in Appendix C. At low angles of attack, the onset of wing rock is actually delayed by the engine flameout. Thus, the likelihood of the F-15 jumping to the spin branch from wing rock is not increased by an engine flameout. However, Fig 5-14 shows a large stable spin region extending from δ_e = -15 degrees to δ_e = 13 degrees. The branch loses stability through Hopf bifurcations at both ends. The positive yawing moment due to the thrust asymmetry creates a much larger stable right spin branch at higher values of δ_e than the symmetric α - δ_e bifurcation diagram. Additionally, the small left spin branch virtually vanishes from the diagram. Fig. 5-15 should produce an opposite effect. The stable right spin branch stretches from δ_e = -26.5 degrees to δ_e = -22 degrees which is smaller and at lower values of δ_e than the symmetric diagrams. The left spin branch also becomes more prevalent. Thus, engine flameouts can be either helpful or harmful, depending on the direction of spin and the engine that flames out.

The yawing moment provided by a thrust asymmetry can be

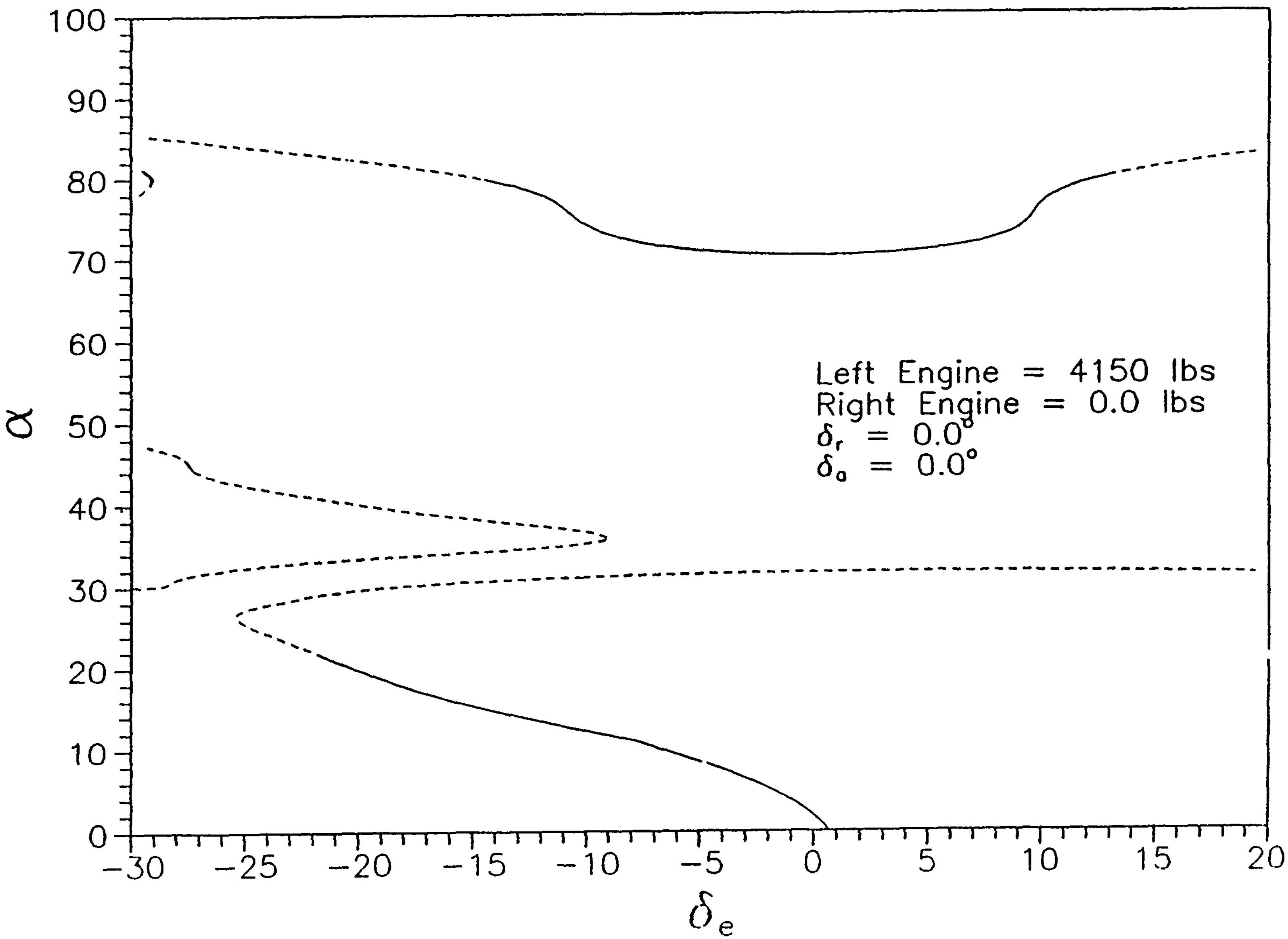

Figure 5-14 Elevator Sweep with Right Engine = 0 Lbs

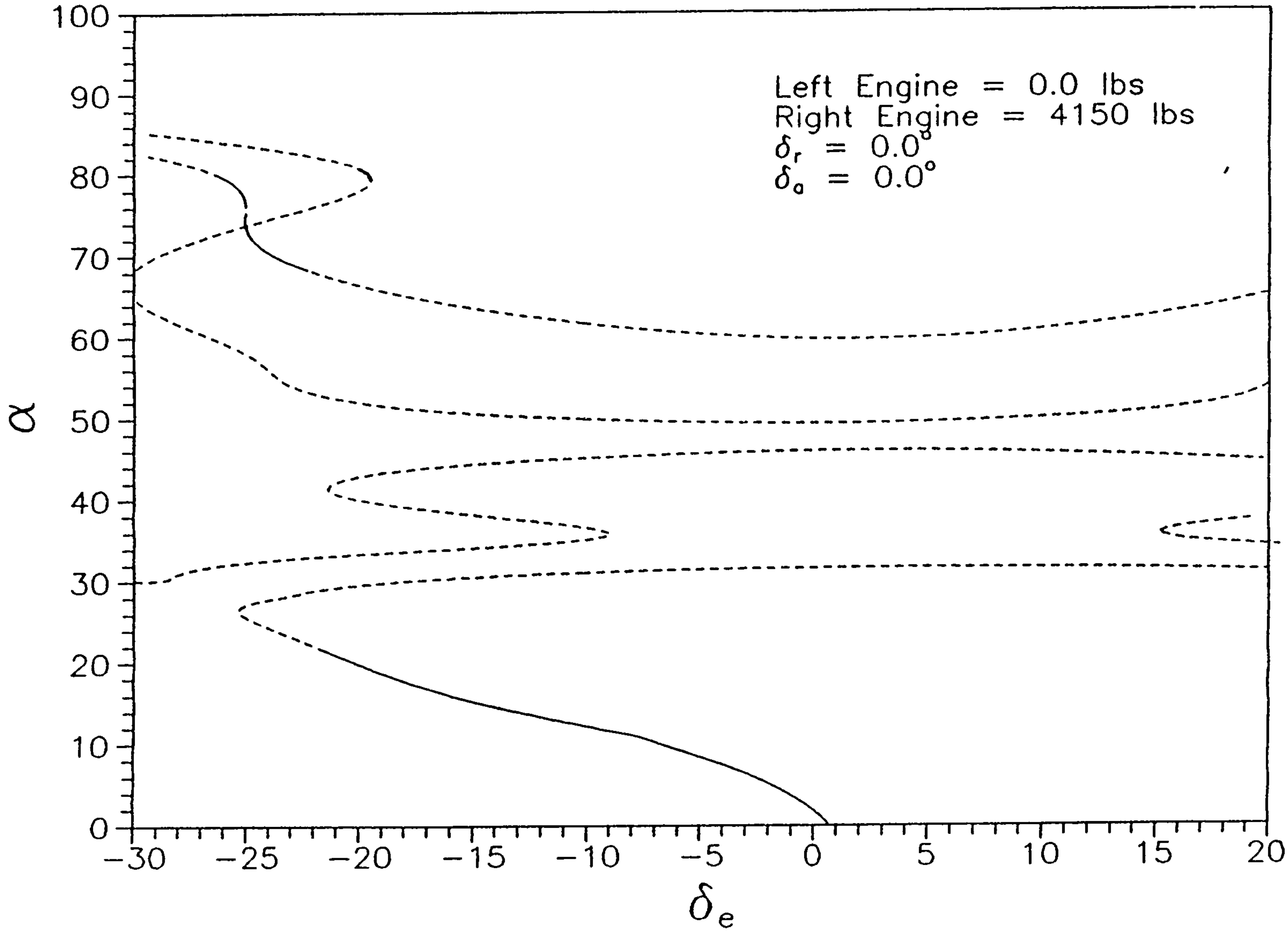

Figure 5-15 Elevator Sweep with Left Engine = 0 Lbs

used to recover from spins. Looking back at Fig. 5-12, the equilibrium branch turns back when the right engine thrust is greater than 15000 pounds. Any setting greater than 15000 lbs. "should" bring the F-15 right back to the stable low angle of attack equilibrium. A simulation was run to see the time history of two imposed asymmetries. The time history shows that the plane enters a unstable limit cycle for a thrust setting of 12000 lbf. A full right engine thrust setting of 25,000 lbf was then tried in the simulation. Fig. 5-16 shows that using the higher thrust asymmetry, the F-15 pushes through the limit cycle and recovers to the low angle of attack stable equilibrium.

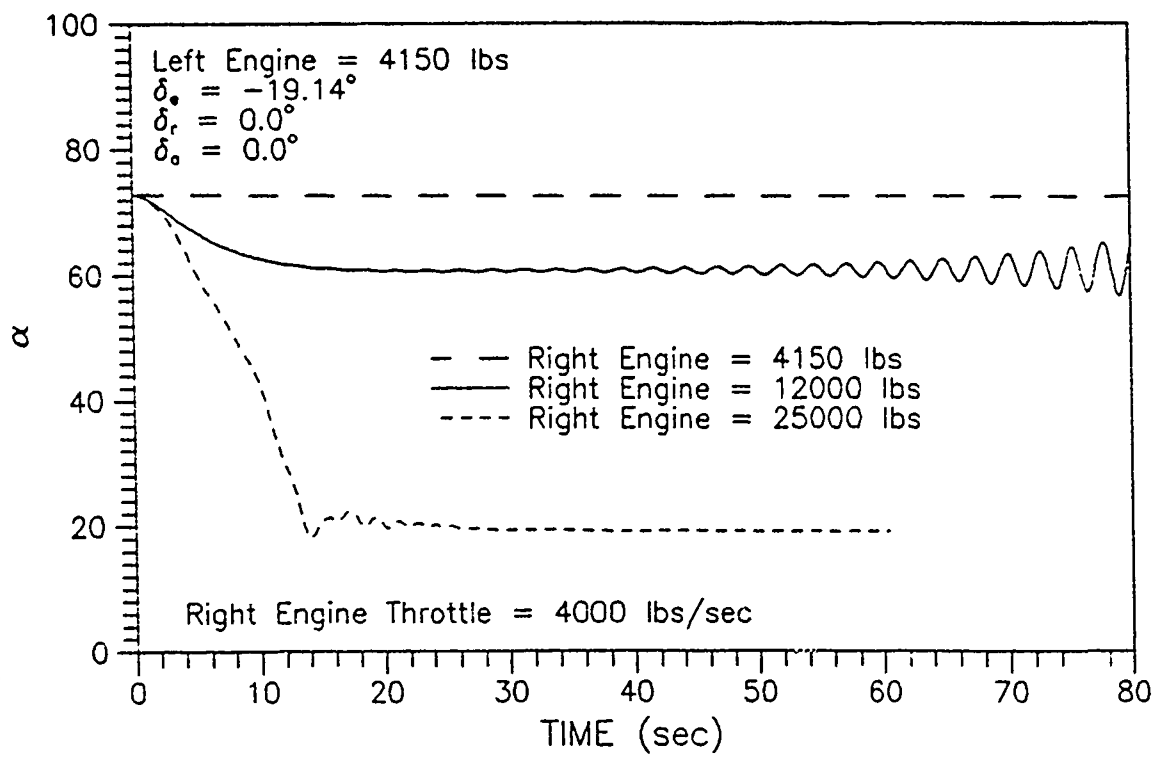

Figure 5-16 Asymmetric Thrust Spin Recovery

This recovery is in a timeframe that could realistically recover the F-15 from the spin (13 seconds).

Asymmetric thrust settings can aid in recovering from spins, however, the same asymmetries that can aid the recovery, can make recovery more difficult if the wrong engine flames out in the spin.

Thrust Vectoring

The capability to vector thrust on an F-15 is currently available only on the F-15 STOL demonstrator. This aircraft has modified nozzles to provide pitch vectoring, but no yaw vectoring capability exists. Pitch and yaw vectoring will be investigated to see how they can influence spin recoveries if a baseline F-15 were fitted with pitch or yaw vectoring nozzles.

Pitch Vectoring

Pitch vectoring can be thought of as an automatic elevator, providing the pilot the capability to control the pitch rate with the engine. The pitch moment created by vectoring the engine exhaust is dependent on the engine thrust and the angle of vectoring. Additionally, vectoring the thrust decreases the force in the x direction and changes the forces in the z direction. The effects of pitch vectoring in aiding the recovery from spins are expected to be small, since the moment produced will not oppose the large yaw angular momentum. Some coupling effects will possibly be helpful in aiding the recovery and the nose down moment should lower the angle of attack and make the aerodynamic controls more effective. Additionally, a nose up moment could produce a deeper flat spin.

An α - δ_{pv} bifurcation diagram was created for each of two different thrust levels (8300 lbs and 29200 lbs) starting from δ_e = -19.14 degrees in the stable right flat spin region. Figs. 5-17 and 5-18 show that a nose down pitching moment ($\delta_{pv} < 0$) will cause the F-15 to remain at approximately the same angle of attack, while a nose up pitching moment ($\delta_{pv} > 0$) will bring about higher angles of attack. The nose down moment will also bring about a loss of stability through a Hopf bifurcation. The higher thrust level will cause the limit cycles to appear at a much lower pitch vector angle. The lower angle of attack and loss of stability could possibly lead to recovery. Additionally, limit cycle behavior appears in the nose up pitch vector for 29200 lbs. These diagrams were not very helpful in trying to understand the dynamics of the pitch vectoring, so additional diagrams plotting p, q, and r versus δ_{pv} were made. Figs. 5-19 and 5-20 show that coupling occurs due to the pitch vectoring. The p - q coupling was mentioned in previous discussions as the cause of the δ_a anomaly. Since p is positive and q is negative, the coupling term drives r

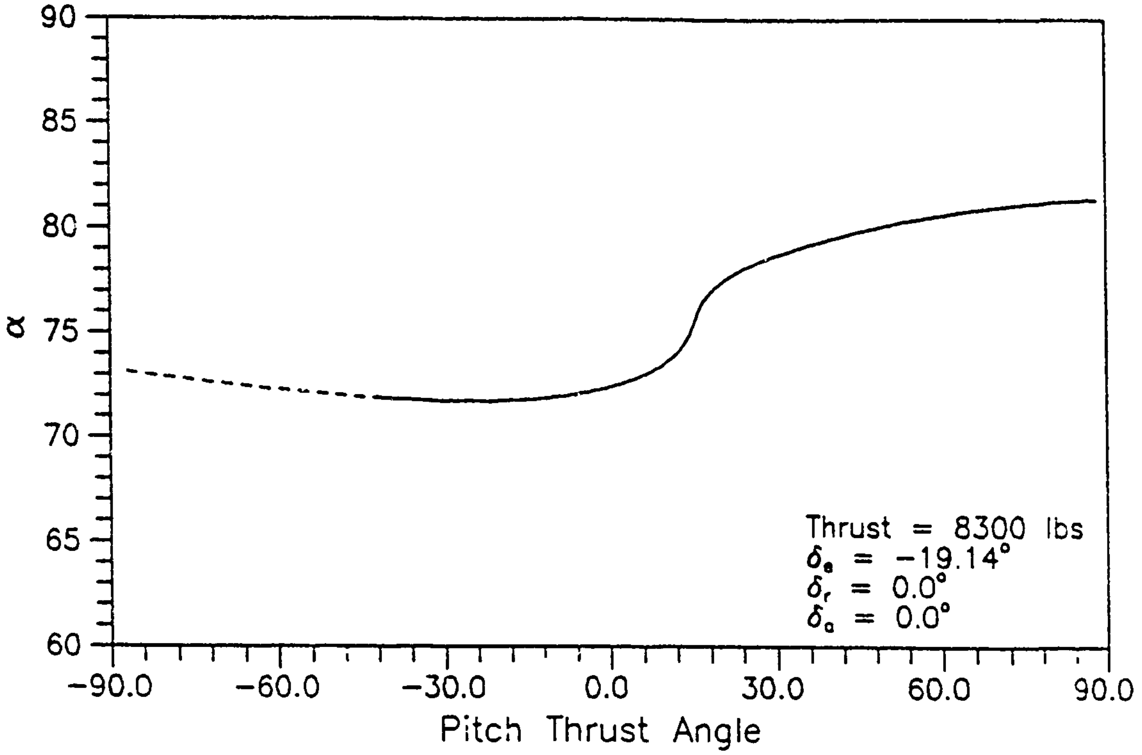

Figure 5-17 Flat Spin Pitch Vectoring, T = 8300 lbs

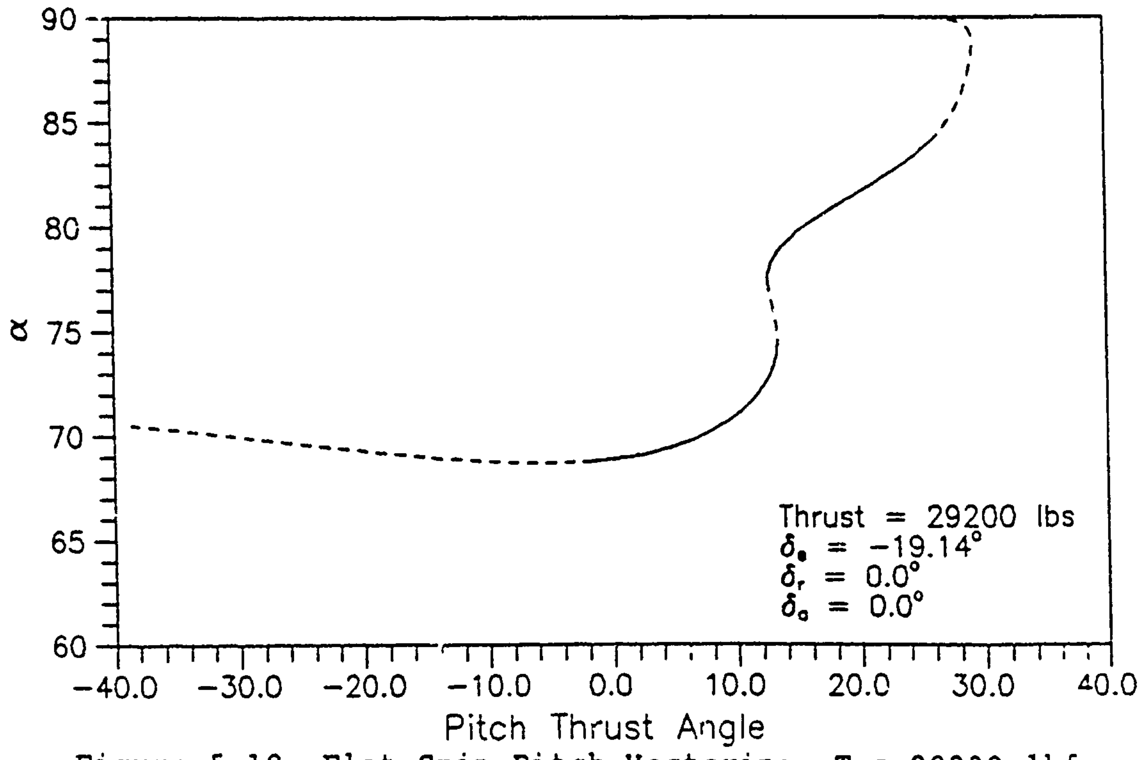

Figure 5-18 Flat Spin Pitch Vectoring, T = 29200 lbf

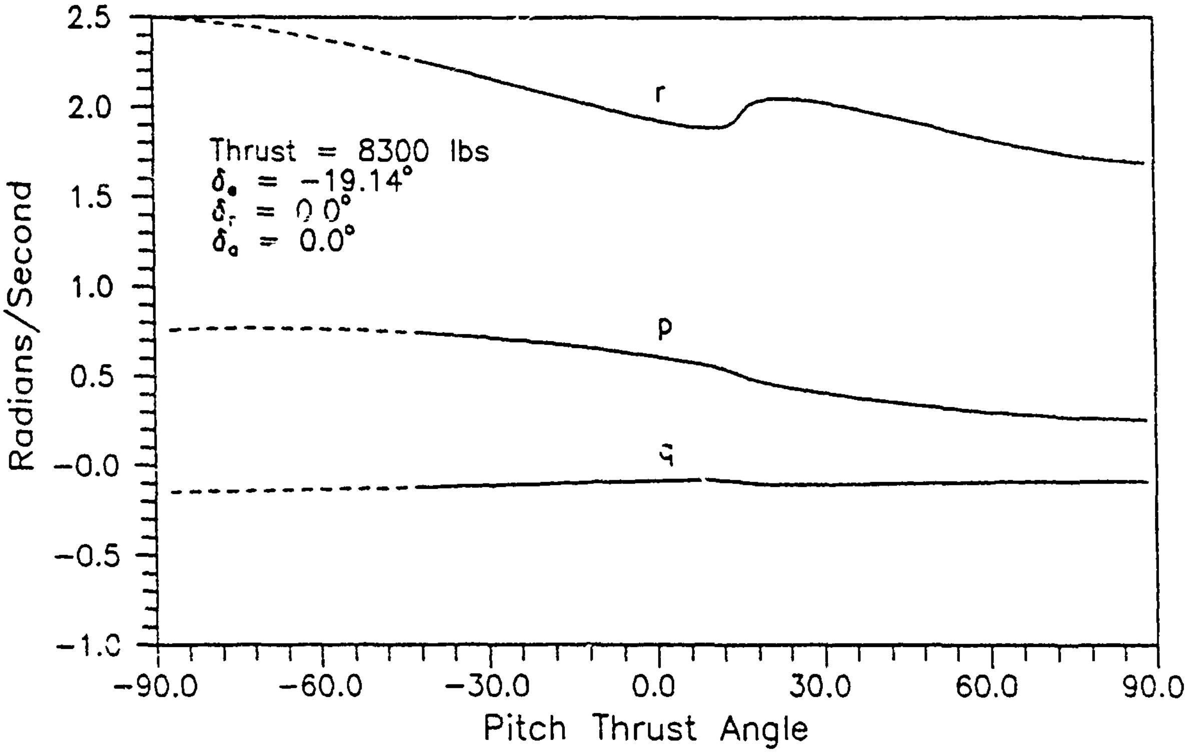

Figure 5-19 Angular Velocities, Pitch Vect, T = 8300 lbf

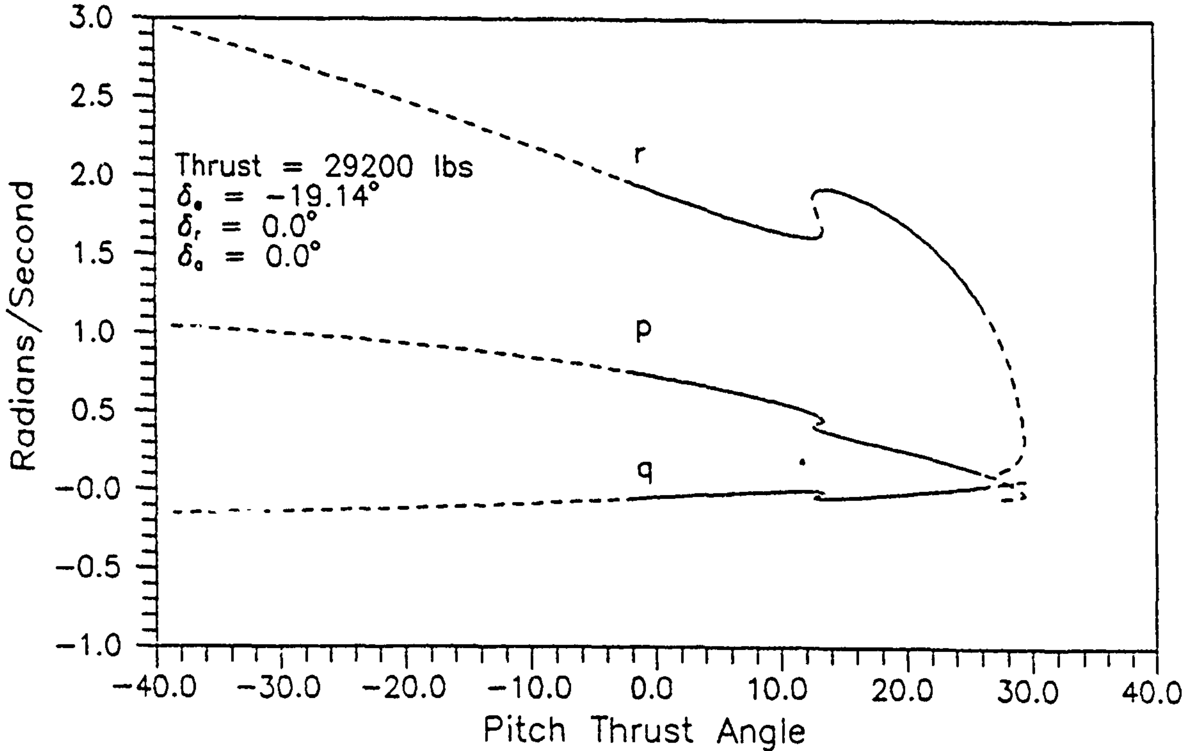

Figure 5-20 Angular Velocities, Pitch Vect, T = 29200 lbf

into the spin direction. If either term changed signs, the coupling would provide an antispin term in $\dot{r}$ and possibly recover the F-15 from the spin. Nose down pitch vectoring actually causes q to become more negative and drives the prospin yaw rate even higher. A nose up pitch vector brings q closer to zero and in the case of Fig. 5-20 actually makes q positive. With the positive q, an antispin coupling results and the F-15 should recover from the spin. This is not intuitive to a pilot since the usual procedure for spin recovery is to release back pressure on the stick which in turn causes a nose down pitching moment. A simulation was run to see if in fact this coupling takes place. Fig. 5-21 doesn't show that a nose up moment will promote the recovery from a spin since the angle of attack remains around 90 degrees. Although Fig. 5-21 shows that the F-15 remains at 90 degrees, Fig. 5-22 qualifies this by showing that all yaw rotation stops. The F-15 is in a deep stall that can be recovered by vectoring the nozzle the other direction. Applying nose down pitch vectoring as an initial command actually increases the yaw rate and produces an oscillatory spin. Again, in the real world an F-15 wouldn't have 60 seconds to recover from a flat spin, but these simulations do show that a nose up pitch vector can theoretically bring about a recovery. Pitch vectoring is therefore useful in recovering the F-15 from spins but not in an intuitive way.

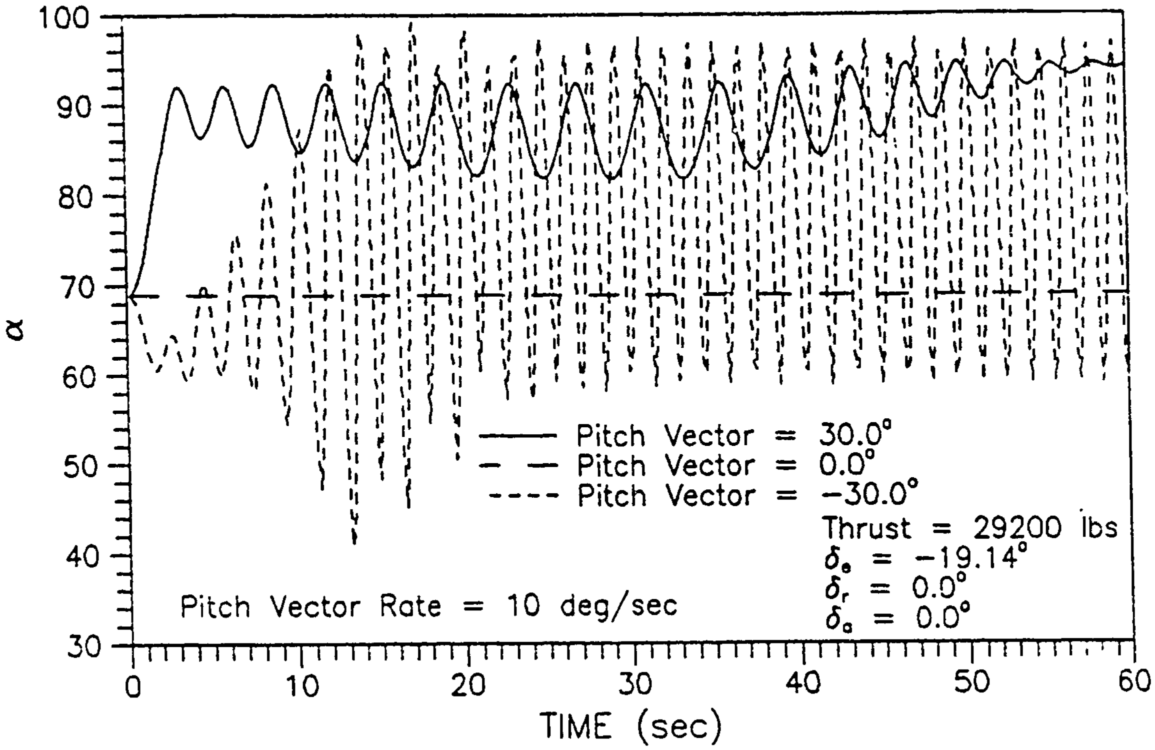

Figure 5-21 Simulation of Pitch Vectoring in a Flat Spin

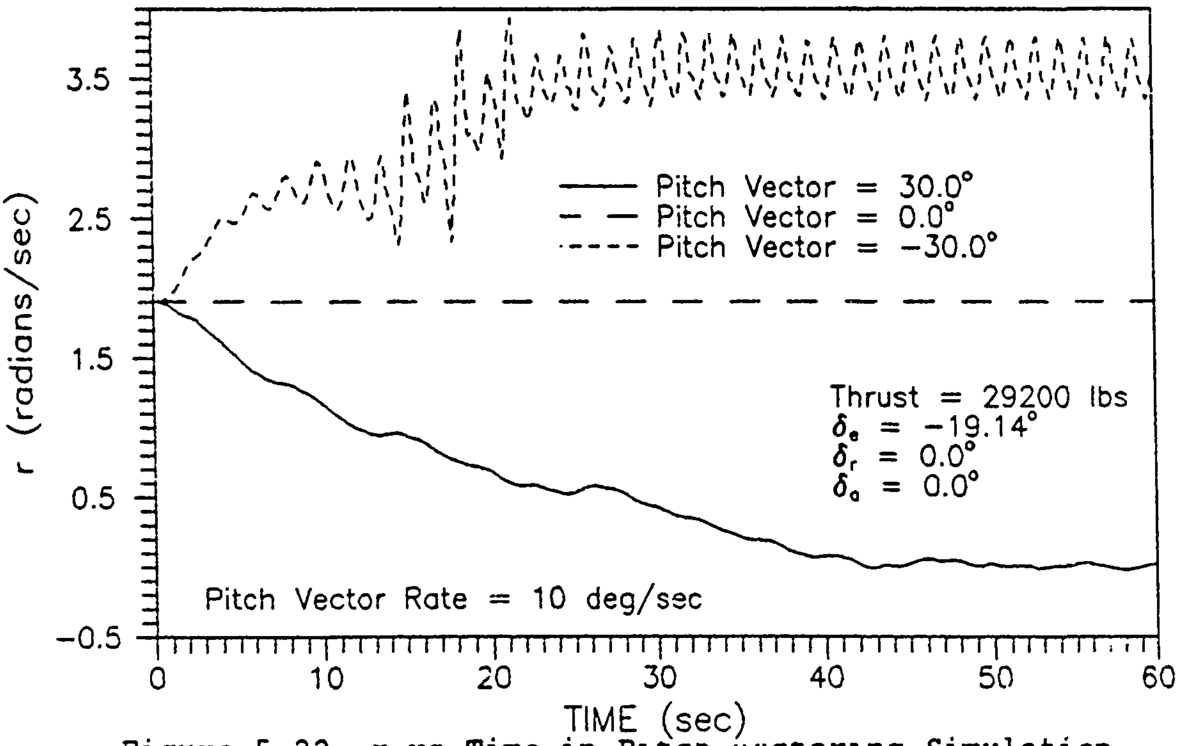

Figure 5-22 r vs Time in Pitch Vectoring Simulation

Yaw Vectoring

Yaw vectoring can also be thought of as an automatic control, providing the pilot control of the yaw moments with the engines. With yaw vectoring, the capability exists to directly oppose the angular momentum in a spin. Thus, yaw vectoring is expected to be the most effective use of thrust to recover from a spin. The effectiveness of yaw vectoring to recover from a spin is directly proportional to the thrust level and the angle of deflection. At low thrust levels, the moment created by vectoring the thrust may be small, even with a large vectoring angle. At high thrust levels, only a small angle may be necessary to recover from the spin.

The global effect of yaw vectoring was found by starting at a low angle of attack equilibrium point and varying the yaw angle for two thrust settings. Figs. 5-23 and 5-24 are the α - δ_{yv} bifurcation diagrams. The diagrams continue up to the high angle of attack regime where both left and right spin branches are found. Looking at the low angle of attack solutions, the equilibrium solutions reach a turning point at a relatively small yaw vector. The F-15 may depart controlled flight at the limit point and jump to the spin branch directly above it. Thus, yaw vectoring capabilities can be dangerous at low angl-s of attack.

Looking at the high α branches, the branch with the large stable portion is the right spin branch. Since a right spin is the only possible spin in this diagram for an undeflected flow, it will be the main topic of discussion. Both diagrams show that an antispin yaw vector ($\delta_{yv} > 0$) will drive the F-15 out of the stable spin and into an oscillatory spin at the Hopf bifurcation. Further yaw vectoring will bring the F-15 to the previously identified small stable branch at $\alpha = 50$ degrees. This is surrounded by additional limit cycles. With enough yaw vectoring, the F-15 will eventually make it through the limit cycles and down to the stable low α equilibrium branch. A prospin yaw vector will drive the F-15 into a deeper, oscillatory flat spin. Although the diagrams are fairly similar in structure, the amount of vectoring necessary to drive the F-15 out of the spin is much less with higher thrust levels. A simulation was run to see how yaw vectoring can bring the F-15 out of the spin. Fig. 5-25 shows that for a small yaw vector (5 degrees), the F-15 begins to oscillate around the Hopf point discussed earlier and eventually is attracted to the low α stable branch. With a 10 degree yaw vector, the F-15 is driven straight down to the low α stable branch. An even larger yaw vector of 20 degrees brings the F-15 down to the low α stable branch even faster, however, without correction, the F-15 will enter a spin in the opposite direction. Looking back at Fig. 5-23 verifies that this

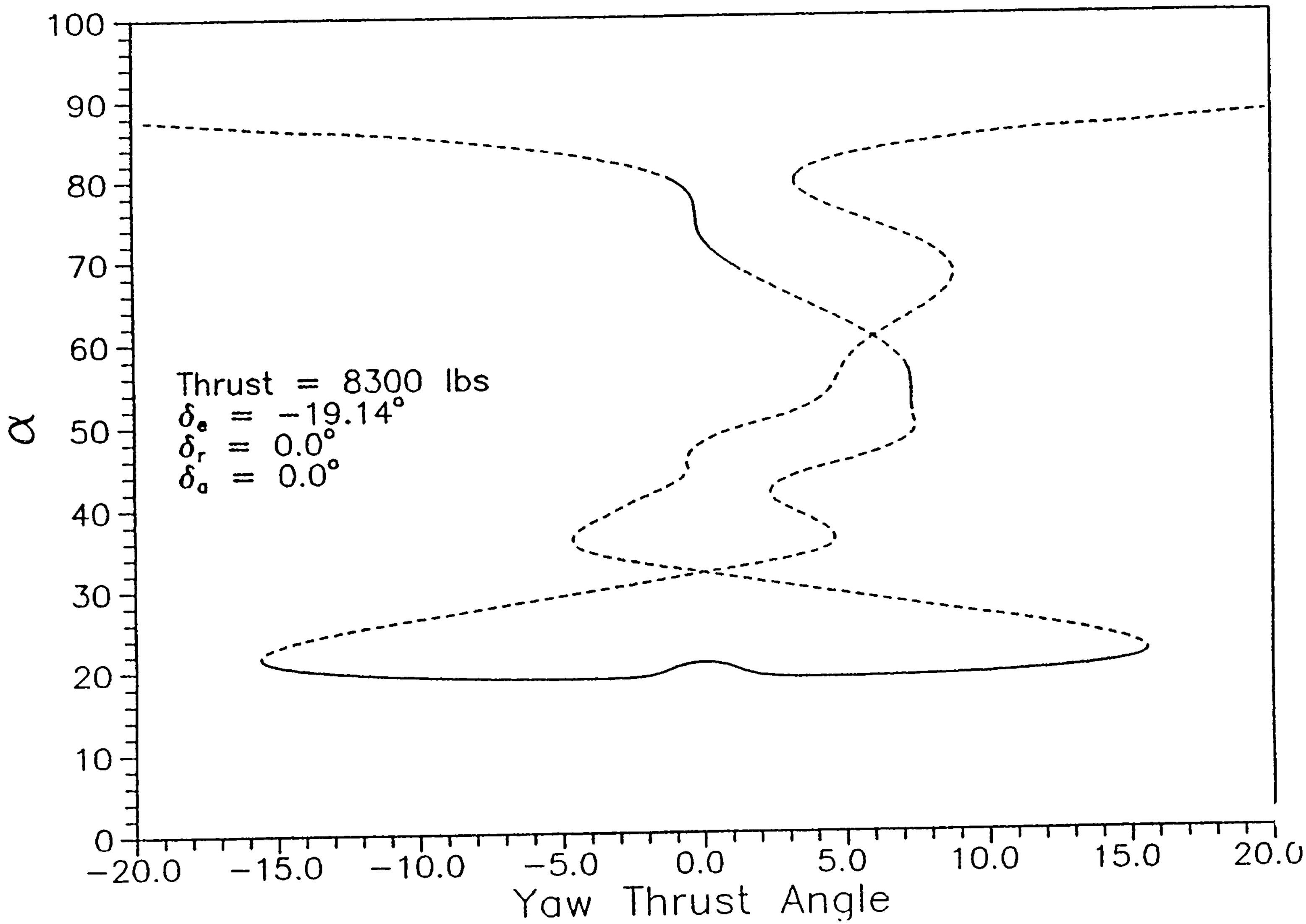

Figure 5-23 Yaw Vectoring T = 8300 lbs.

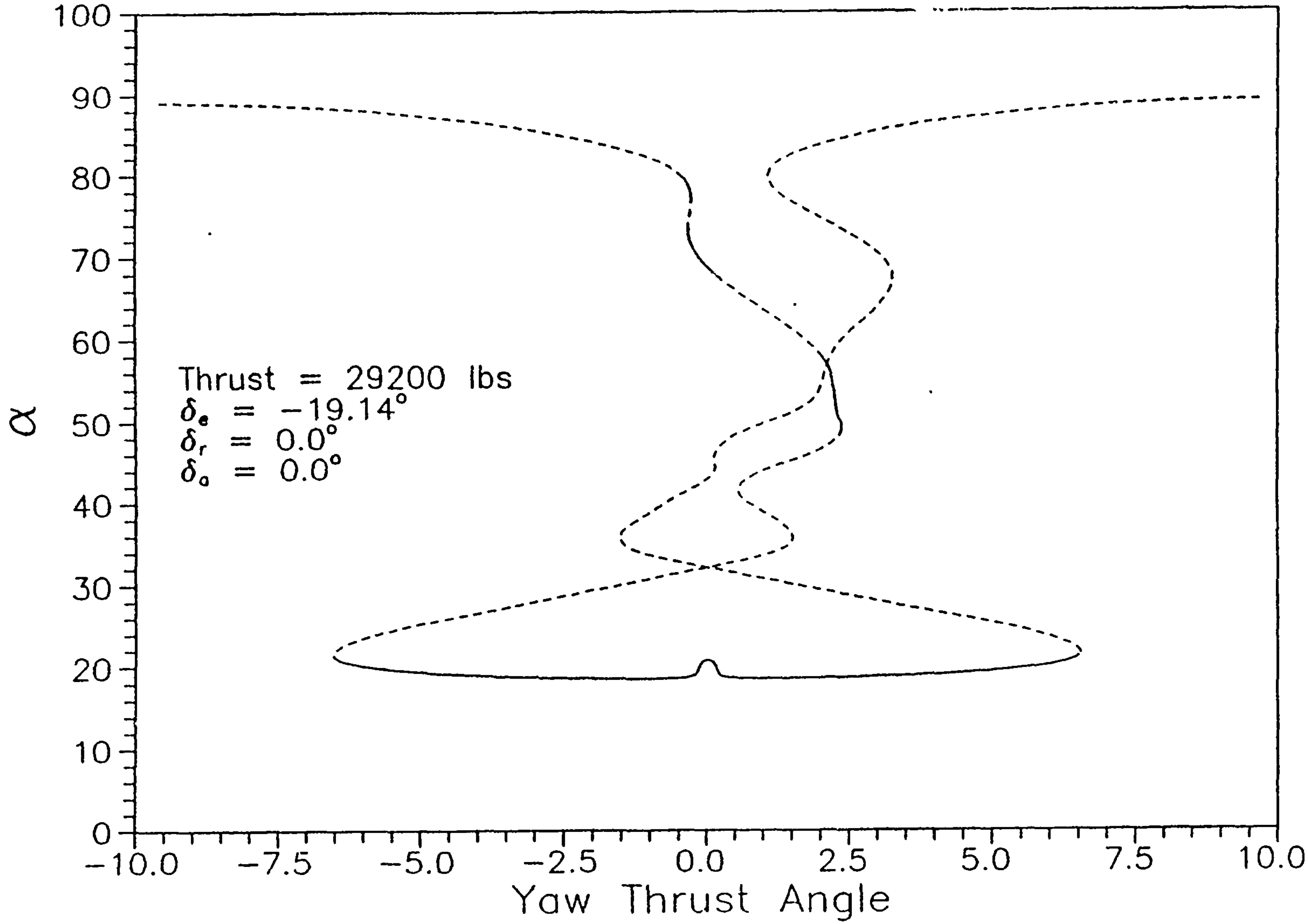

Figure 5-24 Yaw Vectoring T = 29200 lbs.

would indeed happen. The low angle of attack stable branch turns at 16 degrees and the only solution would be the left spin. Fig. 5-26 gives an appreciation as to how quick the rotation in the opposite direction begins if the yaw vector is not removed when the F-15 approaches low angle of attack flight.

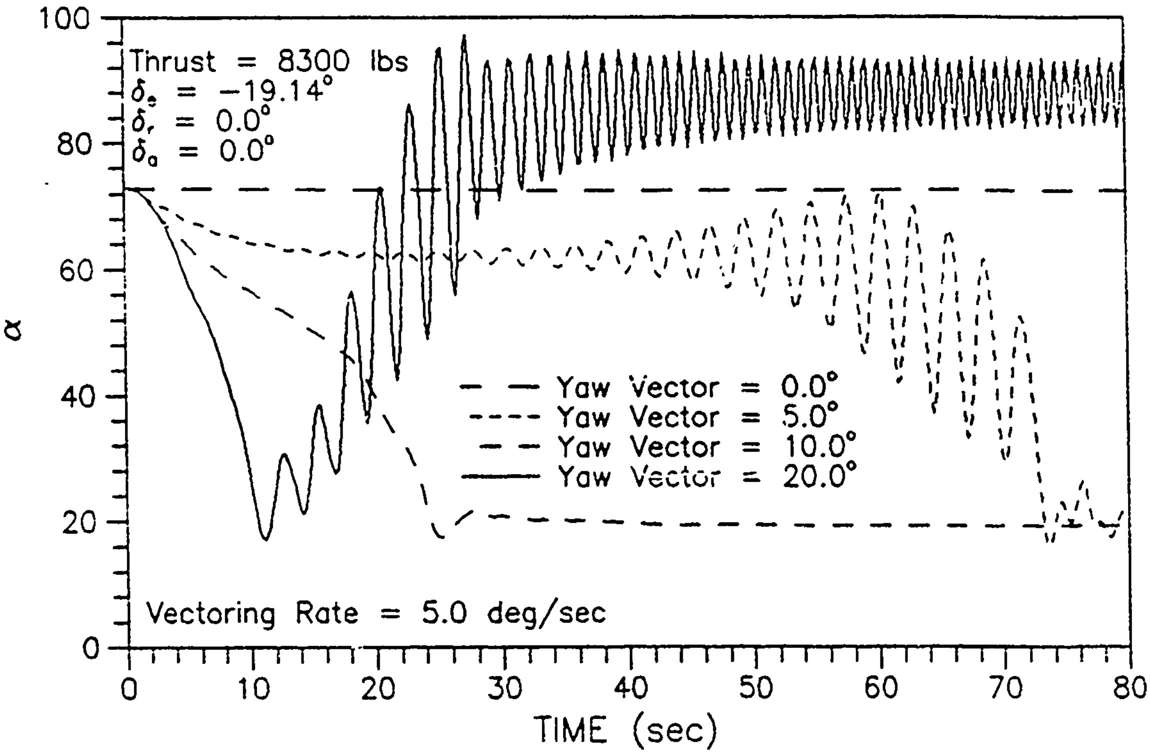

Figure 5-25 Simulation of Yaw Vectoring in a Flat Spin

As expected, yaw vectoring can be very effective in recovering the F-15 from a flat spin. Burk (8) also came to this result in his early research. However, yaw vectoring can lead to jumps to spins if used at low alpha. Additionally, care must be taken to remove yaw vectoring as the F-15 recovers or an inadvertent spin in the opposite direction may be entered.

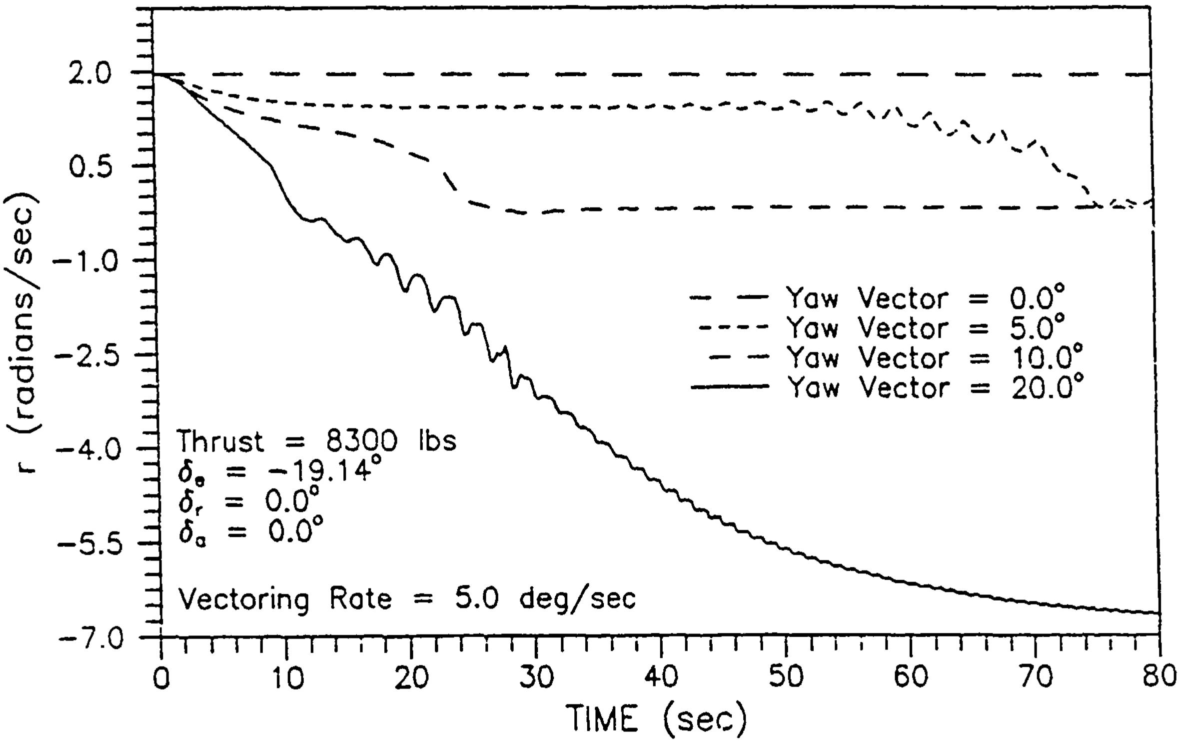

Figure 5-26 r vs Time in Yaw Vectoring Simulation

VI. Conclusions

Bifurcation analysis is a powerful tool in the analysis of nonlinear aircraft behavior. If it is used in conjunction with a realistic model of an aircraft's inertia and aerodynamic coefficients and some trial simulations, it can provide a qualitative idea of the nonlinear behavior of the aircraft. From a single starting point, it can be used to map out an entire spectrum of possible aircraft motions. This study took a fairly realistic model of an F-15, modified it with nozzles that have never been used on an operational F-15, and mapped out how they could be used to help recover from a flat spin. Additionally, spin characteristics due to thrust and thrust asymmetries were identified. The following conclusions were formed from this research:

1. The F-15 model designed by Baumann is a fairly realistic model of the F-15's actual behavior. However, the effectiveness of the rudder at high angles of attack is overestimated in the model. Recovery from the principal spin region identified in the research does not follow the recommended course of action of applying ailerons in the direction of the spin. The model therefore has some shortcomings that create unrealistic aircraft behavior.

2. Thrust affects the spin characteristics of the F-15 by changing the size and location of the stable spin

branches. Additionally, higher levels of thrust make thrust vectoring more effective. Full thrust alone cannot recover the F-15 from a spin, but it can aid other methods of recovering.

3. Asymmetric thrust can be used to recover the F-15 from a flat spin. The same moments that make thrust asymmetries useful can also make spins more difficult to recover from if the wrong engine flames out. Additionally, thrust asymmetries do not lead to jumps to spins and actually may delay the onset of wing rock.

4. Pitch vectoring can be used in a nonintuitive manner to bring about the recovery from a flat spin. Most pilots would argue that a nose up moment would probably deepen a spin, however this research shows that just the opposite occurs. Application of a nose up moment reduces the yaw rate and results in a deep stall which can be more easily recovered from.

5. Yaw vectoring shows to be the most promising method of spin recovery. However care must be taken to remove the yaw vector upon recovery or an inadvertent spin in the opposite direction can occur. The use of yaw vectoring at low α can lead to jumps to spins due to limit point behavior and therefore should be avoided.

Recommendations

The following are recommendations for future research that were identified while pursuing this research:

1. Use rotary balance data in the model. Many previous studies of spin behavior used rotary balance data in their models. F-15 rotary balance data is available but was not used in this study (3,4). This data is nonlinear in angular velocity and more correctly characterizes the actual aerodynamics in a spin. Discrepancies between flight test data and predicted behavior identified in this research may be explained away using the rotary balance data.

2. Plug the thrust vectoring angles into a control system to see how it can be used to minimize wing rock. This offers an ideal method to help keep control of the F-15 at high angles of attack by not having to rely on aerodynamic surfaces.

3. The F-15 used in this study was loaded symmetrically. In the real world, the F-15 is often flown with an asymmetric load of fuel or the weapons. This is a potential cause of many departures in the F-15 and bifurcation theory can be used to better characterize the mechanisms of these departures. Guicheteau (16:7) has applied this in his study of the Alpha Jet.

4. Include the contribution of gyroscopic torques due to the engines. This analysis assumes that they are zero. In reality, they will influence the spin behavior of the

F-15. Guicheteau (16:7) also applies this to the Alpha Jet.

5. The model has an inaccuracy identified ($C_{n\delta r}$) and may contain more that were not identified in this research. Therefore, a thorough refinement of the model's curve fits could make it more realistic in the high α regime.

6. Apply bifurcation theory to one of the new designs (ATF, B-2, C-17) using wind tunnel data to help develop their flight test program or verify flight test results.

Appendix A: F-15B Weight and Balance Data

The physical dimensions and weight and balance data for the F-15B is listed in Table V. The data for the F-15 was obtained from Beck (7) and (23).

Table II. Physical Characteristics of the F-15B

Wing	
Area (Theoretical)	608 sq ft
Aspect Ratio	3.01
Airfoil	
Root	NACA64006.6
Xw 155	NACA64A(x)04.6 (a = 0.8 Mod)
Tip	NACA64A203 (a=0.8 Mod)
Span	42.8 ft
Taper Ratio	0.25
Root Chord (Theoretical)	273.3 in
Tip Chord	68.3 in
Mean Aerodynamic Chord	191.3 in
Leading Edge Sweep Angle	45 degrees
25% Chord Sweep Angle	38.6 degrees
Dihedral	-1 degrees
Incidence	None
Twist at Tip	None
Aileron Area	26.5 sq ft
Flap Area	35.8 sq ft
Speed Brake - Area	31.5 sq ft
Control Surface Movement	
Aileron	+/- 20 degrees
Speedbrake	45 degrees up
Flap	30 degrees down
Horizontal Tail	29 degrees down, 15 degrees up
Rudder	+/- 30 degrees
Vertical Tail	
Area (Theoretical Each)	62.6 sq ft
Rudder Area (Each)	10.0 sq ft
Span	10.3 sq ft
Aspect Ratio	1.70
Root Chord	115.0 in
Tip Chord	30.6 in
Airfoil - Root	NACA0005-64

- Tip	NACA0003.5-64
Taper Ratio	0.27
Leading Edge Sweep Angle	36.6 degrees
25% Chord Sweep Angle	29.7 degrees
Mean Aerodynamic Chord	81.0 in
Cant	2 degrees out
Length ($.25c_w$ to $.25c_h$)	241.0 in
Wetted Area	
Fuselage	1405 sq ft
Nozzles	53 sq ft
Horizontal Tail	216 sq ft
Vertical Tail	257 sq ft
Wing	698 sq ft
Total Area	2629 sq ft
Engine Data (each)	
Non-Afterburning Thrust	14,871 lb
Afterburning Thrust	23,810 lb
Y Direction C.G. Offset	+/- 25.5 in
Z Direction C.G. Offset	0.25 in
Nozzle Pivot C.G. Offset	-20.219 ft
Miscellaneous Data	
Aircraft Length	63.8 ft
Aircraft Height	18.6 ft
Aircraft Volume	1996 cu ft
Aircraft Gross Weight	37000 lbs
C.G. Station X Direction	557.173
Y direction	0.0
Z Direction	116.173
Inertia Data	
I_x	25480 slug-ft^2
I_y	166620 slug-ft^2
I_z	186930 slug-ft^2
I_{xz}	-1000 slug-ft^2

The inertia values are for a basic F-15 with 4 AIM-7F missiles, ammo, 50% fuel and gear up.

Appendix B: Driver Program

```
C     CAPTAIN ROBERT J. MCDONNELL  AFIT GAE-90D
C     MASTERS THESIS
C
C     THIS COMPUTER PROGRAM SOLVES THE NONLINEAR DIFFERENTIAL
C     EQUATIONS OF MOTION FOR THE F-15B AIRCRAFT.  IT IS USED
C     AS AN ANALYTICAL TOOL IN THE SEARCH OF HIGH ANGLE OF ATTACK
C     PHENOMENA (I. E. FLAT SPINS).  THE PROGRAM IS CAPABLE OF
C     VARYING ELEVATOR, AILERON, AND RUDDER DEFLECTIONS, ENGINE
C     THRUST VECTOR (PITCH AND YAW), PORT AND STARBOARD ENGINE
C     THRUST, AND TOTAL THRUST.
C
C     LAST EDITED ON 24 OCT 1990
C
      IMPLICIT DOUBLE PRECISION(A-H,O-Z)
      DIMENSION W(300000), IW(1000)
C
C     OPEN(UNIT=3,FILE='fort.3')
      OPEN(UNIT=4,FILE='fort.4')
      OPEN(UNIT=7,FILE='fort.7')
      OPEN(UNIT=8,FILE='fort.8')
      OPEN(UNIT=9,FILE='fort.9')
      OPEN(UNIT=10,FILE='fort.10')
      OPEN(UNIT=12,FILE='cs')
      OPEN(UNIT=13,FILE='cts')
C
      REWIND 7
      REWIND 8
      REWIND 9
      REWIND 10
      REWIND 3
      REWIND 4
      REWIND 12
      REWIND 13
C
C     CALL AUTO - CONTINUATION & BIFURCATION LOCATION SUBROUTINE
C
      CALL AUTO(W,IW)
C
      STOP
      END
C
      SUBROUTINE FUNC(NDIM,NPAR,U,ICP,PAR,IJAC,F,DFDU,DFDP)
C     ---------- -----------------------------------------
C
      IMPLICIT DOUBLE PRECISION (A-H,O-Z)
      COMMON /KS/ K1,K5,K7,K8,K9,K10,K12,K13,K14,K15,K16,K17
      COMMON /ACDATA/ BWING,CWING,SREF,RHO,RMASS
      DOUBLE PRECISION K1,K5,K7,K8,K9,K10,K12,K13,K14,K15,K16,K17
      COMMON /SEIZE/ CX,CY,CZ,CLM,CMM,CNM
      COMMON /SEIZET/ CXT,CYT,CZT,CLMT,CMMT,CNMT
C
```

```
      DIMENSION DFDU(NDIM,NDIM),DFDP(NDIM,NPAR),DELF1(8),
     +          DELF2(8),U(NDIM),PAR(10),F(NDIM),DX(8)
C
C     INITIALIZE SOME CONSTANTS THAT ARE PASSED THROUGH
C     THE COMMON BLOCK ACDATA
C
C     DATA IS FROM MCAIR REPORT# A4172 AND AFFTC-TR-75-32
C     F-15A APPROACH-TO-STALL/STALL/POST-STALL EVALUATION
C
C     BWING  - A/C WINGSPAN, FT
C     CWING  - A/C MEAN AERODYNAMIC CHORD, FT
C     SREF   - A/C WING REFERENCE AREA, SQ FT
C     RHO    - AIR DENSITY AT 20000 FT ALTITUDE, SLUG/FT^3
C     RMASS  - A/C MASS, SLUGS
C
      BWING=42.8
      CWING=15.94
      SREF=608.
      RHO=.0012673
      RMASS=37000./32.174
C
C      DETERMINE CONSTANTS K1 THROUGH K17.  SOME ARE MADE COMMON AND
C      PASSED TO SUBROUTINE FUNX AND USED IN THE EQUATIONS
C      OF MOTION THERE
C
C      INERTIAS HAVE UNITS OF SLUG-FT^2
C
C      K1 HAS UNITS OF 1/FT
C
C      K6, K8, K11, K14, AND K17 HAVE UNITS OF 1/FT^2
C
C      IX=  25480.0d0
C      IY= 166620.0d0
C      IZ= 186930.0d0
C      IXZ= -1000.0d0
C      K1=0.5d0*RHO*SREF/RMASS
C      K2=(IZ-IY)/IX
C      K3=IXZ*IXZ/(IX*IZ)
C      K4=(IY-IX)/IZ
C      K5=IXZ/IX
C      K6=0.5d0*RHO*BWING*SREF/IX
C      K7=IXZ/IZ
C      K8=0.5d0*RHO*SREF*CWING/IY
C      K9=(IZ-IX)/IY
C      K10=IXZ/IY
C      K11=0.5d0*RHO*SREF*BWING/IZ
C      K12=(K2+K3)/(1.0d0-K3)
C      K13=(1.0d0-K4)*K5/(1.0d0-K3)
C      K14=K6/(1.0d0-K3)
C      K15=(K3-K4)/(1.0d0-K3)
C      K16=(1.0d0+K2)*K7/(1.0d0-K3)
C      K17=K11/(1.0d0-K3)
C
```

```
      K1  = 3.350088890D-04
      K5  =-3.924646781D-02
      K7  =-5.349596105D-03
      K8  = 3.685650971D-05
      K9  = .96897131196
      K10 =-6.001680471D-03
      K12 = .79747314581
      K13 =-9.615755341D-03
      K14 = 6.472745847D-04
      K15 =-.754990553922
      K16 =  K13
      K17 = 8.822851558D-05
C
C     FIND THE VALUES OF F(1) THROUGH F(NDIM).  SUBROUTINES
C     COEFF AND FUNX ARE CALLED ONCE.
C
      CALL COEFF(U,PAR,NDIM,ICP)
C
      CALL FUNX(NDIM,U,F)
C
      IF(IJAC.EQ.0) RETURN
C
C   SET THE VALUES OF DX
C   MODIFIED TO SCALE DX ACCORDING TO VARIABLE
C   13 JUN 88
C
C     DX0=1.0D-9
      DX(1)=DX0*50.0d0
      DX(2)=DX0*10.0d0
      DX(3)=DX0*0.5d0
      DX(4)=DX0*0.25d0
      DX(5)=DX0*0.5d0
      DX(6)=DX0*50.0d0
      DX(7)=DX0*50.0d0
      DX(8)=DX0*0.5d0
C
C     NEXT THE PARTIAL OF F W.R.T. A GIVEN PARAMETER ARE FINITE
C     DIFFERENCED
C
      PTEMP=PAR(ICP)
      PAR(ICP)=PTEMP+DX(1)
      CALL COEFF(U,PAR,NDIM,ICP)
      CALL FUNX(NDIM,U,DELF1)
C
      PAR(ICP)=PTEMP-DX(1)
      CALL COEFF(U,PAR,NDIM,ICP)
      CALL FUNX(NDIM,U,DELF2)
C
        DO 13 I=1,NDIM
C
          DFDP(I,ICP)=(DELF1(I)-DELF2(I))/(2.0d0*DX(1))
C
  13    CONTINUE
```

```
      PAR(ICP)=PTEMP
C
C     THE NEXT DO LOOP CALCULATES THE PARTIAL DERIVATIVE OF F W.R.T.
C     TO U USING FINITE DIFFERENCES.
C
C     SET U(J) EQUAL TO U+DU, THEN CALL COEFF WITH THIS UPDATED
C     STATE VECTOR.  THIS IS DONE SIMILARLY WITH U-DU
C
      DO 20 J=1,NDIM
C
         UTEMP=U(J)
C
         U(J)=UTEMP+DX(J)
         CALL COEFF(U,PAR,NDIM,ICP)
         CALL FUNX(NDIM,U,DELF1)
C
         U(J)=UTEMP-DX(J)
         CALL COEFF(U,PAR,NDIM,ICP)
         CALL FUNX(NDIM,U,DELF2)
C
         DO 16 I=1,NDIM
            DFDU(I,J)=(DELF1(I)-DELF2(I))/(2.0d0*DX(J))
   16       CONTINUE
C
         U(J)=UTEMP
C
   20 CONTINUE
      RETURN
      END
      SUBROUTINE FUNX(NDIM,U,F)
C     ---------- -------------
C
C     SUBROUTINE FUNX EVALUATES THE NDIM EQUATIONS GIVEN THE
C     STATE VECTOR U.
C
C     NDIM- THE DIMENSION OF THE PROBLEM
C     U   - THE VECTOR OF STATES ALPHA, BETA, ... (INPUT)
C     F   - THE VECTOR RESULT OF FUNCTION EVALUATIONS (OUTPUT)
C
      IMPLICIT DOUBLE PRECISION (A-H,O-Z)
      COMMON /SEIZE/ CX,CY,CZ,CLM,CMM,CNM
      COMMON /SEIZET/ CXT,CYT,CZT,CLMT,CMMT,CNMT
      COMMON /KS/ K1,K5,K7,K8,K9,K10,K12,K13,K14,K15,K16,K17
      DOUBLE PRECISION K1,K5,K7,K8,K9,K10,K12,K13,K14,K15,K16,K17
      DIMENSION U(NDIM),F(NDIM)
C
C     SET TRIGONOMETRIC RELATIONSHIPS OF THE STATES ALPHA, BETA,
C     THETA, AND PHI AND THEN SET P, Q, R, AND VTRFPS
C
      IWRITE=1
C
      DEGRAD=57.29577951D0
C
```

```
      CA=COS(U(1)/DEGRAD)
      SA=SIN(U(1)/DEGRAD)
      CB=COS(U(2)/DEGRAD)
      SB=SIN(U(2)/DEGRAD)
      CTHE=COS(U(6)/DEGRAD)
      STHE=SIN(U(6)/DEGRAD)
      CPHI=COS(U(7)/DEGRAD)
      SPHI=SIN(U(7)/DEGRAD)
C
      P=U(3)
      Q=U(4)
      R=U(5)
      VTRFPS=1000.0d0*U(8)
C
C     SET THE GRAVITATIONAL CONSTANT, FT/SEC
C
      G=32.1740d0
C
C    THE FOLLOWING SYSTEM OF NONLINEAR DIFFERENTIAL EQUATIONS
C    GOVERN AIRCRAFT MOTION
C
C    UPDATED FOR PROPER DEGREE-RADIAN UNITS AND PROPERLY
C    SCALED VELOCITY EQUATION:  7 JUN 88
C
C   ****** ALPHA DOT ******
C
C   F(1)=ALPHA-DOT
C
  1   F(1)=Q+(-(K1*VTRFPS*CX-G*STHE/VTRFPS+R*SB)*SA+(K1*VTRFPS
     +         *CZ+(G*CTHE*CPHI/VTRFPS)-P*SB)*CA)/CB
      F(1)=F(1)*DEGRAD
C
C   ****** BETA DOT ******
C
C   F(2)=BETA-DOT
C
  2   F(2)=-((K1*VTRFPS*CX-G*STHE/VTRFPS)*SB+R)*CA+(K1*VTRFPS*CY
     +   +G*CTHE*SPHI/VTRFPS)*CB-((K1*VTRFPS*CZ+G*CTHE*CPHI/VTRFPS)
     +   *SB-P)*SA
      F(2)=F(2)*DEGRAD
C
C   ****** P DOT ******
C
C   F(3)=P-DOT
C
  3   F(3)=-K12*Q*R+K13*P*Q+K14*(CLM+K7*CNM)*VTRFPS*VTRFPS
C
C   ****** Q DOT ******
C
C   F(4)=Q-DOT
C
  4   F(4)=K8*VTRFPS*VTRFPS*CMM+K9*P*R+K10*(R*R-P*P)
C
```

```
C     ****** R DOT ******
C
C     F(5)=R-DOT
C
    5    F(5)=K15*P*Q-K16*Q*R+K17*VTRFPS*VTRFPS*(K5*CLM+CNM)
C
C     ****** THETA DOT ******
C
C     F(6)=THETA-DOT
C
    6    F(6)=Q*CPHI-R*SPHI
         F(6)=F(6)*DEGRAD
C
C     ****** PHI DOT ******
C
C     F(7)=PHI-DOT
C
    7    F(7)=P+Q*(STHE/CTHE)*SPHI+R*(STHE/CTHE)*CPHI
         F(7)=F(7)*DEGRAD
C
C     ****** V DOT ******
C
C     F(8)=VTRFPS-DOT  (SCALED BY A FACTOR OF 1000)
C
    8    F(8)=U(8)*((K1*VTRFPS*CX-G*STHE/VTRFPS)*CA*CB+(K1*VTRFPS*CY
     +  +G*CTHE*SPHI/VTRFPS)*SB
     +  +(K1*VTRFPS*CZ+G*CTHE*CPHI/VTRFPS)*SA*CB)
C
         RETURN
         END
C
         SUBROUTINE STPNT(NDIM,U,NPAR,ICP,PAR)
C        ---------- --------------------------
C
C        THIS SUBROUTINE SETS THE VALUES OF THE STATES AND PARAMETERS
C        AT THE START OF THE ANALYSIS.  THE STATES AND CONTROL SURFACE
C        SETTINGS REPRESENT AN EQUILIBRIUM STATE OF THE AIRCRAFT
C
         IMPLICIT DOUBLE PRECISION (A-H,O-Z)
C
         DIMENSION U(NDIM),PAR(10)
C        U(1) - ALPHA, DEG
C        U(2) - BETA, DEG
C        U(3) - P, RAD/SEC
C        U(4) - Q, RAD/SEC
C        U(5) - R, RAD/SEC
C        U(6) - THETA, DEG
C        U(7) - PHI, DEG
C        U(8) - TRUE VELOCITY, IN THOUSANDS OF FT/SEC
C
C        THE STARTING POINT (VECTOR)
C
         OPEN(UNIT=15,FILE='fort.15')
```

```
      REWIND (15)
C
      READ(15,*) U(1)
      READ(15,*) U(2)
      READ(15,*) U(3)
      READ(15,*) U(4)
      READ(15,*) U(5)
      READ(15,*) U(6)
      READ(15,*) U(7)
      READ(15,*) VTRFPS
      U(8)=VTRFPS/1000.0d0
C
C     PAR(1)=DELESD
C     PAR(2)=DRUDD       THE PARAMETERS, IN DEGREES
C     PAR(3)=DDA
C     PAR(4)=ENGPA  PORT ENGINE THRUST, POUNDS/1000
C     PAR(5)=ENGSA  STARBORD ENGINE THRUST, POUNDS/1000
C     PAR(6)=TPTAL  PITCH THRUST VECTOR, DEG
C     PAR(7)=TYTAL  YAW THRUST VECTOR, DEG
C     PAR(8)=TTHRST  TOTAL THRUST, POUNDS/1000
C
      READ(15,*) PAR(1)
      READ(15,*) PAR(2)
      READ(15,*) PAR(3)
      READ(15,*) PAR(4)
      READ(15,*) PAR(5)
      READ(15,*) PAR(6)
      READ(15,*) PAR(7)
      READ(15,*) PAR(8)
C
      RETURN
      END
C
      SUBROUTINE INIT
C     ---------- ----
C
      IMPLICIT DOUBLE PRECISION(A-H,O-Z)
C
      COMMON /BLCSS/ NDIM,ITMX,NPAR,ICP,IID,NMX,IPS,IRS
      COMMON /BLCPS/ NTST,NCOL,IANCH,NMXPS,IAD,NPR,NWTN,ISP,ISW1
      COMMON /BLDLS/ DS,DSMIN,DSMAX,IADS
      COMMON /BLLIM/ RL0,RL1,A0,A1,PAR(10)
      COMMON /BLOPT/ ITNW,MXBF,IPLT,ICP2,ILP
      COMMON /BLEPS/ EPSU,EPSL,EPSS,EPSR
C
C IN THIS SUBROUTINE THE USER SHOULD SET THOSE CONSTANTS
C THAT REQUIRE VALUES DIFFERENT FROM THE DEFAULT VALUES
C ASSIGNED IN THE LIBRARY SUBROUTINE DFINIT.  FOR A DESCRIPTION
C OF THESE CONSTANTS SEE THE DOCUMENTATION CONTAINED IN THE
C LIBRARY.  COMMON BLOCKS CORRESPONDING TO CONSTANTS THAT THE USER
C WANTS TO CHANGE MUST BE INSERTED ABOVE.  THESE COMMON BLOCKS
C SHOULD OF COURSE BE IDENTICAL TO THOSE IN DFINIT.
C
```

```
      DSMAX = 10.0d0
      DSMIN =0.00000010d0
      EPSU  = 1.0D-07
      EPSL  = 1.0D-07
      EPSS  = 1.0D-05
      EPSR  = 1.0D-07
      IAD   = 1
      ILP   = 1
      ITMX  = 40
      ITNW  = 20
      MXBF  = 5
      NDIM  = 8
      NPAR  = 8
C
      OPEN(UNIT=25,FILE='fort.25')
      REWIND (25)
C
      READ(25,*) RL0,RL1
      READ(25,*) A0,A1
      READ(25,*) DS
      READ(25,*) NMX
      READ(25,*) NTST,NCOL,NMXPS,NPR
      READ(25,*) ISP,IRS,ICP,ICP2,IPLT,IPS
      READ(25,*) ISW1
      RETURN
      END
C
      SUBROUTINE BCND
C     ---------- ----
C
      RETURN
      END
C
      SUBROUTINE ICND
C     ---------- ----
C
      RETURN
      END
C
      SUBROUTINE COEFF(U,PAR,NDIM,ICP)
C     ---------- -------------------
C
      IMPLICIT DOUBLE PRECISION (A-H,O-Z)
      COMMON /ACDATA/ BWING,CWING,SREF,RHO,RMASS
      COMMON /SEIZE/ CX,CY,CZ,CLM,CMM,CNM
      COMMON /SEIZET/CXT,CYT,CZT,CLMT,CMMT,CNMT
      DIMENSION U(NDIM),PAR(10)
C
C   THE PRIMARY SOURCE OF THESE COEFFICIENT EQUATIONS IS SUBROUTINE
C   ARO10 FROM MCAIR CODE USED IN THE F15 BASELINE SIMULATOR.
C
C   MOST OF THE COEFFICIENTS USED IN THE EQUATIONS WERE COMPUTED
C   USING SAS WITH RAW DATA FROM THE F15 SIMULATOR DATA TABLES.
```

```
C
C   THIS SUBROUTINE IS CALLED BY THE DRIVER PROGRAM FOR THE AUTO
C   SOFTWARE.  IT MERELY TAKES INPUTS ON THE A/C STATE, CONTROL
C   SURFACE POSITIONS, AND THRUST VALUES  AND RETURNS THE
C   APPROPRIATE AERO COEFFICIENTS CX, CY, CZ, CL, CM, AND CN.
C
C   INPUTS TO THIS SUBROUTINE
C
C   AL      - ANGLE OF ATTACK, DEG
C   BETA    - SIDESLIP ANGLE, DEG
C   DDA     - AILERON DEFLECTION ANGLE, DEG
C   DELEDD  - DIFFERENTIAL TAIL DEFLECTION ANGLE, DEG
C   DELESD  - SYMMETRICAL TAIL DEFLECTION ANGLE, DEG
C   DRUDD   - RUDDER DEFLECTION, POSITIVE TRAILING EDGE LEFT, DEG
C   P       - ROLL RATE, RAD/SEC
C   Q       - PITCH RATE, RAD/SEC
C   R       - YAW RATE, RAD/SEC
C   ENGPA   - PORT ENGINE THRUST, POUNDS/1000
C   ENGSA   - STARBOARD ENGINE THRUST, POUNDS/1000
C   TYTAL   - YAW THRUST ANGLE, DEG
C   TPTAL   - PITCH THRUST ANGLE, DEG
C   TTHRST  - TOTAL THRUST, POUNDS/1000
C   VTRFPS  - TRUE AIRSPEED, FT/SEC
C
C   INTERMEDIATE VARIABLES USED IN THIS SUBROUTINE
C
C   ABET    - ABSOLUTE VALUE OF BETA, DEG
C   ARUD    - ABSOLUTE VALUE OF RUDDER DEFLECTION, DEG
C   BWING   - WING SPAN, FEET
C   CA      - COSINE RAL (RAL IN RADIANS)
C   CD      - COEFFICIENT OF DRAG
C   CL      - BASIC LIFT COEFFICIENT
C   CWING   - MEAN AERODYNAMIC CHORD, FEET
C   DAHD    - DIFFERENTIAL ELEVATOR DEFLECTION, DEG
C   DAHLD   - LEFT AILERON DEFLECTION, DEG
C   DAHRD   - RIGHT AILERON DELFECTION, DEG
C   DELEDR  - DIFFERENTIAL TAIL DEFLECTION ANGLE, RAD
C   DELESR  - SYMMETRIC TAIL DEFLECTION ANGLE, RAD
C   ENGP    - PORT ENGINE THRUST, POUNDS
C   ENGS    - STARBOARD ENGINE THRUST, POUNDS
C   PTAL    - PITCH THRUST VECTOR, RAD
C   QBARS   - DYNAMIC PRESSURE TIMES WING REFERENCE AREA, LBF
C   RABET   - ABSOLUTE VALUE OF BETA, RADIANS
C   RAL     - ABSOLUTE VALUE OF ALPHA, RADIANS
C   RARUD   - ABSOLUTE VALUE OF RUDDER, RADIANS
C   SA      - SINE RAL (RAL IN RADIANS)
C   YTAL   - YAW THRUST VECTOR, RAD
C
C   OUTPUTS FROM THIS SUBROUTINE
C
C   CX      - BASIC AXIAL FORCE COEFFICIENT, BODY AXIS, + FORWARD
C   CY      - BASIC SIDE FORCE COEFFICIENT, BODY AXIS, + RIGHT
C   CZ      - BASIC NORMAL FORCE COEFFICIENT, BODY AXIS, + DOWN
```

```
C   CLM      - BASIC ROLLING MOMENT COEFFICIENT, BODY AXIS, + R WING
C              DOWN
C   CMM      - BASIC PITCHING MOMENT COEFFICIENT, BODY AXIS, + NOSE UP
C   CNM      - BASIC YAWING MOMENT COEFFICIENT, BODY AXIS, + NOSE RIGHT
C
C    ANGLES USED IN CALCULATING CL, CLLDB, ..., ARE IN RADIANS. THIS
C    IS BECAUSE RADIANS WERE USED IN THE CURVE FITTING PROGRAM TO
C    OBTAIN THE COEFFICIENTS OF THE ALPHA, BETA, ..., TERMS IN THE
C    FOLLOWING EQUATIONS.
C
C   MOMENT REFERENCE CENTER WAS SET IN ARO10 PROGRAM AS:
C
C     DATA CMCGR /.2565/, CNCGR /.2565/
C
C   THE AERO STABILITY DATA WAS TAKEN REFERENCED TO THESE CG
C   LOCATIONS.  THE MOMENTS OF INERTIA AND OTHER AIRCRAFT DATA
C   ARE FOR A CLEAN CONFIGURATION TEST AIRCRAFT WITH A CG AT
C   THE SAME CG.  AS A RESULT, THERE IS NO 'CG OFFSET' TO BE
C   COMPUTED.
C
      IWRITE=0
C
      AL=U(1)
      BETA=U(2)
      P=U(3)
      Q=U(4)
      R=U(5)
      THETA=U(6)
      PHI=U(7)
      VTRFPS=U(8)*1000.
C
      DELESD=PAR(1)
      DRUDD=PAR(2)
      DDA=PAR(3)
      ENGPA=PAR(4)
      ENGSA=PAR(5)
      TPTAL=PAR(6)
      TYTAL=PAR(7)
      TTHRST=PAR(8)
C
      DEGRAD=57.29577951
      DELESR=DELESD/DEGRAD
      YTAL=TYTAL/DEGRAD
      PTAL=TPTAL/DEGRAD
C
C     IF BLOCK TO CHANGE TOTAL THRUST
C
      IF(ICP.EQ.8)THEN
        DIFT=PAR(4)-PAR(5)
        THALF=TTHRST/2.0d0
        ENGPA=THALf+DIFT/2.0d0
        ENGSA=THALF-DIFT/2.0d0
      ENDIF
```

```
C
      ENGP=ENGPA*1000.0
      ENGS=ENGSA*1000.0
C
      QBARS=0.5d0*RHO*VTRFPS*VTRFPS*SREF
      CO2V=CWING/(2.0d0*VTRFPS)
      BO2V=BWING/(2.0d0*VTRFPS)
      QSB=BWING*QBARS
      ARUD=ABS(DRUDD)
      RARUD=ARUD/DEGRAD
      RAL=AL/DEGRAD
      ABET=ABS(BETA)
      RABET=ABET/DEGRAD
C
C*********************************************************************
C
C
C  NEW SECTION OF CODE - 1) ALL THE AERODYNAMIC COEFFICIENTS IN
C                           THIS VERSION OF THE DRIVER PROGRAM
C                           ARE TAKEN DIRECTLY FROM THE 1988
C                           F15 AEROBASE (0.6 MACH, 20000 FEET)
C
C                        2) THIS SECTION SUMMARIZES THE
C                           AERODYNAMIC COEFFICIENTS AS TO WHAT
C                           THEY ARE AND HOW THEY ARE USED.
C                           THE FIRST ACCRONYM IS THE JOVIAL NAME
C                           OF THE AERODYNAMIC COEFFICIENT (CFX1,
C                           ETC), THE SECOND ACCRONYM IS THE
C                           F15 AEROBASE CODE OR CTAB NAME
C                           (ATAB15, ETC).  A BRIEF DEFINITION
C                           OF THE AERODYNAMIC COEFFICIENT IS ALSO
C                           PROVIDED.
C
C                        3) THERE IS ALSO A SECTION THAT PROVIDES
C                           A TABLE OF CONVERSIONS BETWEEN WHAT
C                           THE VARIABLE IS CALLED IN THE ORIGINAL
C                           SECTION OF THIS PROGRAM
C                           AND ITS NAME IN THE 1988 F15 AEROBASE.
C                           FOR THE SAKE OF CONTINUITY THE
C                           ORIGINAL PROGRAM NAME IS USED AND
C                           THE 1988 F15 AEROBASE NAME
C                           IS PROVIDED AS BOOK KEEPING
C                           INFORMATION.
C********* CFX ****************************************************C
C
C  CFX = FORCE IN STABILITY AXIS X DIRECTION (CD IN BODY AXIS)
C        (FUNCTION OF CL OR CFZ1)
C  CFX = CFX1 + CXRB + STORE INCREMENTS + CXDSPD + DCXLG + DCD
C
C  CFX1 = ATAB15 = PERFORMANCE DRAG COEFFICIENT - CD
C  CXRB = ATAB22 = DELTA CD DUE TO CG (=0.0)
C  CXDSPD = ATAB27 = DELTA CD DUE TO SPEEDBRAKE (NORMALLY = 0.0436)
C                    SET TO 0 SINCE THIS STUDY IS CONCERNED
```

```
C                    WITH HIGH ANGLES
C                    OF ATTACK PHENOMENON (>40 DEGREES) AND BECAUSE
C                    THE SPEEDBRAKE WILL NOT DEPLOY AT ANGLES OF
C                    ATTACK GREATER THAN 15 DEGREES.
C  DCXLG = ATAB19 = DELTA CD DUE TO REYNOLD'S NUMBER  (=-0.0005)
C  DCD = BTAB03 = DELTA CD DUE TO 2-PLACE CANOPY (F15B) (=0.0005)
C        ******* NOTE THAT DCXLG AND DCD CANCEL EACH OTHER *******
C
C*********** CFY *************************************************C
C
C  CFY = FORCE IN BODY AXIS Y DIRECTION
C  CFY = CFY1*EPA02 + CYDAD*DAILD + [CYDRD*DRUDD*DRFLX5]*EPA43
C        +[CYDTD*DTFLX5 + DTFLX6]*DTALD + CFYP*PB + CFYR*RB
C        +CYRB + STORE INCREMENTS + DCYB*BETA
C
C  CFY1  = ATAB16 = BASIC SIDE FORCE COEFFICIENT - CY(BETA)
C  EPA02 = ATAB21 = BETA MULTIPLIER TABLE
C  CYDAD = ATAB75 = SIDE FORCE COEFFICIENT DUE TO AILERON DEFLECTION
C  DAILD          = AILERON DEFLECTION (DEG)
C  CYDRD = ATAB69 = SIDE FORCE COEFFICIENT DUE TO RUDDER DEFLECTION
C  DRUDD          = RUDDER DEFLECTION  (DEG)
C  DRFLX5 = ATAB88 = FLEX MULTIPLIER ON CYDRD (=0.89)
C  EPA43 = ATAB30 = MULTIPLIER ON CNDR, CLDR, CYDR DUE TO SPEEDBRAKE
C                  (=1.0)
C  CYDTD = ATAB72 = SIDE FORCE COEFFICIENT DUE TO DIFFERENTIAL TAIL
C                  DEFLECTION - CYDDT
C  DTFLX5 = ATAB10 = FLEX MULTIPLIER ON CYDTD (=0.975)
C  DTFLX6 = ATAB77 = FLEX INCREMENT TO CYDTD (=0.0)
C  DTALD           = DIFFERENTIAL TAIL DEFLECTION (DEG) WHICH IS
C                    DIRECTLY PROPORTIONAL TO AILERON DEFLECTION AND
C                    IS PRIMARILY USED TO ASSIST IN ROLLING THE
C                    F-15B (DTALD=0.3*DAILD)
C  CFYP = ATAB13 = SIDE FORCE COEFFICIENT DUE TO ROLL RATE (CYP)
C  PB            = (PEOBB*SPAN)/(2*VILWF)
C                  PEOBB = ROLL RATE IN RAD/SEC = P
C                  SPAN = WING SPAN = 42.8 FEET = BWING
C                  VILWF = VELOCITY IN FT/SEC = VTRFPS
C  CFYR = ATAB07 = SIDE FORCE COEFFICIENT DUE TO YAW RATE (CYR)
C  RB            = (REOBB*SPAN)/(2*VILWF)
C                  REOBB = YAW RATE IN RAD/SEC = R
C  CYRB = ATAB93 = ASSYMETRIC CY AT HIGH ALPHA (ANGLE OF ATTACK)
C  DCYB          = 0.0  THERE IS NO INCREMENT DELTA CYB (SIDE FORCE)
C                 DUE TO A 2-PLACE CANOPY ON THE F15B.  THIS IS
C                 BECAUSE THE SAME CANOPY IS USED ON BOTH THE
C                 BASELINE F15A AND THE F15B.  THE SIDEFORCE IS THE
C                 SAME FOR BOTH VERSIONS OF THE F15 AND ALREADY
C                 INCLUDED IN THE BASIC SIDE FORCE (CFY1).  THE TWO
C                 PLACE CANOPY IS MOUNTED DIFFERENTLY HOWEVER, SO
C                 THERE IS A DIFFERENCE IN YAWING AND ROLLING MOMENT.
C                 (SEE DCNB AND DCLB)
C
C*********** CFZ **************************************************C
```

```
C
C  CFZ = FORCE IN STABILITY AXIS Z DIRECTION (CL IN BODY AXIS)
C  CFZ = CFZ1 + CZDSPD + STORE INCREMENTS + DCL*BETA
C
C
C  CFZ1 = ATAB17 = BASIC LIFT COEFFICIENT - CL
C  CZDSPD = ATAB26 = DELTA CL DUE TO SPEEDBRAKE
C                    SET TO 0 DUE TO THE REASONS GIVEN ABOVE IN CXDSPD
C  DCL = BTAB01 = DELTA CL DUE TO 2-PLACE CANOPY (F15B) (=0.0)
C
C********** CLM ****************************************************C
C
C  CML = TOTAL ROLLING MOMENT COEFFICIENT IN BODY AXIS
C  CML = CML1*EPA02 + CLDAD*DAILD + [CLDRD*DRUDD*DRFLX1]*EPA43 +
C        [CLDTD*DTFLX1 + DTFLX2]*DTALD + CMLP*PB + CMLR*RB +
C        STORE INCREMENTS + CLDSPD + DCLB*BETA
C  CML1 = ATAB01 = BASIC ROLLING MOMENT COEFFICIENT - CL(BETA)
C  EPA02 = ATAB21 = BETA MULTIPLIER TABLE
C  CLDAD = ATAB73 = ROLL MOMENT COEFFICIENT DUE TO AILERON DEFLECTION
C                   -(CLDA)
C  DAILD          = AILERON DEFLECTION (DEG)
C  CLDRD = ATAB67 = ROLLING MOMENT COEFFICIENT DUE TO RUDDER
C                   DEFLECTION  -(CLD)
C  DRUDD          = RUDDER DEFLECTION (DEG)
C  DRFLX1 = ATAB80 = FLEX MULTIPLIER ON CLDRD (=0.85)
C  EPA43 = ATAB30 = MULTIPLIER ON CNDR, CLDR, CYDR DUE TO SPEEDBRAKE
C                   (=1.0)
C  CLDTD = ATAB70 = ROLL MOMENT COEFFICIENT DUE TO DIFFERENTIAL TAIL
C                   DEFLECTION - CLDD
C  DTFLX1 = ATAB04 = FLEX MULTIPLIER ON CLDTD (=0.975)
C  DTFLX2 = ATAB84 = FLEX INCREMENT TO CLDTD (=0.0)
C  DTALD           = DIFFERENTIAL TAIL DEFLECTION (DEG) WHICH IS
C                    DIRECTLY PROPORTIONAL TO AILERON DEFLECTION AND
C                    IS PRIMARILY USED TO ASSIST IN ROLLING THE F-15B
C                    (DTALD = 0.3*DAILD)
C  CMLP = ATAB02 = ROLL DAMPING DERIVATIVE -CLP
C  PB            = (PEOBB*SPAN)/(2*VILWF)
C                   PEOBB = ROLL RATE IN RAD/SEC = P
C                   SPAN = WING SPAN = 42.8 FEET = BWING
C                   VILWF = VELOCITY IN FT/SEC = VTRFPS
C  CMLR = ATAB11 = ROLLING MOMENT COEFFICIENT DUE TO YAW RATE - CLR
C  RB            = (REOBB*SPAN)/(2*VILWF)
C                 REOBB = YAW RATE IN RAD/SEC = R
C  CLDSPD = ATAB29 = DELTA CL DUE TO SPEEDBRAKE
C                    SET TO 0 DUE TO THE REASONS GIVEN ABOVE IN CXDSPD
C  DCLB = BTAB04 = INCREMENT DELTA CLB (ROLLING MOMENT) DUE TO 2-PLACE
C                 CANOPY FROM PSWT 499
C
C*********** CMM ***************************************************C
```

```
C
C  CMM = TOTAL PITCHING MOMENT COEFFICIENT IN STABILITY AXIS
C        (BODY AXIS - AS WELL)
C  CMM = CMM1 + CMMQ*QB + STORE INCREMENTS + CMDSPD + DCM
C  CMM1 = ATAB03 = BASIC PITCHING MOMENT COEFFICIENT - CM
C  CMMQ = ATAB05 = PITCH DAMPING DERIVATIVE - CMQ
C  QB            = (QEOBB*MAC)/(2*VILWF)
C                  QEOBB = PITCH RATE IN RAD/SEC = Q
C                  MAC = MEAN AERODYNAMIC CHORD = 15.94 FEET = CWING
C                  VILWF = VELOCITY IN FT/SEC = VTRFPS
C  CMDSPD = ATAB25 = DELTA CM DUE TO SPEEDBRAKE
C                    SET TO 0 DUE THE REASONS GIVEN ABOVE IN CXDSPD
C  DCM = BTAB02 = DELTA CM DUE TO 2-PLACE CANOPY (F15B) (=0.0)
C
C*********** CNM ***********************************************C
C
C  CMN = TOTAL YAWING MOMENT COEFFICIENT IN BODY AXIS
C  CMN = CMN1*EPA02 + CNDAD*DAILD + [CNDRD*DRUDD*DRFLX3]*EPA43
C        +[CNDTD*DTLX3 + DTFLX4]*DTALD + CMNP*PB + CMNR*RB + CNRB
C        +DCNB2*EPA36 + STORE INCREMENTS + CNDSPD + DCNB*BETA
C  CMN1 = ATAB12 = BASIC YAWING MOMENT COEFFICIENT  - CN (BETA)
C  EPA02 = ATAB21 = BETA MULTIPLIER TABLE
C  CNDAD = ATAB74 = YAW MOMENT COEFFICIENT DUE TO AILERON
C                   DEFLECTION -CNDA
C  DAILD =        = AILERON DEFLECTION (DEG)
C  CNDRD = ATAB68 = YAWING MOMENT COEFFICIENT DUE TO RUDDER
C                   DEFLECTION -CNDR
C  DRUDD          = RUDDER DEFLECTION (DEG)
C  DRFLX3 = ATAB85 = FLEX MULTIPLIER ON CNDRD
C  EPA43 = ATAB30 =  MULTIPLIER ON CNDR, CLDR, CYDR DUE TO SPEEDBRAKE
C  CNDTD = ATAB71 = YAWING MOMENT COEFFICIENT DUE TO DIFFERENTIAL TAIL
C                   DEFLECTION - CNDDT
C  DTFLX3 = ATAB08 = FLEX MULTIPLIER ON CNDTD
C  DTFLX4 = ATAB09 = FLEX INCREMENT ON CNDTD  (=0.0)
C  DTALD =         = DIFFERENTIAL TAIL DEFLECTION (DEG) WHICH IS
C                    DIRECTLY PROPORTIONAL TO AILERON DEFLECTION
C                    AND IS PRIMARILY USED TO ASSIST IN ROLLING
C                    THE F-15B (DTALD = 0.3*DAILD)
C  CMNP = ATAB06 = YAWING MOMENT COEFFICIENT DUE TO ROLL RATE - CNP
C  PB            = (PEOBB*SPAN)/(2*VILWF)
C                  PEOBB=ROLL RATE IN RAD/SEC = P
C                  SPAN = WING SPAN = 42.8 FT = BWING
C                  VILWF = VELOCITY IN FT/SEC = VTRFPS
C  CMNR = ATAB14 = YAW DAMPING DERIVATIVE - CNR
C  RB            = (REOBB*SPAN)/(2*VILWF)
C                  REOBB = YAW RATE IN RAD/SEC = R
C  CNRB = ATAB86 = ASSYMETRIC CN AT HIGH ALPHA
C  DCNB2 = ATAB44 = DELTA CNB WITH STABILATOR EFFECT - DELCNB (=0.0)
C  EPA36 = ATAB94 = MULTIPLIER ON DCNB2  (=BETA)
C  CNDSPD = ATAB28 = DELTA CN DUE TO SPEEDBRAKE
C                    SET TO 0 DUE TO THE REASONS GIVEN ABOVE IN CXDSPD
C  DCNB = BTAB05 = INCREMENT DELTA CNB (YAWING MOMENT) DUE TO
```

```
C                  2-PLACE CANOPY (F15B)
C
C*************************************************************************C
C
C  MISCELLANEOUS COEFFICIENTS AND NAME CONVERSION TABLE
C
C       1988 F15             ORIGINAL
C       AEROBASE NAME        PROGRAM NAME       DEFINITION
C       *************        ************       **********
C
C       AL77D                AL                 ANGLE OF ATTACK
C                                               (DEG)
C       BE77D                BETA               SIDESLIP ANGLE
C                                               (DEG)
C       BE77D                RBETA              SIDESLIP ANGLE
C                                               (RAD)
C       BO77D                ABET               ABSOLUTE VALUE OF
C                                               SIDESLIP ANGLE
C                                               (DEG)
C       DAILA                DAILA              ABSOLUTE VALUE OF
C                                               AILERON DEFLEC-
C                                               TION (DEG)
C       DAILD                DDA                AILERON DEFLEC-
C                                               TION (DEG)
C       DRUABS               ARUD               ABSOLUTE VALUE OF
C                                               RUDDER DEFLEC-
C                                               TION (DEG)
C       DRUABS               RARUD              ABSOLUTE VALUE OF
C                                               RUDDER DEFLEC-
C                                               TION (RAD)
C       DRUDD                DRUDD              RUDDER DEFLECTION
C                                               (DEG)
C       DSTBD                DELESD(R)          AVERAGE
C                                               STABILATOR
C                                               DEFLECTION
C                                               DEG (RAD)
C       DTALD                DELEDD(R)          DIFFERENTIAL TAIL
C                                               DEFLECTION
C                                               DEG (RAD)
       RBETA=BETA/DEGRAD
       DAILA=ABS(DDA)
C
       PB=(P*BWING)/(2.0d0*VTRFPS)
       QB=(Q*CWING)/(2.0d0*VTRFPS)
       RB=(R*BWING)/(2.0d0*VTRFPS)
C
C      THE F-15B AERO DATA TABLES DO NOT CONTAIN STABILITY COEFFICIENT
C      DATA FOR BETA AND RUDDER DEFLECTION ,DRUDD, LESS THAN 0
C      DEGREES.  THE ABSOLUTE VALUE OF BETA, ABET, AND THE ABSOLUTE
C      VALUE OF RUDDER DEFLECTION, ARUDD, ARE USED IN THE FOLLOWING
C      EQUATIONS.  IN RADIANS THESE PARAMETERS ARE RABET AND RARUD,
C      RESPECTIVELY.  IN SOME CASES THE COEFFICIENT IS MULTIPLIED BY A
C      -1 FOR PARAMETER VALUES LESS THAN ZERO.
```

```
C
C     EPA02 IS A MULTIPLIER THAT ADJUSTS THE PARTICULAR COEFFICIENT
C     IT IS WORKING ON (CFY1,CML1,CMN1) BY CHANGING THAT PARTICULAR
C     COEFFICIENTS SIGN (POSITIVE OR NEGATIVE) DEPENDENT ON THE SIGN
C     OF THE SIDESLIP ANGLE (BETA).  IF BETA IS NEGATIVE THEN
C     EPA02=-1.0.  IF BETA IS POSITIVE THEN EPA02=1.0.  SINCE THIS
C     FUNCTION IS DISCONTINUOUS AT THE ORIGIN A CUBIC SPLINE HAS
C     BEEN EMPLOYED TO REPRESENT THIS FUNCTION IN ORDER THAT
C     AUTO CAN RUN.
C
      IF (BETA .LT. -1.0) THEN
      EPA02S= -1.0d0
      ENDIF
C
      IF ((BETA .GE. -1.0) .AND. (BETA .LE. 1.0)) THEN
      EPA02S=-1.0d0+(1.50d0*((BETA+1.0d0)**2.0d0))-
     1 (0.50d0*((BETA+1.0d0)**3.0d0))
      ENDIF
C
      IF (BETA .GT. 1.0) THEN
      EPA02S=1.0d0
      ENDIF
C
      IF (BETA .LT. -5.0) THEN
      EPA02L= -1.0d0
      ENDIF
C
      IF ((BETA .GE. -5.0) .AND. (BETA .LE. 5.0)) THEN
      EPA02L=-1.0d0+(0.060d0*((BETA+5.0d0)**2.0d0))-
     1 (0.0040d0*((BETA+5.0d0)**3.0d0))
      ENDIF
C
      IF (BETA .GT. 5.0) THEN
      EPA02L=1.0d0
      ENDIF
C
C     ***** DIFFERENTIAL ELEVATOR *****
C
C     DTALD=0.30d0*DAILD
      DELEDD=0.30d0*DDA
      DELEDR=0.30d0*(DDA/DEGRAD)
C
C**********  CFZ  ****************************************************C
C
      CFZ1=-0.00369376+(3.78028702*RAL)+(0.6921459*RAL*RAL)-(5.0005867
     +*(RAL**3))+(1.94478199*(RAL**4))+(0.40781955*DELESR)+(0.10114579
     +*(DELESR*DELESR))
C
      CFZ=CFZ1
C
C*********  CFX  *****************************************************C
C
      CL=CFZ1/57.29578
```

```
C
C     THIS CONVERSION OF CFZ1 TO CL IS AN ARTIFACT FROM THE
C     CURVE FITTING PROCESS WHERE ALL THE INDEPENDENT VARIABLES
C     WERE ANGLES THAT WERE CONVERTED FROM DEGREES TO RADIANS.
C     IT JUST SO HAPPENED THAT FOR CFX1 ONE OF THE VARIABLES
C     WAS NOT AN ANGLE BUT A DIMENSIONLESS COEFFICIENT.
C
      CFX1=0.01806821+(0.01556573*CL)+(498.96208868*CL*CL)
     +-(14451.56518396*(CL**3))+(2132344.6184755*(CL**4))
C
C     TRANSITIONING FROM LOW AOA DRAG TABLE TO HIGH AOA DRAG TABLE
C
      CFX2=0.0267297-(0.10646919*RAL)+(5.39836337*RAL*RAL)
     +-(5.0086893*(RAL**3))+(1.34148193*(RAL**4))+
     +(0.20978902*DELESR)+(0.30604211*(DELESR**2))+0.09833617
C
      A1=20.0d0/DEGRAD
      A2=30.0d0/DEGRAD
      A12=A1+A2
      BA=2.0/(-A1**3+3.*A1*A2*(A1-A2)+A2**3)
      BB=-3.0d0*BA*(A1+A2)/2.0d0
      BC=3.0d0*BA*A1*A2
      BD=BA*A2**2*(A2-3.0d0*A1)/2.0d0
      F1=BA*RAL**3+BB*RAL**2+BC*RAL+BD
      F2=-BA*RAL**3+(3.0d0*A12*BA+BB)*RAL**2.0d0-
     +   (BC+2.0d0*A12*BB+3.0d0*A12**2*BA)*RAL+
     +   BD+A12*BC+A12**2*BB+A12**3*BA
C
      IF (RAL .LT. A1) THEN
C
        CFX=CFX1
C
      ELSEIF (RAL .GT. A2) THEN
C
        CFX=CFX2
C
      ELSE
C
        CFX=CFX1*F1+CFX2*F2
C
      ENDIF
C
C*********  CFY  ****************************************************C
C
      DTFLX5=0.975d0
      DRFLX5=0.89d0
C
      CFY1=-0.05060386-(0.12342073*RAL)+(1.04501136*RAL*RAL)
     +-(0.17239516*(RAL**3))-(2.90979277*(RAL**4))
     ++(3.06782935*(RAL**5))-(0.88422116*(RAL**6))
     +-(0.06578812*RAL*RABET)-(0.71521988*RABET)-(0.00000475273
     +*(RABET**2))-(0.04856168*RAL*DELESR)-(0.05943607*RABET*DELESR)+
     +(0.02018534*DELESR)
```

```
C
      IF (RAL .LT. .52359998) THEN
C
      CFYP=0.014606188+(2.52405655*RAL)-(5.02687473*(RAL**2))
     +-(106.43222962*(RAL**3))+(256.80215423*(RAL**4))
     ++(1256.39636248*(RAL**5))
     +-(3887.92878173*(RAL**6))-(2863.16083460*(RAL**7))+
     +(17382.72226362*(RAL**8))-(13731.65408408*(RAL**9))
      ENDIF
C
      IF ((RAL .GE. .52359998) .AND. (RAL .LE. .610865)) THEN
C
      CFYP=0.00236511+(0.52044678*(RAL-0.52359998))-(12.8597002*(RAL-
     +0.52359998)**2)+(75.46138*(RAL-0.52359998)**3)
      ENDIF
C
      IF (RAL .GT. 0.610865) THEN
C
      CFYP=0.0d0
      ENDIF
C
      IF (RAL .LT. -0.06981) THEN
C
      CFYR=0.35d0
      ENDIF
C
      IF ((RAL .GE. -0.06981) .AND. (RAL .LT. 0.0)) THEN
C
      CFYR=0.34999999+(35.4012413*(RAL+0.06981)**2)-(493.33441162*
     +(RAL+0.06981)**3)
      ENDIF
C
      IF ((RAL .GE. 0.0) .AND. (RAL .LE. 0.523599)) THEN
C
      CFYR=0.35468605-(2.26998141*RAL)+(51.82178387*RAL*RAL)
     +-(718.55069823*(RAL**3))
     ++(4570.00492172*(RAL**4))-(14471.88028351*(RAL**5))+
     +(22026.58930662*(RAL**6))-(12795.99029404*(RAL**7))
      ENDIF
C
      IF ((RAL .GT. 0.523599) .AND. (RAL .LE. 0.61087)) THEN
C
      CFYR=0.00193787+(1.78332495*(RAL-0.52359903))-(41.63198853*(RAL-
     +0.52359903)**2)+(239.97909546*(RAL-0.52359903)**3)
      ENDIF
C
      IF (RAL .GT. 0.61087) THEN

      CFYR=0.0d0
      ENDIF
C
      IF (RAL .LT. 0.55851) THEN
C
```

```
      CYDAD=-0.00020812+(0.00062122*RAL)+(0.00260729*RAL*RAL)
     ++(0.00745739*(RAL**3))-(0.0365611*(RAL**4))
     +-(0.04532683*(RAL**5))+(0.20674845*(RAL**6))
     +-(0.13264434*(RAL**7))-(0.00193383*(RAL**8))
      ENDIF
C
      IF ((RAL .GE. 0.55851) .AND. (RAL .LT. 0.61087)) THEN
C
      CYDAD=0.00023894+(0.00195121*(RAL-0.55851001))+(0.02459273
     +*(RAL-0.55851001)**2)-(0.1202244*((RAL-0.55851001)**3))
      ENDIF
C
      IF (RAL .GE. 0.61087) THEN
C
      CYDAD=0.27681285-(2.02305395*RAL)+(6.01180715*RAL*RAL)
     +-(9.24292188*(RAL**3))+(7.59857819*(RAL**4))
     +-(2.8565527*(RAL**5))+(0.25460503*(RAL**7))
     +-(0.01819815*(RAL**9))
      ENDIF
C
C
C     IF (RAL .LE. 0.0) THEN
C     EPA43=1.0d0
C     ENDIF
C     IF (RAL .GT. 0.0 AND .LE. 0.6283185) THEN
C     0.6283185 RADIANS = 36 DEGREES
C     EPA43=0.9584809+(4.13369452*RAL)-(18.31288396*RAL*RAL)+
C    +(19.5511466*(RAL**3))-(1.09295946*RAL*DSPBD)+(0.17441033*
C    +DSPBD*DSPBD)
C     ENDIF
C     IF (RAL .GT. 0.6283185) THEN
      EPA43=1.0d0
C     ENDIF
C          ***********************************************************
C          *  NOTE - THE PARAMETER EPA43 IS A MULTIPLIER ON RUDDER  *
C          *  EFFECTIVENESS DUE TO SPEEDBRAKE.  THIS TABLE IS ALSO  *
C          *  LIMITED TO 36 DEG AOA.  HOWEVER, THERE IS NO AERODY   *
C          *  NAMIC EFFECT FOR ANGLES OF ATTACK LESS THAN 16 DEG,   *
C          *  AND THE SPEEDBRAKE IS AUTOMATICALLY RETRACTED AT AOA  *
C          *  GREATER THAN 15 DEG.  THEREFORE, THIS TABLE SHOULD    *
C          *  NOT BE NECESSARY FOR THE ORDINARY OPERATION OF THE    *
C          *  AIRCRAFT                                              *
C          ***********************************************************
C
      CYDRD=0.00310199+(0.00119963*RAL)+(0.02806933*RAL*RAL)
     +-(0.12408447*(RAL**3))-(0.12032121*(RAL**4))
     ++(0.79150279*(RAL**5))-(0.86544347*(RAL**6))
     ++(0.27845115*(RAL**7))+(0.00122999*RAL*RARUD)+(0.00145943
     +*RARUD)-(0.01211427*RARUD*RARUD)+(0.00977937*(RARUD**3))
C
      CYDTD=-0.00157745-(0.0020881*RAL)+(0.00557239*RAL*RAL)
     +-(0.00139886*(RAL**3))+(0.04956247*(RAL**4))
     +-(0.0135353*(RAL**5))-(0.11552397*(RAL**6))
```

```
     ++(0.11443452*(RAL**7))-(0.03072189*(RAL**8))-(0.01061113*
     +(RAL**3)*DELESR)-(0.00010529*RAL*RAL*DELESR*DELESR)
     +-(0.00572463*RAL*DELESR*DELESR)
     ++(0.01885361*RAL*RAL*DELESR)-(0.01412258*RAL*(DELESR**2))
     +-(0.00081776*DELESR)+(0.00404354*(DELESR**2))-
     +(0.00212189*(DELESR**3))+(0.00655063*(DELESR**4))
     ++(0.03341584*(DELESR**5))
C
      RALY1=0.6108652
      RALY2=90.0d0/DEGRAD
      RBETY1=-0.0872665
      RBETY2=0.1745329
C
      AY=0.1640d0
      ASTARY=0.95993
      BSTARY=0.087266
C
      ZETAY=(2.0D0*ASTARY-(RALY1+RALY2))/(RALY2-RALY1)
      ETAY=(2.0D0*BSTARY-(RBETY1+RBETY2))/(RBETY2-RBETY1)
C
      X=(2.0D0*RAL-(RALY1+RALY2))/(RALY2-RALY1)
      Y=(2.0D0*RBETA-(RBETY1+RBETY2))/(RBETY2-RBETY1)
C
      FY=((5.0D0*(ZETAY**2))-(4.0D0*ZETAY*X)-1.0D0)*(((X**2)-1.0D0)
     +**2)*(1.0D0/(((ZETAY**2)-1.0D0)**3))
C
      GY=((5.0D0*(ETAY**2))-(4.0D0*ETAY*Y)-1.0D0)*(((Y**2)-1.0D0)**2)
     +*(1.0D0/(((ETAY**2)-1.0D0)**3))
C
      CYRB=AY*FY*GY
C
      IF (RAL .LT. 0.6108652) THEN
C
      CYRB=0.0d0
      GOTO 500
      ENDIF
C
      IF ((RBETA .LT. -0.0872665) .OR. (RBETA .GT. 0.1745329)) THEN
C
      CYRB=0.0d0
      GOTO 500
      ENDIF
C
  500 CFY=(CFY1*EPA02L)+(CYDAD*DDA)+(CYDRD*DRUDD*DRFLX5*EPA43)+
     +((CYDTD*DTFLX5)*DELEDD)+(CFYP*PB)+(CFYR*RB)
     ++CYRB
C
C************  CLM  ************************************************C
C
      DTFLX1=0.9750d0
      DRFLX1=0.850d0
C
      CML1=-0.00238235-(0.04616235*RAL)+(0.10553168*RAL*RAL)
```

```
     ++(0.10541585*(RAL**3))-(0.40254765*(RAL**4))
     ++(0.32530491*(RAL**5))-(0.08496121*(RAL**6))
     ++(0.00112288*(RAL**7))-(0.05940477*RABET*RAL)-
     +(0.07356236*RABET)-(0.00550119*RABET*RABET)+(0.00326191
     +*(RABET**3))
C
      IF (RAL .LT. 0.29671) THEN
C
      CMLP=-0.24963201-(0.03106297*RAL)+(0.12430631*RAL*RAL)
     +-(8.95274618*(RAL**3))+(100.33109929*(RAL**4))
     ++(275.70069578*(RAL**5))-(1178.83425699*(RAL**6))
     +-(2102.66811522*(RAL**7))+(2274.89785551*(RAL**8))
      ENDIF
C
      IF ((RAL .GE. 0.29671) .AND. (RAL .LT. 0.34907)) THEN
C
      CMLP=-0.1635261-(3.77847099*(RAL-0.29671001))+(147.47639465
     +*(RAL-0.29671001)**2)-(1295.94799805*(RAL-0.29671001)**3)
      ENDIF
C
      IF (RAL .GE. 0.34907) THEN
C
      CMLP=-1.37120291+(7.06112181*RAL)-(13.57010422*RAL*RAL)
     ++(11.21323850*(RAL**3))
     +-(4.26789425*(RAL**4))+(0.6237381*(RAL**5))
      ENDIF
C
      IF (RAL .LT. 0.7854) THEN
C
      CMLR=0.03515391+(0.59296381*RAL)+(2.27456302*RAL*RAL)
     +-(3.8097803*(RAL**3))
     +-(45.83162842*(RAL**4))+(55.31669213*(RAL**5))+
     +(194.29237485*(RAL**6))-(393.22969953*(RAL**7))+(192.20860739*
     +(RAL**8))
      ENDIF
C
      IF ((RAL .GE. 0.7854) .AND. (RAL .LE. 0.87266)) THEN
C
      CMLR=0.0925579071-(0.6000000238*(RAL-0.7853999734))
     ++(1.3515939713*((RAL-0.7853999734)**2))
     ++(29.0733299255*((RAL-0.7853999734)**3))
      ENDIF
C
      IF (RAL .GT. 0.87266) THEN
C
      CMLR=-311.126041+(1457.23391042*RAL)-(2680.19461944*RAL*RAL)+
     +(2361.44914738*(RAL**3))-(893.83567263*(RAL**4))+(68.23501924*
     +(RAL**6))-(1.72572994*(RAL**9))
      ENDIF
C
```

```
      CLDAD=0.00057626+(0.00038479*RAL)-(0.00502091*RAL*RAL)
     ++(0.00161407*(RAL**3))+(0.02268829*(RAL**4))
     +-(0.03935269*(RAL**5))+(0.02472827*(RAL**6))
     +-(0.00543345*(RAL**7))+(0.0000007520348*DELESR*RAL)+
     +(0.000000390773*DELESR)
C
      CLDRD=0.00013713-(0.00035439*RAL)-(0.00227912*RAL*RAL)
     ++(0.00742636*(RAL**3))+(0.00991839*(RAL**4))
     +-(0.04711846*(RAL**5))+(0.046124*(RAL**6))
     +-(0.01379021*(RAL**7))+(0.00003678685*RARUD*RAL)+
     +(0.00001043751*RARUD)-(0.00015866*RARUD*RARUD)+(0.00016133
     +*(RARUD**3))
C
      CLDTD=0.00066663+(0.00074174*RAL)+(0.00285735*RAL*RAL)
     +-(0.02030692*(RAL**3))-(0.00352997*(RAL**4))
     ++(0.0997962*(RAL**5))-(0.14591227*
     +(RAL**6))+(0.08282004*(RAL**7))
     +-(0.0168667*(RAL**8))+(0.00306142*(RAL**3)*DELESR)
     +-(0.00110266*RAL*RAL*(DELESR**2))+(0.00088031*RAL*
     +(DELESR**2))-(0.00432594*RAL*RAL*DELESR)-
     +(0.00720141*RAL*(DELESR**3))
     +-(0.00034325*DELESR)+(0.00033433*(DELESR**2))+(0.00800183
     +*(DELESR**3))-(0.00555986*(DELESR**4))-(0.01841172*(DELESR**5))
C
      IF (RAL .LT. 0.0) THEN
C
      DCLB=-0.000060d0
      ENDIF
C
      IF ((RAL .GE. 0.0) .AND. (RAL .LE. 0.209434)) THEN
C
      DCLB=-0.000060d0+(0.0041035078*RAL*RAL)-(0.0130618699*(RAL**3))
      ENDIF
C
      IF (RAL .GT. 0.209434) THEN
C
      DCLB=0.0d0
      ENDIF
C
      CML=(CML1*EPA02S)+(CLDAD*DDA)+(CLDRD*DRUDD*DRFLX1*EPA43)+
     +((CLDTD*DTFLX1)*DELEDD)+(CMLP*PB)+(CMLR*RB)+(DCLB*BETA)
C
C**************  CMM  *********************************************C
C
      CMM1=0.00501496-(0.08004901*RAL)-(1.03486675*RAL*RAL)
     +-(0.68580677*(RAL**3))+(6.46858488*(RAL**4))
     +-(10.15574108*(RAL**5))+
     +(6.44350808*(RAL**6))-(1.46175188*(RAL**7))
     ++(0.24050902*RAL*DELESR)
     +-(0.42629958*DELESR)-(0.03337449*DELESR*DELESR)
     +-(0.53951733*(DELESR**3))
C
C     modified 25 Jul 90 to use new curve fit for CMQ
```

```
C
C          OLD EQUATION
C
C      IF (RAL .LE. 0.25307) THEN
C
C      CMMQ=-3.8386262+(13.54661297*RAL)+(402.53011559*RAL*RAL)
C     +-(6660.95327122*(RAL**3))-(62257.89908743*(RAL**4))
C     ++(261526.10242329*(RAL**5))
C     ++(2177190.33155227*(RAL**6))-(703575.13709062*(RAL**7))-
C     +(20725000.34643054*(RAL**8))-(27829700.5333364?*(RAL**9))
C      ENDIF
C
C      IF ((RAL .GT. 0.25307) .AND. (RAL .LT. 0.29671)) THEN
C
C      CMMQ=-8.4926528931-(2705.3000488281*(RAL-0.2530699968))
C     ++(123801.5*(RAL-0.2530699968)**2)
C     +-(1414377*(RAL-0.2530699968)**3)
C      ENDIF
C
C      IF (RAL .GE. .29671) THEN
C
C      CMMQ=47.24676075-(709.60757056*RAL)+(3359.08807193*RAL*RAL)-
C     +(7565.32017266*(RAL**3))+(8695.1858091*(RAL**4))
C     +-(4891.77183313*(RAL**5))+(1061.55915089*(RAL**6))
C      ENDIF
C
C      CMMQ vs. alpha n degrees
C
C          NEW EQUATION
C
C      convert alpha to degrees
C
       A=RAL*DEGRAD
c
       F1=-4.33509d0+A*(-0.141624d0+A*(0.0946448d0+A*(-0.00798481d0
      + +A*(-0.00168344d0+A*(0.000260037d0+A*(6.64054d-6+A*(
      + -2.20055d-6+A*(-2.74413d-8+A*(7.14476d-9+A*
      + 2.07046d-10)))))))))
c
       F2=-302.567+a*(106.288+a*(-14.7034+A*(1.02524+A*(-0.0393491
      + +A*(0.00084082+A*(-9.365e-6+A*4.2355e-8))))))
c
       F3=1724.99+A*(-158.944+A*(5.59729+A*(-0.0949624+A*(
      + 0.000779066+A*(-2.47982e-6)))))
c
c     ramp functions
c
       R1=1.0-0.75*(A-10.0)**2+0.25*(A-10.0)**3
       R2=1.0-R1
       R3=1.0-7.5*(A-40.0)**2/62.5+(A-40.0)**3/62.5
       R4=1.0-R3
c
       IF(A.LT.10.0)THEN
```

```
        CMMQ=F1
      ELSEIF(A.LT.12.0)THEN
        CMMQ=F1*R1+F2*R2
      ELSEIF(A.LT.40.0)THEN
        CMMQ=F2
      ELSEIF(A.LT.45.0)THEN
        CMMQ=F2*R3+F3*R4
      ELSE
        CMMQ=F3
      ENDIF
C
      CMM=CMM1+(CMMQ*QB)
C
C************  CNM  *************************************************C
C
      DTFLX3=0.9750d0
      DRFLX3=0.890d0
C
      CMN1=0.01441512+(0.02242944*RAL)-(0.30472558*(RAL**2))
     ++(0.14475549*(RAL**3))
     ++(0.93140112*(RAL**4))-(1.52168677*(RAL**5))+
     +(0.90743413*(RAL**6))-(0.16510989*(RAL**7))
     +-(0.0461968*(RAL**8))
     ++(0.01754292*(RAL**9))-(0.17553807*RAL*RABET)+
     +(0.15415649*RAL*RABET*DELESR)
     ++(0.14829547*(RAL**2)*(RABET**2))
     +-(0.11605031*(RAL**2)*RABET*DELESR)
     +-(0.06290678*(RAL**2)*(DELESR**2))
     +-(0.01404857*(RAL**2)*(DELESR**2))
     ++(0.07225609*RABET)-(0.08567087*(RABET**2))
     ++(0.01184674*(RABET**3))
     +-(0.00519152*RAL*DELESR)+(0.03865177*RABET*DELESR)
     ++(0.00062918*DELESR)
C
      CNDRD=-0.00153402+(0.00184982*RAL)-(0.0068693*RAL*RAL)
     ++(0.01772037*(RAL**3))
     ++(0.03263787*(RAL**4))-(0.15157163*(RAL**5))+(0.18562888
     +*(RAL**6))-(0.0966163*(RAL**7))+(0.01859168*(RAL**8))+(0.0002587
     +*RAL*DELESR)-(0.00018546*RAL*DELESR*RBETA)-(0.00000517304*RBETA)
     +-(0.00102718*RAL*RBETA)-(0.0000689379*RBETA*DELESR)-(0.00040536
     +*RBETA*RARUD)-(0.00000480484*DELESR*RARUD)
     +-(0.00041786*RAL*RARUD)
     ++(0.0000461872*RBETA)+(0.00434094*(RBETA**2))
     +-(0.00490777*(RBETA**3))
     ++(0.000005157867*RARUD)+(0.00225169*RARUD*RARUD)-(0.00208072
     +*(RARUD**3))
C
      IF (RAL .LT. 0.55851) THEN
C
      CMNP=-0.00635409-(1.14153932*RAL)+(2.82119027*(RAL**2))+
     +(54.4739579*(RAL**3))-(140.89527667*(RAL**4))-(676.73746128*
     +(RAL**5))+(2059.18263976*(RAL**6))+(1579.41664748*(RAL**7))
     +-(8933.08535712*(RAL**8))+(6806.54761267*(RAL**9))
```

```
      ENDIF
C
      IF ((RAL .GE. 0.55851001) .AND. (RAL .LE. 0.61087)) THEN
C
      CMNP=-.07023239+(1.085815*(RAL -0.55851))
     ++(8.852651*((RAL-.55851)**2))-(192.6093*((RAL-0.55851)**3))
      ENDIF
C
      IF (RAL .GT. 0.61087) THEN
C
      CMNP=-71.03693533+(491.32506715*RAL)
     +-(1388.11177979*(RAL**2))+
     +(2033.48621905*(RAL**3))
     +-(1590.91322362*(RAL**4))+(567.38432316*(RAL**5))
     +-(44.97702536*(RAL**7))+(2.8140669*(RAL**9))
      ENDIF
C
      IF (RAL .LE. -.069813) THEN
C
      CMNR= -0.28050d0
      ENDIF
C
      IF ((RAL .GT. -.069813) .AND. (RAL .LT. 0.0)) THEN
C
      CMNR=-0.2804999948+(35.9903717041*(RAL+.0698129982)**2)
     +-(516.1574707031*(RAL+.0698129982)**3)
      ENDIF
C
      IF ((RAL .GE. 0.0) .AND. (RAL .LE. 0.78539801)) THEN
C
      CMNR=-.28071511-(2.52183924*RAL)+(68.90860031*(RAL**2))
     +-(573.23100511*(RAL**3))+(2009.08725005*(RAL**4))
     +-(3385.15675307*(RAL**5))
     ++(2730.49473149*(RAL**6))-(848.12322034*(RAL**7))
      ENDIF
C
      IF ((RAL .GT. 0.78539801) .AND. (RAL .LT. 0.95993102)) THEN
C
      CMNR=-0.1096954+(0.52893072*(RAL-0.78539801))-(6.09109497*(RAL-
     +0.78539801)**2)+(17.47834015*(RAL-0.78539801)**3)
      ENDIF
C
      IF (RAL .GE. 0.95993102) THEN
C
      CMNR=-0.110d0
      ENDIF
C
      CNDTD=0.00058286+(0.0007341*RAL)-(0.00746113*RAL*RAL)
     +-(0.00685223*(RAL**3))
     ++(0.03277271*(RAL**4))-(0.02791456*(RAL**5))
     ++(0.00732915*(RAL**6))
     ++(0.00120456*RAL*DELESR)-(0.00168102*DELESR)+(0.0006462*
     +DELESR*DELESR)
```

```
C
      CNDAD=0.00008228887-(0.00014015*RAL)-(0.0013493*RAL*RAL)+
     +(0.00020487*(RAL**3))+(0.00561241*(RAL**4))
     +-(0.00634392*(RAL**5))
     ++(0.00193323*(RAL**6))-(2.05815E-17*(RAL*DAILA))+(3.794816E-17*
     +(DAILA**3))
C
      DCNB=-2.500E-4
C
      RALN1=0.69813
      RALN2=90.0d0/DEGRAD
      RBETN1=-0.174532
      RBETN2=0.34906
C
      AN=0.034d0
      ASTARN=1.0472d0
      BSTARN=0.087266
C
      ZETAN=(2.0D0*ASTARN-(RALN1+RALN2))/(RALN2-RALN1)
      ETAN=(2.0D0*BSTARN-(RBETN1+RBETN2))/(RBETN2-RBETN1)
C
      XN=(2.0D0*RAL-(RALN1+RALN2))/(RALN2-RALN1)
      YN=(2.0D0*RBETA-(RBETN1+RBETN2))/(RBETN2-RBETN1)
C
      FN=((5.0D0*(ZETAN**2))-(4.0D0*ZETAN*XN)-1.0D0)*
     +(((XN**2)-1.0D0)**2)/(((ZETAN**2)-1.0D0)**3)
C
      GN=((5.0D0*(ETAN**2))-(4.0D0*ETAN*YN)-1.0D0)*
     +(((YN**2)-1.0D0)**2)/(((ETAN**2)-1.0D0)**3)
C
      CNRB=AN*FN*GN
C
      IF (RAL .LT. 0.69813) THEN
C
      CNRB=0.0d0
      GOTO 1000
      ENDIF
C
      IF ((RBETA .LT. -0.174532) .OR. (RBETA .GT. 0.34906)) THEN
C
      CNRB=0.0d0
      GOTO 1000
      ENDIF
C
 1000 CMN=(CMN1*EPA02S)+(CNDAD*DDA)+((CNDRD*DRUDD*DRFLX3)*EPA43)+
     +((CNDTD*DTFLX3)*DELEDD)+(CMNP*PB)+(CMNR*RB)+(DCNB*BETA)
     ++CNRB
C
C***********  THRUST TERMS  ***********************************C
```

```
C
C     THIS SECTION DETERMINES THE EFFECT OF THE THRUST VALUES FOR
C     ADDITION TO CX, CY, CZ, CLM, CMM, AND CNM VALUES DETERMINED
C     ABOVE AND CONTAIN THE FOLLOWING VARIABLES:
C     CPTAL  - COSINE OF PITCH VECTOR ANGLE
C     SPTAL  - SINE OF PITCH VECTOR ANGLE
C     CYTAL  - COSINE OF YAW VECTOR ANGLE
C     SYTAL  - SINE OF YAW VECTOR ANGLE
C     ENGPQ  - PORT ENGINE THRUST/(QBAR*S)
C     ENGSQ  - STARBOARD ENGINE THRUST/(QBAR*S)
C     CXENGP - COEFFICIENT OF PORT ENGINE THRUST IN X DIRECTION
C     CXENGS - COEFFICIENT OF SBRD ENGINE THRUST IN X DIRECTION
C     CXT    - COEFFICIENT OF TOTAL THRUST IN X DIRECTION
C     CYENGP - COEFFICIENT OF PORT ENGINE THRUST IN Y DIRECTION
C     CYENGS - COEFFICIENT OF SRBD ENGINE THRUST IN Y DIRECTION
C     CYT    - COEFFICIENT OF TOTAL THRUST IN Y DIRECTION
C     CZENGP - COEFFICIENT OF PORT ENGINE THRUST IN Z DIRECTION
C     CZENGS - COEFFICIENT OF STARBOARD ENGINE THRUST IN Z DIRECTION
C     CZT    - COEFFICIENT OF TOTAL THRUST IN Z DIRECTION
C     CLMT   - ROLL MOMENT COEFFICIENT DUE TO THRUST
C     CMMT   - PITCH MOMENT COEFFICIENT DUE TO THRUST
C     CNMT   - YAW MOMENT COEFFICIENT DUE TO THRUST
C
      CPTAL=COS(PTAL)
      SPTAL=SIN(PTAL)
      CYTAL=COS(YTAL)
      SYTAL=SIN(YTAL)
      CRAL=COS(RAL)
      SRAL=SIN(RAL)
C
      ENGPQ=ENGP/QBARS
      ENGSQ=ENGS/QBARS
C
      CXENGP=ENGPQ*CPTAL*CYTAL
      CXENGS=ENGSQ*CPTAL*CYTAL
      CXT=CXENGP+CXENGS
C
      CYENGP=ENGPQ*CPTAL*SYTAL
      CYENGS=ENGSQ*CPTAL*SYTAL
      CYT=CYENGP+CYENGS
C
      CZENGP=ENGPQ*SPTAL
      CZENGS=ENGSQ*SPTAL
      CZT=CZENGS+CZENGP
C
      CLMT=(CZENGS-CZENGP)*(25.5d0/12.0d0)/BWING
C
      CMMT=CXT*(0.25d0/12.0d0)/CWING+
     +     CZT*20.219d0/CWING
C
      CNMT=(CXENGP-CXENGS)*(25.5d0/12.0d0)/BWING-
     +     CYT*20.219d0/BWING
C
```

```
      CX=CFZ*SRAL-CFX*CRAL+CXT
      CY=CFY+CYT
      CZ=-(CFZ*CRAL+CFX*SRAL)+CZT
      CLM=CML+CLMT
      CMM=CMM+CMMT
      CNM=CMN+CNMT
C
C     THE 0.25/12.0 IS THE Z OFFSET OF THE THRUST FROM THE CG
C     THE 20.219 IS THE X OFFSET OF THE THRUST FROM THE CG
C     THE 25.5/12.0 IS THE Y OFFSET OF THE THRUST FROM THE CG
C
C    RETURN CX, CY, CZ, CLM, CMM, CNM TO CALLING PROGRAM.
C
C
      RETURN
      END
```

Appendix C: Complete Bifurcation Diagrams

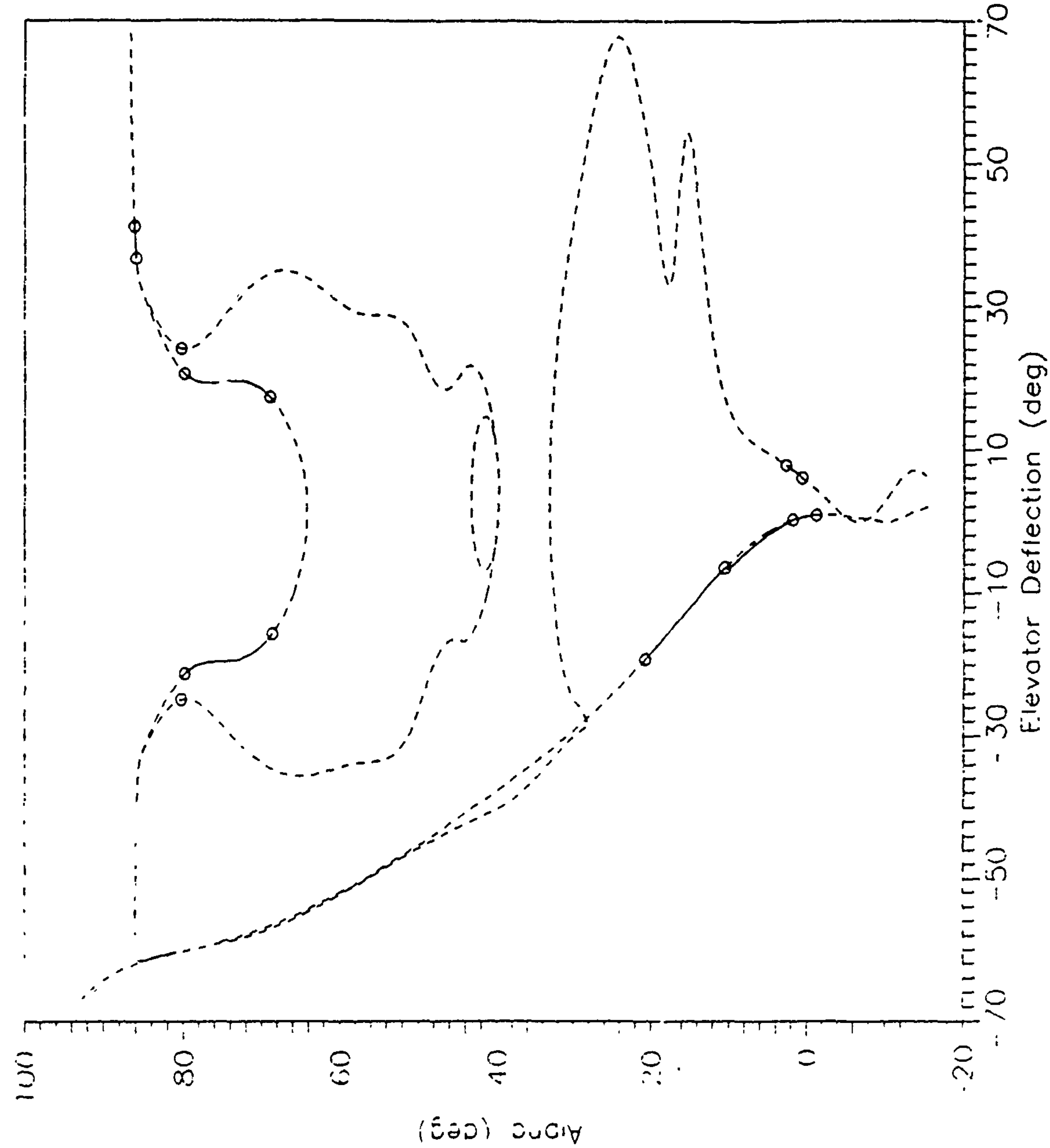

Figure C-1 Bifurcation Diagram of Elevator Sweep, T = 8300

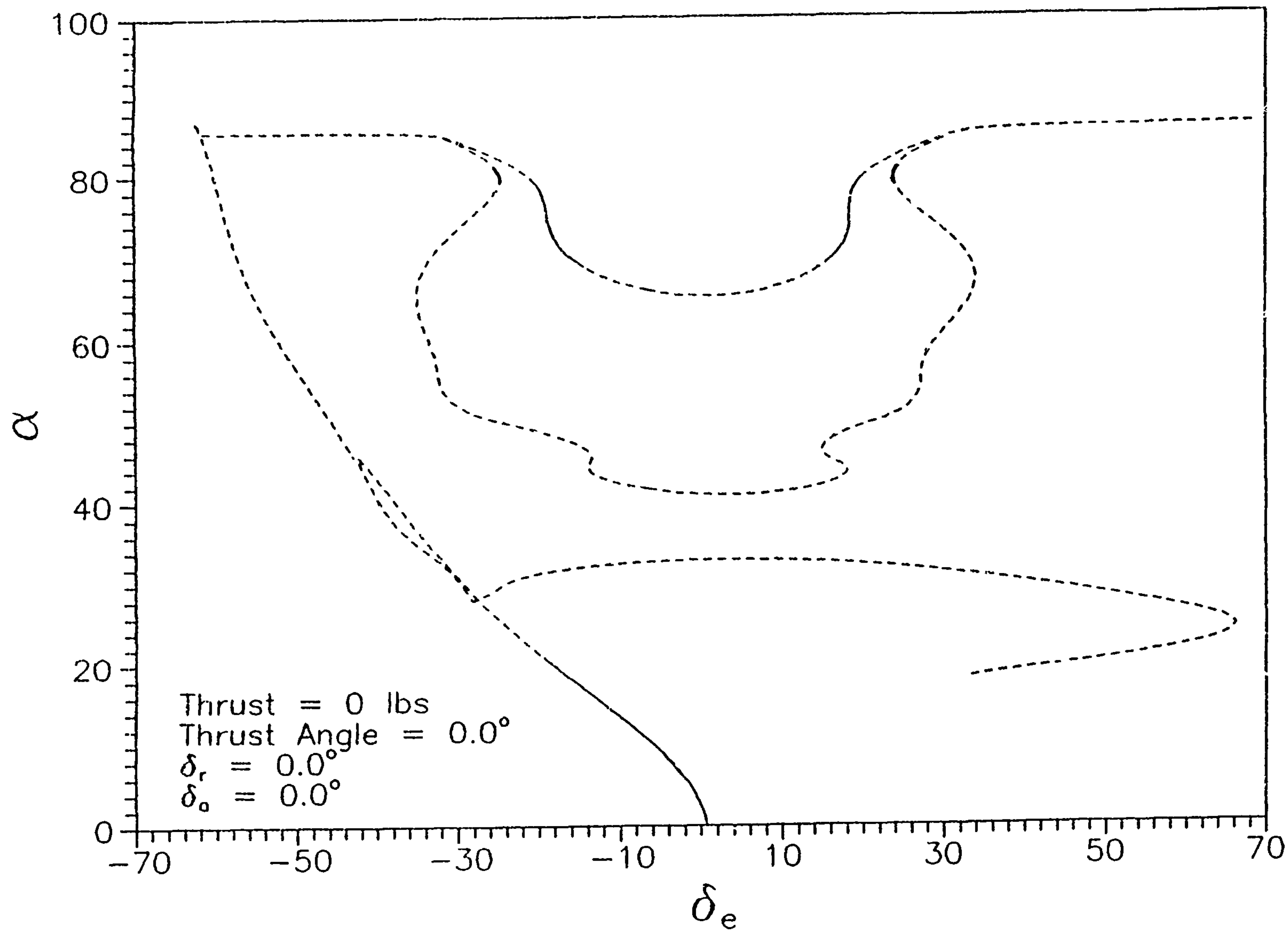

Figure C-2 Bifurcation Diagram of Elevator Sweep, T = 0 lbs

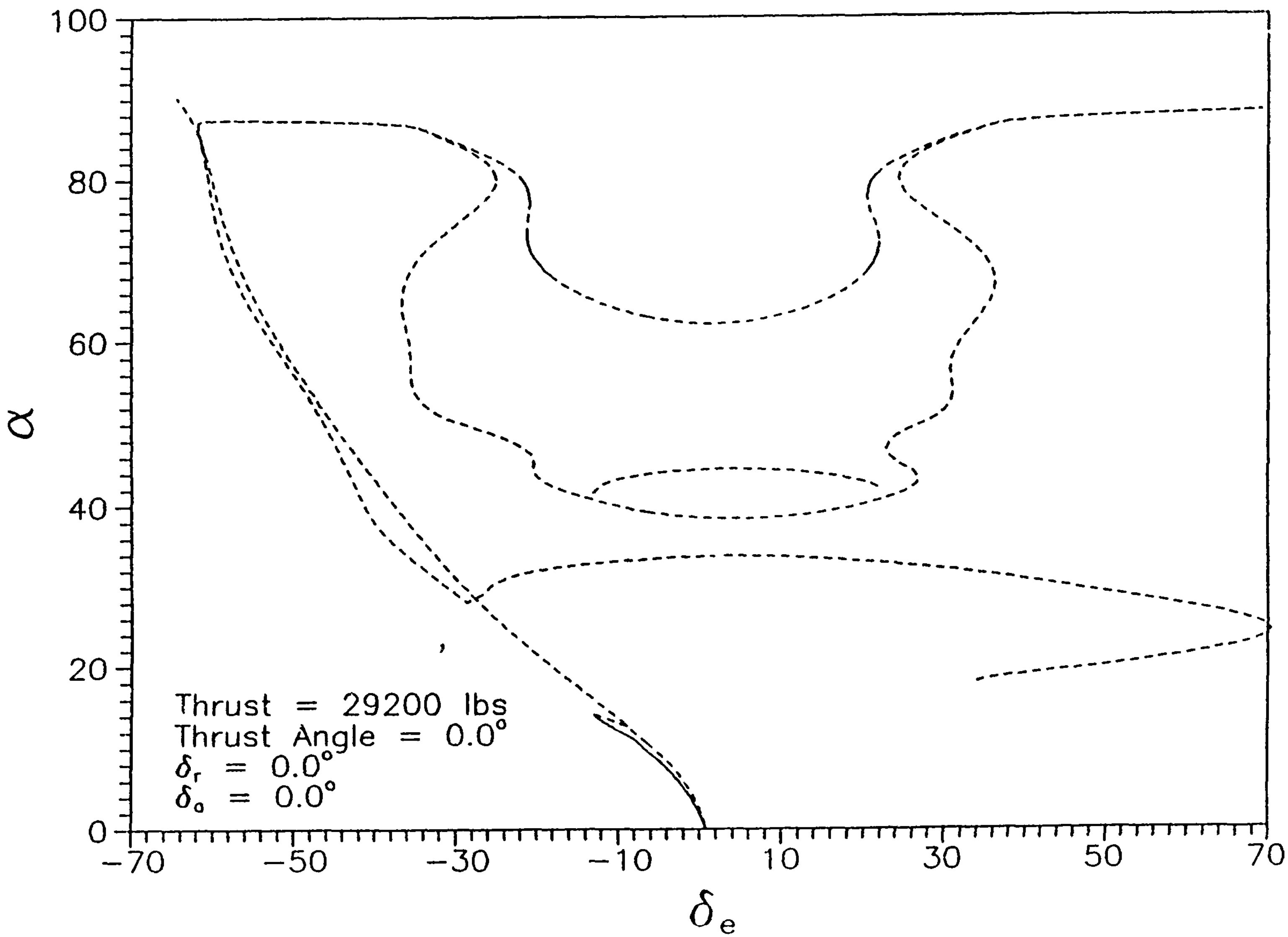

Figure C-3 Bifurcation Diagram of Elevator Sweep, T = 29200lbs

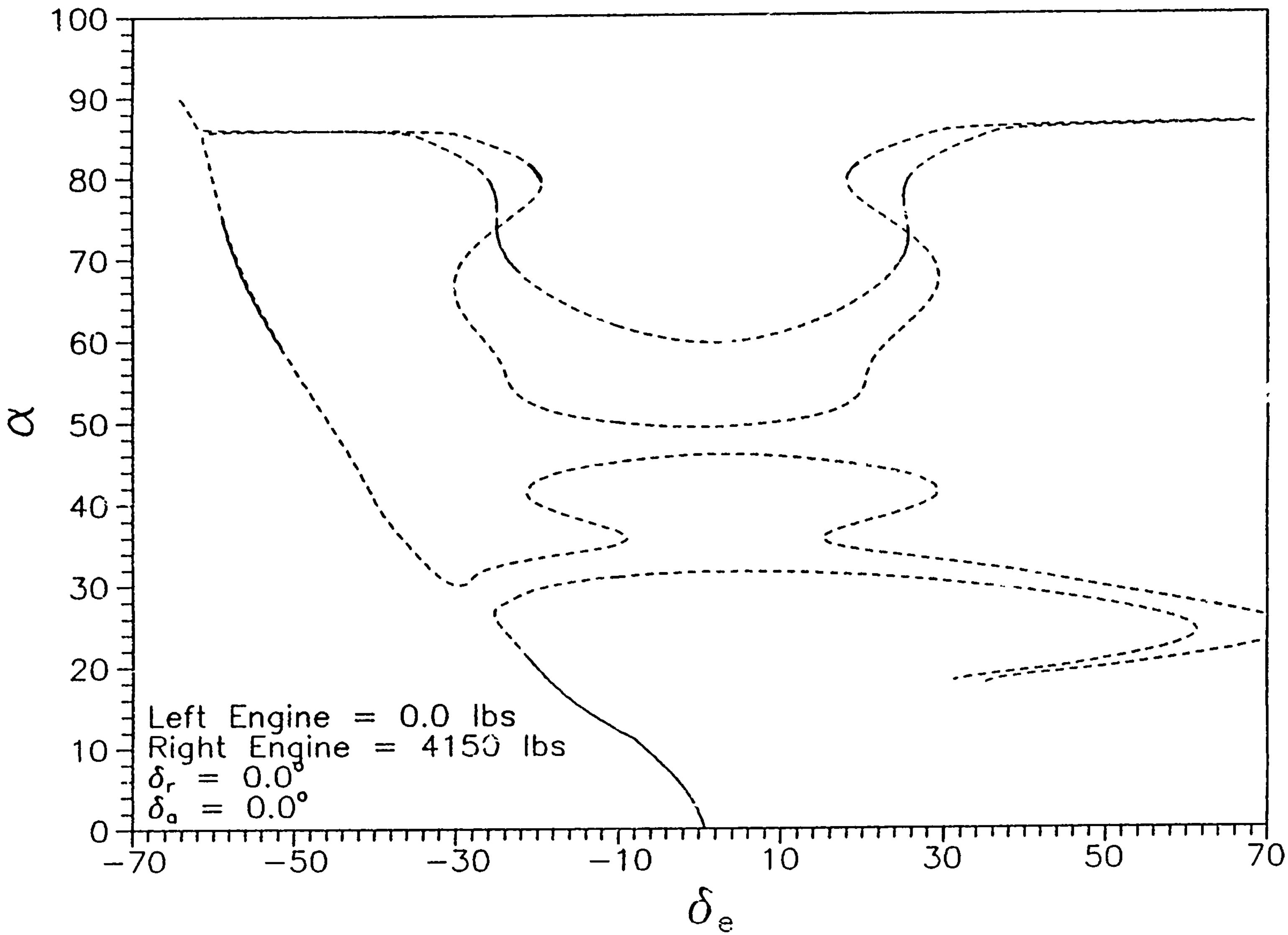

Figure C-4 Bifurcation Diagram of Elevator Sweep, Left Engine = 0 lbs

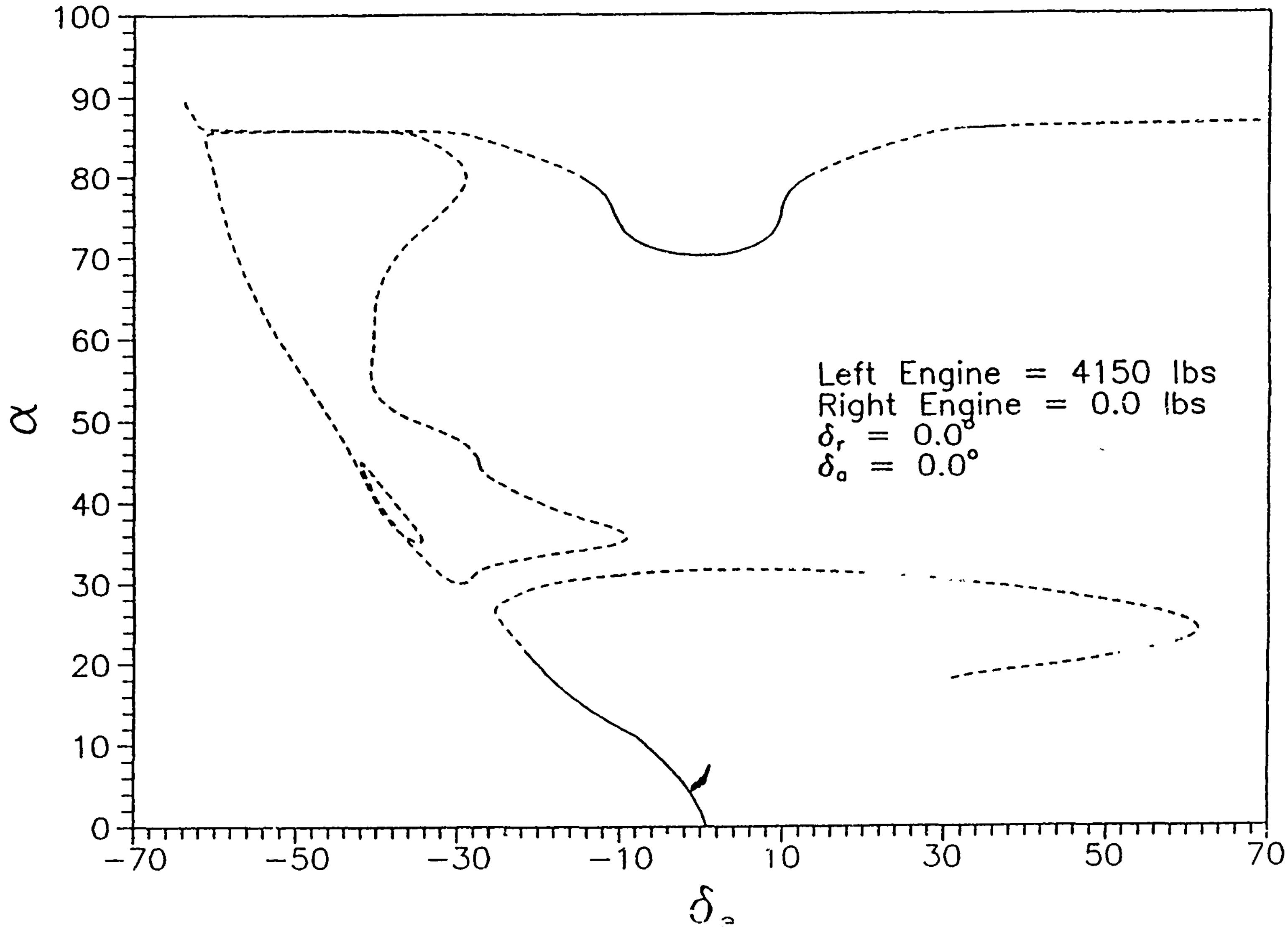

Figure C-5 Bifurcation Diagram of Elevator Sweep, Right Engine = 0 lbs

Bibliography

1. Adams, W.M., Jr. *Analytic Prediction of Aircraft Equilibrium Spin Characteristics*, NASA Technical Note D-6926, 1972.

2. Anderson, J. "Agile Fighter Aircraft Simulation," *27th Aerospace Sciences Meeting*. Paper no 89-0015. American Institute of Aeronautics and Astronautics: Reno, NV January 9-12, 1989.

3. Barnhart, Billy. *F-15 Rotary Balance Data for an Angle-of-Attack Range of 8 Degrees to 90 Degrees*. NASA Contractor Report CR-3478, May 1982.

4. Barnhart, Billy. *Analysis of Rotary Balance Data for the F-15 Airplane Including the Effect of Conformal Fuel Tanks*. NASA Contractor Report CR-3479, April 1982.

5. Barth, Capt Thomas J. *Determination of High Angle-of-Attack Stability of the F-15B Aircraft Using Bifurcation Analysis*. MS Thesis, AFIT/GAE/AA/87D-1. School of Engineering, Air Force Institute of Technology (AU), Wright-Patterson AFB OH, December 1987.

6. Baumann, Capt Daniel D. *F-15B High Angle-of-Attack Phenomena and Spin Prediction Using Bifurcation Analysis*. MS Thesis, AFIT/GAE/ENY/89D-01. School of Engineering, Air Force Institute of Technology (AU), Wright-Patterson AFB OH, December 1989.

7. Beck, Capt Jeffery A. *Bifurcation Analysis of a Model Fighter Aircraft with Control Augmentation*. MS Thesis, AFIT/GAE/ENY/89D-02. School of Engineering, Air Force Institute of Technology (AU), Wright-Patterson AFB OH, December 1989.

8. Burk, Sanger M. *Analytical Determination of the Mechanism of an Airplane Spin Recovery with Different Applied Yawing Moments by the Use of Rotary-Balence Data*, NACA Technical Note 3321, December 1954.

9. Carrol, James V. and Raman K. Mehra. "Bifurcation Analysis of Nonlinear Aircraft Dynamics," AIAA paper 82-4254, *Journal of Guidance and Control*, 5: 529-536 (September-October 1982).

10. Chambers, Joseph R. "High Angle-of-Attack Aerodynamics: Lessons Learned," *AIAA 4th Applied Aerodynamics Conference*. Paper no 86-1774-CP. San Diego, Ca: American Institute of Aeronautics and Astronautics, June 9-11, 1986.

11. Doedel, Eusebius and Jean Pierre Kernévez. *Software for Continuation Problems in Ordinary Differential Equations with Applications*. May 1986.

12. Etkin, Bernard. *Dynamics of Atmospheric Flight*. New York: John Wiley & Sons, Inc., 1972.

13. Grafton, Sue B. *A Study to Determine Effects of Applying Thrust on Recovery from Incipient and Developed Spins for Four Airplane Configurations*, NASA Technical Note D-3416, June 1966.

14. Grantham, William D. and Stanley H. Scher. *Analytical Investigation and Prediction of Spin and Recovery Characteristics of the North American X-15 Airplane*. NASA Technical Memorandum X-294, October 1960.

15. Guicheteau, P. "Bifurcation Theory Applied to the Study of Control Losses on Combat Aircraft," *La Recherche Aérospataile*, 1982.

16. Guicheteau, P. Bifurcation Theory in Flight Dynamics; An Application to a Real Combat Aircraft. CAS 90 Congress Paper no. 1990-116, Stockhlolm (Sweden): ONERA, September 9-14 1990.

17. Hawkins, Capt Carl A. *Application of Bifurcation And Catastrophe Theories to the Near Stall Flight Mechanics*. MS Thesis. Massachusetts Institute of Technology, December 1985 (AD-A167697).

18. Hui, W.H. and M. Tobak. "Bifurcation Analysis of Aircraft Pitching Motions About Large Mean Angles of Attack," *Journal of Guidance and Control*, 7 (January-February 1984).

19. Jahnke, Craig C. *Application of Dynamical Systems Theory to Nonlinear Aircraft Dynamics*. PhD Dissertation. Division of Engineering and Applied Sciences, California Institue of Technology, Pasadena Ca, January 1990.

20. Jahnke, Craig C. and Fred E.C. Culick. "Application of Dynamical Systems Theory to Nonlinear Aircraft Dynamics," *AIAA Atmospheric Flight Mechanics Conference*. Paper no 88-4372. Washington D.C: American Institute of Aeronautics and Astronautics, August 1988.

21. Jahnke, C. and F. Culick. "Application of Dynamical Systems Theory to the High Angle of Attack Dynamics of the F-14," *28th Aerospace Sciences Meeting*. Paper no 90-0221. Reno, NV: American Institute of Aeronautics and Astronautics, January 8-11, 1990.

22. McDonnell Aircraft Company. *F-15 Stability and Control and Flying Qualities, Part III Spin Studies*. Report No. MDC A0503, 31 July 1972.

23. McDonnell Aircraft Company. *F/TF-15 Stability Derivatives, Mass and Inertia Characteristics Flight Test Basis, Part II Aerodynamic Coefficients and Stability and Control Derivatives*. Report No. MDC A4172

24. Neihouse, Anshal I., Walter J. Klinar, and Stanley H. Scher. *Status of Spin Research for Recent Airplane Designs*, NASA Technical Report R-57, 1960.

25. Planeaux, J.B. and T.J. Barth. "High Angle-of-Attack Dynamic Behavior of a Model High-Performance Fighter Aircraft," *AIAA Atmospheric Flight Mechanics Conference*. Paper no 88-4368. Washington, D.C.: American Institute of Aeronautics and Astronautics, August 1988

26. Planeaux, J.B., J.A. Beck, and D.D. Baumann. "Bifurcation Analysis of a Model Fighter Aircraft with Control Augmentation," *AIAA Atmospheric Flight Mechanics Conference*. Paper no 90-2836. Washington D.C.: American Institute of Aeronautics and Astronautics, August 1990.

27. "Rockwell/MBB X-31 Makes Second Flight reaching 20,000-Ft. Altitude, Mach 0.6," *Aviation Week and Space Technology*. October 22, 1990, p. 117.

28. Ropelewski, Robert R. "Modified F-15 Will Investigate Advanced Control Concepts," *Aviation Week and Space Technology*. February 11, 1985, pp. 51-53.

29. Scher, Stanley H. *An Analytical Investigation of Airplane Spin-Recovery Motion by Use of Rotary-Balence Aerodynamic Data*, NACA Technical Note 3188, June 1954.

30. Scher, Stanley H., Ernie L. Anglin, and George F. Lawerence. *Analytical Investigation of Effect of Spin Entry Technique on Spin and Recovery Characteristics for a 60 Degree Delta-Wing Airplane*," NASA Technical Note D-156, December 1959.

31. Schneider, Garret L. *Minimum Time Turns Using Vectored Thrust.* M.S. Thesis, AFIT/GAE/AA/84D-24. School oof Engineering, Air Force Institute of Technology (AU), Wright-Patterson AFB OH, December 1984.

32. Schy, A.A., and M.E. Hannah. "Prediction of Jump Phenomena in Roll-Coupled Maneuvers of Airplanes," *Journal of Aircraft*, 14: 375-382 (April 1977).

33. Seydel, Rüdiger. *From Equilibrium to Chaos: Practical Bifurcation and Stability Analysis.* New York: Elsevier Press, 1988.

34. *USAF Series F-15A/B/C/D Aircraft Flight Manual,* TO 1F-15A-1, 15 January 1984

35. Young, J.W., A.A. Schy, and K.G. Johnson. "Prediction of Jump Phenomena in Aircraft Maneuvers, including Nonlinear Aerodynamic Effects," *Journal of Guidance and Contrcl*, 1: 26-31 (January-Febuary 1978).

36. Zagaynov, G.I. and M.G. Goman. "Bifurcation Analysis of Critical Aircraft Flight Regimes," *International Council of the Aeronautical Sciences*, 84: 217,223, 1984.

Vita

Captain Robert J. McDonnell was born on 8 August 1962 in Evanston, Illinois. He graduated from Edina West High School, Edina, Minnesota, in 1980 and received an appointment to the U.S. Air Force Academy in Colorado Springs, Colorado. He graduated from the Academy in 1984 with a Bachelor of Science in Engineering Mechanics and was assigned to the 6595th Shuttle Test Group at Vandenberg AFB, Ca. He served in various capacities, including Orbiter Test Controller, while in the 6595 STG from July 1984 until December 1986. He was reassigned to the 6595th Test and Evaluation Group, Vandenberg AFB, when the 6595 STG was deactivated. There he served as a Small ICBM Launch Controller until entering the School of Engineering, Air Force Institute of Technology, in May 1989.

Permanent Address: 5301 W 64th St
Edina, Mn 55435

REPORT DOCUMENTATION PAGE

Form Approved
OMB No 0704-0188

1. AGENCY USE ONLY (*Leave blank*)

2. REPORT DATE: Dec 1990

3. REPORT TYPE AND DATES COVERED: Master's Thesis

4. TITLE AND SUBTITLE
Investigation of the High Angle of Attack Dynamics of the F-15B Using Bifurcation Analysis

5. FUNDING NUMBERS

6. AUTHOR(S)
Captain Robert J. McDonnell

7. PERFORMING ORGANIZATION NAME(S) AND ADDRESS(ES)
Air Force Institute of Tecnology
WPAFB, OH 45433-6583

8. PERFORMING ORGANIZATION REPORT NUMBER
AFIT/GAE/ENY/90D-16

9. SPONSORING/MONITORING AGENCY NAME(S) AND ADDRESS(ES)

10. SPONSORING/MONITORING AGENCY REPORT NUMBER

11. SUPPLEMENTARY NOTES

12a. DISTRIBUTION/AVAILABILITY STATEMENT
Approved for Public Release;
Distribution Unlimited

12b. DISTRIBUTION CODE

13. ABSTRACT (*Maximum 200 words*)
Previous studies predicted the F-15B high angle of attack and flat spin behavior using bifurcation analysis. The purpose of this thesis research was to use bifurcation analysis to predict the F-15B high angle of attack and flat spin behavior as a function of variable thrust, asymmetric thrust, and thrust vectoring. Using a previously developed model of the F-15B, bifurcation analysis and continuation methods were used to map out the equilibrium and periodic solutions of the model as a function of the thrust parameters. A baseline bifurcation diagram, as a function of alpha and elevator deflection, was developed. Thrust was varied and changes were identified. Thrust asymmetries were introduced and their effect on entering and recovering from spins was identified. Thrust vectoring was introduced to see how pitch and yaw vectoring can aid in the entry and recovery from spins. Where deemed necessary, time history simulations were presented to further explain F-15B behavior

14. SUBJECT TERMS
Aerodynamic Stability, Equations of Motion, Spins
Bifurcation, Thrust, Thrust Vectoring

15. NUMBER OF PAGES: 122

16. PRICE CODE

17. SECURITY CLASSIFICATION OF REPORT	18. SECURITY CLASSIFICATION OF THIS PAGE	19 SECURITY CLASSIFICATION OF ABSTRACT	20. LIMITATION OF ABSTRACT
Unclassified	Unclassified	Unclassified	UL

GENERAL INSTRUCTIONS FOR COMPLETING SF 298

The Report Documentation Page (RDP) is used in announcing and cataloging reports. It is important that this information be consistent with the rest of the report, particularly the cover and title page. Instructions for filling in each block of the form follow It is important to ***stay within the lines*** to meet ***optical scanning requirements***.

Block 1. Agency Use Only *(Leave blank)*

Block 2. Report Date Full publication date including day, month, and year, if available (e.g. 1 Jan 88). Must cite at least the year

Block 3. Type of Report and Dates Covered. State whether report is interim, final, etc. If applicable, enter inclusive report dates (e.g. 10 Jun 87 - 30 Jun 88).

Block 4. Title and Subtitle. A title is taken from the part of the report that provides the most meaningful and complete information. When a report is prepared in more than one volume, repeat the primary title, add volume number, and include subtitle for the specific volume On classified documents enter the title classification in parentheses.

Block 5. Funding Numbers. To include contract and grant numbers; may include program element number(s), project number(s), task number(s), and work unit number(s) Use the following labels:

C	- Contract	PR	- Project
G	- Grant	TA	- Task
PE	- Program Element	WU	- Work Unit Accession No.

Block 6. Author(s) Name(s) of person(s) responsible for writing the report, performing the research, or credited with the content of the report. If editor or compiler, this should follow the name(s).

Block 7. Performing Organization Name(s) and Address(es). Self-explanatory

Block 8. Performing Organization Report Number. Enter the unique alphanumeric report number(s) assigned by the organization performing the report.

Block 9. Sponsoring/Monitoring Agency Name(s) and Address(es). Self-explanatory.

Block 10. Sponsoring/Monitoring Agency Report Number *(If known)*

Block 11. Supplementary Notes Enter information not included elsewhere such as. Prepared in cooperation with .; Trans of ., To be published in . When a report is revised, include a statement whether the new report supersedes or supplements the older report

Block 12a. Distribution/Availability Statement. Denotes public availability or limitations. Cite any availability to the public. Enter additional limitations or special markings in all capitals (e.g. NOFORN, REL, ITAR).

DOD - See DoDD 5230.24, "Distribution Statements on Technical Documents."
DOE - See authorities.
NASA - See Handbook NHB 2200.2.
NTIS - Leave blank.

Block 12b. Distribution Code.

DOD - Leave blank.
DOE - Enter DOE distribution categories from the Standard Distribution for Unclassified Scientific and Technical Reports.
NASA - Leave blank.
NTIS - Leave blank.

Block 13. Abstract. Include a brief *(Maximum 200 words)* factual summary of the most significant information contained in the report.

Block 14. Subject Terms. Keywords or phrases identifying major subjects in the report.

Block 15. Number of Pages. Enter the total number of pages.

Block 16. Price Code. Enter appropriate price code *(NTIS only)*.

Blocks 17. - 19. Security Classifications. Self-explanatory. Enter U.S. Security Classification in accordance with U.S. Security Regulations (i.e , UNCLASSIFIED). If form contains classified information, stamp classification on the top and bottom of the page.

Block 20. Limitation of Abstract. This block must be completed to assign a limitation to the abstract. Enter either UL (unlimited) or SAR (same as report). An entry in this block is necessary if the abstract is to be limited If blank, the abstract is assumed to be unlimited.